UNIVERSITY OF CALIFORNIA SAN DIEGO

Mechanisms of Mitochondrial tRNA Regulation: Transcriptional Pausing and RNA Processing

A Dissertation submitted in partial satisfaction of the requirements
for the degree Doctor of Philosophy

in

Biochemistry and Molecular Biophysics

by

Jubilee Haddasah Muñozvilla

Committee in charge:

Professor Tatiana Mishanina, Chair
Professor Susan Ackerman
Professor Colleen McHugh
Professor Navtej Toor
Professor Brian Zid

2026

The Dissertation of Jubilee Haddasah Muñozvilla is approved, and it is acceptable in quality and form for publication on microfilm and electronically.

University of California San Diego

2026

DEDICATION

To my parents, Sergio Yoseph and Lennierose Rut, who have supported and believed in me throughout my academic journey, this PhD is partially yours too. To my younger siblings, Serg, Nafti, Willie, Arik, Richie, Binnie, Kuky and Debbie, who are always up for adventures and who made the house a home. To Papi Memo and Papi Cincho, for teaching me the value of hard work, and finding joy in the little things. To Mami Cuca and Mami Chiqui, who taught me the value of kindness and hospitality. To Tatiana, who believed in me and became more than a mentor, a friend. To all the friends that have gotten on and off my train of life, or have stayed connected, especially my Johnnys, Ari, Adam, and Dafna, who provided valuable life lessons and who were there when it mattered the most. To my students, Sushi, Aves, Linh, and Aaron, for giving me the opportunity to build their scientific foundation and to be their mentor. To Dr. An Hsieh, who walked so I could run. To Dr. Amy Moskun, Dr. Jason Schwans, Dr. Ivan Martinez, Dr. Vas, Dr. Jeff Bradbury, Dr. Ryan Babiar, Dr. Scottie Henderson, Dr. Sean Bonness and Dr. Chase Tydell, who guided me throughout my undergraduate career and beyond. You have been, and will always remain, the foundation of my scientific development. And to Mama K, whose memory made me brave. Thank you to H-shem who gave me the strength and courage to finish the Ph.D. B"H

EPIGRAPH

"Nothing is worth doing without being a little bit scared."
Anonymous

"A dream you don't fight for, can haunt you the rest of your life."
Robots

TABLE OF CONTENTS

LIST OF FIGURES

Chapter 1

Chapter 2

Chapter 3

Chapter 4

ACKNOWLEDGEMENTS

I would like to thank and acknowledge Professor Tatiana Mishanina for her support as the chair of my committee but also as my PhD advisor. Through many laughs, brainstorming sessions, and emotional moments, her mentorship and guidance has proved invaluable. Thank you for giving me the opportunity to complete a PhD in your lab and for encouraging creativity. Thank you for all the undergraduate outreach opportunities we have been able to create together and for allowing me to actively live my dream of impacting student lives at the early stages of their career. I would also like to thank and acknowledge Professor Elizabeth Komives for her support as director of the Biochemistry and Molecular Biophysics program. Her encouragement throughout the PhD, guidance with MBTG, and support post-candidacy, is the reason I have reached this step.

I would also like to acknowledge and thank my committee members. It has been a challenging journey, but your support and feedback during our meetings have helped to shape my PhD journey. I especially would like to thank Professor Sue Ackerman for her valuable guidance on my research, as well as for her openness and perspective during the thoughtful conversations we shared, which provided meaningful support during challenging times.

I would like to acknowledge Dr. An Hsieh for their support and guidance in my early years of graduate school. Thank you for teaching me about POLRMT transcriptional pausing and taking me under your wing. But also thank you for teaching me the resilience necessary to finish the PhD and standing up for yourself when it matters most. I would like to acknowledge Dr. Ravish Sharma, Dr. Mukesh Mahajan, and Dr. Sean Reardon, for their guidance in project direction. Thank you for the brainstorming talks and the suggestions, your advice was truly invaluable for my paper's direction.

I would also like to acknowledge my undergraduate student mentees, Avery Ontiveros, Linh Tran, and Aaron Bagaoisan. Thank you for the foundational work you input into these mitochondrial projects and for teaching me the value of mentorship.

Chapter 2, in part, has been submitted for publication of the material as it may appear in Journal of Biological Chemistry, 2026, Munozvilla, Jubilee; Ontiveros, Avery; Mishanina, Tatiana, ASBMB Journals, 2026. The dissertation author was the primary researcher and author of this paper.

Chapter 3, in full, is a reprint of the material as it appears in BioProtocol, 2023, Hsieh, An; Reardon, Sean; Munozvilla-Cabellon, Jubilee; Shen, Jiayu; Patel, Smita; Mishanina, Tatiana. The dissertation author was the co-investigator and co-author of this paper.

Chapter 4 contains unpublished material. The dissertation author was the primary author of this chapter.

VITA

2019 Associate of Science in Chemistry and Biology, Cerritos Community College

2021 Bachelor of Science in Biochemistry, California State University Long Beach

2023 Master of Science in Biochemistry and Molecular Biophysics, University of California San Diego

2026 Doctor of Philosophy in Biochemistry and Molecular Biophysics, University of California San Diego

PUBLICATIONS

Muñozvilla, J.H., Ontiveros, A., Mishanina, T. (in revision)
"Pathogenic human mitochondrial tRNA variants impair RNA processing by compromising 5′ leader removal." https://doi.org/10.64898/2026.03.25.714317

Hsieh, A., Reardon, S., Muñozvilla-Cabellon, J., Shen, Jiayu., Patel, S., Mishanina, T.
"Expression and Purification of Recombinant Human Mitochondrial RNA Polymerase (POLRMT) and the Initiation Factors TFAM and TFB2M." Bio-protocol 13(23): e4892. 2023. https://doi.org/10.21769/bioprotoc.4892

FIELD OF STUDY

Major Field: Biochemistry
Studies in mitochondrial tRNA transcription
Professor Tatiana Mishanina

ABSTRACT OF THE DISSERTATION

Mechanisms of Mitochondrial tRNA Regulation: Transcriptional Pausing and RNA Processing

by

Jubilee Haddasah Muñozvilla

Doctor of Philosophy in Biochemistry and Molecular Biophysics

University of California San Diego, 2026

Professor Tatiana Mishanina, Chair

Mitochondria are essential organelles within a eukaryotic cell, with their own genome (mtDNA) responsible for cellular energy production through oxidative phosphorylation. The mtDNA-encoded mitochondrial transfer RNAs (mt-tRNAs), despite comprising only a small fraction of the mitochondrial genome, account for a disproportionate number of disease-associated

mutations. Many of these mutations disrupt mitochondrial gene expression and lead to severe mitochondrial disorders. However, the molecular mechanisms by which mt-tRNA sequence variation affect transcription and RNA maturation are insufficiently characterized. Understanding how these mutations alter the mt-tRNA life cycle is key to identify early points of dysfunction and for development of targeted therapeutic strategies. The goal of this dissertation is to define how mt-tRNA sequence variation influences transcriptional pausing on mt-tRNA encoding sequences and mt-tRNA processing, towards establishing mechanistic links between these processes and mitochondrial disease.

Chapter 1, which serves as an introduction to the dissertation, provides an overview of mitochondrial transcription machinery and mt-tRNA processing, with the emphasis on the role of mt-tRNAs in coordinating RNA maturation.

In Chapter 2, I investigate how disease-associated mutations within the acceptor stem of mt-tRNATyr impair 5' leader processing, disrupt interactions with the MRPP1/2 processing complex, and support a directional 5'-to-3' maturation pathway. This work further demonstrates that defects in upstream mt-tRNAs can propagate to downstream mt-tRNAs within clusters, revealing coordinated processing dependencies.

Chapter 3 describes the development and optimization of the recombinant expression and purification strategies for key components of the human mitochondrial transcription machinery, including POLRMT, TFAM, and TFB2M. Through this work, I participated in establishing a robust biochemical platform for studying mitochondrial transcription in vitro, enabling mechanistic investigations of transcriptional regulation.

In Chapter 4, I study transcriptional pausing by POLRMT and demonstrate that a disease-associated mutation (m.T616C) within mt-tRNAPhe abolishes a sequence-dependent pause.

Through scaffold-based transcription assays, I show that this mutation disrupts transcriptional dynamics, linking mtDNA sequence variation to early defects in the mt-tRNA life cycle and suggesting a role for pausing in coordinating RNA folding and downstream processing.

Overall, my work establishes a mechanistic framework connecting mt-tRNA sequence variation to defects in transcriptional pausing and coordinated mt-tRNA maturation. These findings provide new insight into how disease-associated mutations disrupt mitochondrial gene expression and highlight early stages of the mt-tRNA life cycle as critical points of vulnerability.

Chapter 1 Introduction

1.1 Overview

Eukaryotic cells are presumed to have evolved from an endosymbiotic event in which a Gram-negative α-proteobacterium was enveloped by a fermentative Asgard archaeal host cell, roughly 1.5-2 billion years ago[1]. The α-proteobacterium subsequently transitioned into what is now recognized as mitochondria. Each mammalian cell contains multiple copies of mitochondria, ranging from as few as 4 in platelets to as many as 8,000 in cardiomyocytes, reflecting the energetic demands of each cell type[1]. Human mitochondria contain their own DNA (mtDNA), encoding thirteen essential protein subunits of the oxidative phosphorylation (OXPHOS) complexes responsible for producing the majority of cellular adenosine triphosphate (ATP)[1,2]. Because mitochondria are the primary generators of cellular energy in the form of ATP, they are commonly referred to as the "powerhouses of the cell". Cells containing genetically identical mitochondrial genomes are considered homoplasmic, whereas those harboring a mixture of mtDNA sequence variations are referred to as heteroplasmic[3,4]. In humans, the multicopy nature of mtDNA, combined with the potential for heteroplasmy, introduces unique challenges for maintaining proper mitochondrial gene expression and function. In addition to energy production, mitochondria function as biosynthetic hubs, generating metabolic intermediates that are either exported or further processed to produce diverse biomolecules such as steroids, phospholipids, amino acids and iron-sulfur clusters for essential enzyme activity[1].

Mitochondrial genes are transcribed by a single mitochondrial RNA polymerase (RNAP), producing a ~16,600 nucleotide-long polycistronic transcripts in which protein-coding sequences

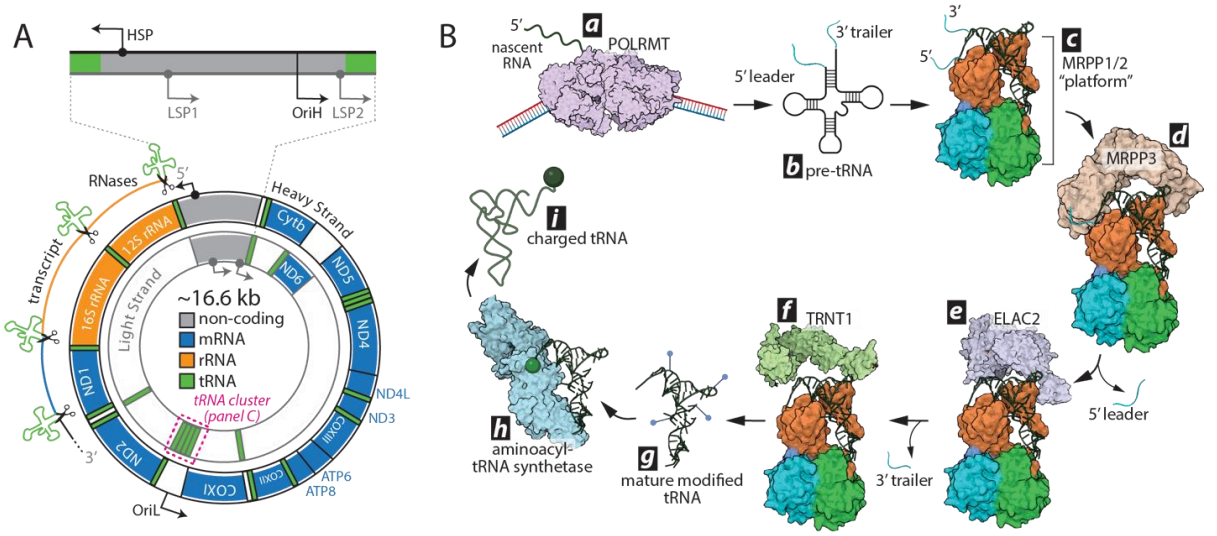

Figure 1 | Mitochondrial DNA and the tRNA life cycle | (A) Map of human mitochondrial genome (mtDNA), with the $tRNA^{Tyr}$ cluster highlighted in magenta. (B) Life cycle of mitochondrial tRNA starting with transcription by human mitochondrial RNA polymerase, POLRMT (*a*), nascent RNA folding into a precursor tRNA containing the 5' leader and 3' trailer (*b*), pre-tRNA association with by MRPP1/2 (*c*, PDB ID: 7ONU), 5' leader processing by MRPP3 (*d*, PDB ID: 7ONU), 3'trailer processing by ELAC2 (*e*, PDB: 8Z1G), 3'-CCA tail addition by TRNT1 (*f*, PDB ID: 4X4W), tRNA modification by "writer enzymes" (*g*), aminoacylation by the respective tRNA aminoacyl synthetase (*h*, PDB ID: 2PID), and mature mt-tRNA release (*i*).

are arranged in tandem (Fig. 1A)[2,5]. These long transcripts require precise and coordinated processing to generate mature and functional RNA species. Processing of the primary transcript requires excision of intervening mitochondrial tRNAs (mt-tRNAs) by the mitochondrial endonucleases RNase P and RNase Z at the 5' and 3' end, respectively (Fig. 1B)[6-11]. Sequence alterations in mt-tRNA genes associated with mitochondrial diseases have been shown to impair mitochondrial transcript processing, observed as decreased levels of mature mt-tRNAs in northern blots of patient cell lines, and increased abundance of unprocessed transcripts detected by RNA-seq[12-14]. Therefore, understanding how mt-tRNA sequence variations impact RNA processing is essential for defining the molecular basis of mitochondrial disease.

In addition to post-transcriptional mt-tRNA processing, RNA synthesis by RNAP represents an important regulatory layer in RNA maturation. In bacterial and nuclear systems, RNAP pausing is a well-characterized transcriptional mechanism that influences RNA folding,

coordinates transcription with downstream processes (e.g., translation and splicing), and modulates gene expression by controlling transcriptional progression (e.g., elongation rate and premature termination) regulates gene expression[15]. However, the extent to which transcriptional pausing contributes to mitochondrial RNA maturation, and the effects of disease-associated mtDNA mutations on pausing, are understudied.

1.2 Transcription and pausing in the mitochondria

Transcription in the mitochondria is initiated by the coordinated binding of mitochondrial transcription factor A (TFAM) to the non-coding region of mtDNA, which houses the heavy strand promoter (HSP) and two light strand promoters (LSP1 and LSP2). TFAM bends the DNA and recruits mitochondrial RNAP (POLRMT in humans) to the promoter region; the mitochondrial transcription factor B2 (TFB2M) then binds and "melts" the promoter region to allow POLRMT transcription initiation[5,16-18]. HSP is responsible for transcription in the "outer" sequence of the mitochondrial genome, encoding fourteen tRNAs, two mitochondrial rRNAs, and twelve OXPHOS mRNA sequences (Fig. 1A)[16-20]. LSP2 enables transcription of the "inner" sequence of the mitochondrial genome, encoding eight tRNAs and one OXPHOS mRNA sequences, and LSP1 invokes transcription of the regulatory non-coding 7S RNA that promotes POLRMT dimerization to "sponge up" POLRMT and inhibit transcription[5,16,19-21]. The transcription elongation factor, TEFM, stabilizes an actively transcribing POLRMT on the DNA template, thereby promoting processive transcription, reducing nascent RNA structure-stabilized transcriptional pause duration, and reducing premature termination[19,22,23].

Pausing occurs when RNAP encounters specific nucleic acid sequence signals that induce a catalytically inactive conformation, temporarily preventing nucleotide addition[15] (Fig. 2A). In bacteria, this paused state mediates transcription termination, nascent RNA folding, or recruitment of RNA translational machinery[15,24,25]. In eukaryotic nucleic systems, RNAP II has frequent pauses

downstream of the promoter, proposed to occur as a checkpoint to control gene expression, as well as splicing and chromatin rearrangement[25-27]. In recent work, POLRMT has been observed to recognize and pause at a universally conserved pause, suggesting the possibility of conserved underlying mechanisms and functional roles for transcriptional pausing across evolution[28]. A consensus elemental pause motif for POLRMT has been identified and is distributed throughout the mitochondrial genome. Notably, these pause-inducing sequences are enriched on the light-strand transcript relative to the heavy strand, potentially reflecting the "G-richness" of the light-strand template, which may promote formation of G-quadruplex structures in the nascent RNA that stabilize the paused polymerase[28,29].

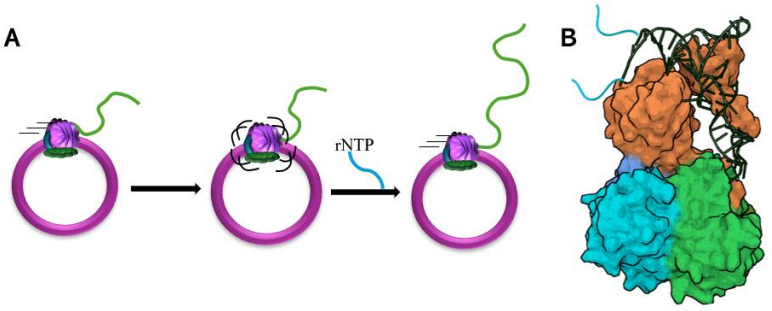

Figure 2 | Pausing Schematic and MRPP1/2 bound to mt-tRNA | (A) Schematic of pausing mechanism where POLRMT (purple) pauses on mtDNA (magenta) continuing transcription of the RNA transcript (green) after addition of the incoming nucleotide. (B) Schematic of MRPP1 (orange, PDB ID: 7ONU) and MRPP2 (Blue, green, indigo, PDB ID: 7ONU) as a protein complex folding and positioning the mt-tRNA (dark green) for cleavage of the 5' leader and the 3' trailer sequences (light blue).

Because transcriptional pausing is linked to nascent RNA folding, it may play a role in shaping mt-tRNA structure during transcription. This is particularly relevant in the context of mitochondrial disease, where point mutations and deletions may alter pausing behavior and affect RNA folding and processing. However, the impact of the disease-associated mtDNA mutations on transcriptional pausing remains largely unexplored.

1.3 Processing machinery of mitochondrial tRNAs: RNase P and RNase Z

Mitochondrial transcripts are synthesized as long polycistronic RNAs in which tRNAs are interspersed between mRNA and rRNA sequences, a genomic organization described as "the tRNA punctuation model." In this model, excision of individual mt-tRNAs from the primary

transcript enables the release of tRNA, adjacent mRNAs, and rRNAs, positioning tRNAs as both structural elements of the translational machinery and key regulators of mitochondrial gene expression (Fig. 1A)[1,16,20].

Most mt-tRNAs have their 5' leader (5' adjacent piece of the polycistron) processed by human mitochondrial RNase P, a multiprotein complex comprised of the methyltransferase TRMT10C (MRPP1), four copies of dehydrogenase SDR5C1 (MRPP2), and the endonuclease PRORP (MRPP3), which together mediate hydrolysis of the precursor mt-tRNA (pre-tRNA) 5' leader[6-11,30-32]. The TRMT10C (MRPP1) also methylates the conserved purine (A or G) at the position 9 of mt-tRNAs, a modification thought to stabilize the final tRNA fold, whereas SDR5C1 (MRPP2) has lost its dehydrogenase activity in the context of the mitochondrial RNase P complex. While PRORP functions as a stand-alone protein-only nuclease in some eukaryotes (e.g., plant mitochondria and plastids), its activity in human mitochondria is entirely dependent on its interactions with MRPP1/2, which act as a structural and functional platform for precursor tRNA (pre-tRNA) substrate positioning[6-8]. The MRPP1/2 subcomplex is widely considered as a "maturation platform", facilitating proper alignment of pre-tRNAs for coordinated and sequential enzymatic processing steps[8,10,11]. In contrast to mitochondrial RNase P, nuclear-encoded pre-tRNAs are cleaved at the 5' end by the evolutionarily and structurally divergent nuclear riboprotein RNase P, which is a ribozyme composed of the catalytic RNA and multiple accessory protein subunits[31]. Cleavage of the 3' trailer (3' adjacent piece of the polycistron) is carried out by RNase Z, which contains the same MRPP1/2 subcomplex in association with the ELAC2 endonuclease (Fig. 1B)[30,31]. ELAC2 also processes nuclear-encoded pre-tRNAs. Unlike in mitochondria, ELAC2 does not require MRPP1/2 for assistance in cleavage of nuclear-encoded pre-tRNAs due

to the additional tertiary structural features of nuclear tRNAs that are absent from the "eroded" mt-tRNAs described below[31].

A defining feature of mt-tRNAs is their deviation from canonical cytosolic tRNA structure. Seventeen out of the 22 mt-tRNAs lack conserved nucleotides within the D- and T-loops that stabilize the classical "L-shaped" tertiary structure via kissing-loop interactions (also referred to as the "elbow"), resulting in decreased intrinsic structural stability for mt-tRNAs and increased reliance on MRPP1/2-mediated stabilization[31]. MRPP1/2 is proposed to compensate for these deficiencies by stabilizing the folded conformation of mt-tRNAs via extensive shape and charge complementarity with the tRNA and conserved nucleotide contacts within the anticodon loop, thereby enabling efficient processing, not only by PRORP and ELAC2, but also by downstream maturation enzymes such as the 3'-CCA cap adding protein, TRNT1 (Fig. 2B)[32]. Studies further suggest that MRPP1/2 enforces an ordered 5' leader first, 3' trailer second cleavage hierarchy as structural work has proposed ELAC2 is prevented from cleaving the 3' trailer when the 5' leader is still attached due to the steric clash between the 5' leader and one of ELAC2 domains in an MRPP1/2-engaged pre-tRNA substrate[31,32].

Following cleavage of both the 5' leader and the 3' trailer, MRPP1/2 is proposed to remain associated with the tRNA during addition of the 3'-CCA cap by TRNT1, suggesting coordinated interactions between processing and maturation proteins (Fig. 1B)[32]. Addition of the 3'-CCA cap not only enables aminoacylation, but also acts as an antideterminant for RNase Z, preventing cleavage of the 3'-added CCA cap and ensuring mt-tRNA maturation progresses unidirectionally[32]. Subsequent aminoacylation by the mt-tRNAs respective aminoacyl tRNA synthetase "charges" the tRNA with its corresponding amino acid, preparing the mt-tRNA for translation (Fig. 1B).

Experimental evidence indicates that unprocessed transcripts containing the 5' leader were not associated with the mitochondrial ribosome, suggesting that 5' leader processing is a prerequisite for translation[33]. In contrast to nuclear-encoded mRNAs, which can remain in non-ribosome bound states for extended periods (approx. 176 min), mitochondrial mRNAs exhibit rapid turnover, spending approximately 5 min in non-bound states and degrading within approximately 74 min[33]. However, while mRNA turnover has been characterized, the kinetics of mt-tRNA biogenesis and degradation remain poorly understood due to the low mt-tRNA cellular abundance compared to total cell RNA levels, extensive post-transcriptional modifications, abundant tertiary structural motifs (e.g., kissing loops), and short length (~70 nt) that poses challenges to traditional RNA sequencing approaches[3,33,34]. The post-transcriptional modifications include methylating purine nucleotides or uridine isomerization to pseudouridine to stabilize the mt-tRNA tertiary structure, enhance codon-anticodon interactions, and prevent premature tRNA degradation[3]. Notably, many of these modifications depend on precise recognition of specific nucleotide identities, making them particularly sensitive to sequence variations[3]. Mutations at post-transcriptional modification sites can prevent installation of these modifications, disrupting tRNA folding and stability, contributing to mitochondrial diseases. For example, a loss of taurinomethyl modification at the wobble base in mt-tRNA$^{Leu(UUR)}$ and mt-tRNA^{Lys} resulting in severely reduced respective codon recognition and translation, manifesting as mitochondrial encephalopathy and myoclonic epilepsy[3,12].

At each stage of processing, MRPP1/2-mediated interactions provide checkpoints that ensure correct progression of mt-tRNA maturation. Disruptions to this system, either through mutations in processing enzymes or sequence variations within mt-tRNAs themselves (see next section for examples), can impair maturation and ultimately compromise mitochondrial function[12-

[14,35,36]. Thus, defining how specific mt-tRNA mutations alter coordinated processing steps is key for understanding the mechanistic basis of mitochondrial diseases.

1.4 Mitochondrial diseases associated with mt-tRNA gene deviations

Studies of both nuclear-encoded and mitochondrial tRNAs have demonstrated that efficient RNA processing and maturation depend on the correct folded shape of the substrate rather than the exact nucleotide sequence at the cleavage site. Early studies with nuclear RNase P showed that efficient processing requires conserved structural features within the acceptor stem and tertiary core of the tRNA, establishing a model in which substrate architecture is a large determinant of enzyme recognition for processing[37].

More recent studies with nuclear-encoded and cytoplasm-localized tRNAs have further shown that sequence variants can impair processing through effects on RNA structure. A disease-associated C50U substitution located on the T-stem in the neuron-specific cytoplasmic $tRNA^{Arg(UCU)}$ (n-Tr20) reduced RNase P cleavage efficiency ~20-fold, despite the substitution being located distal to the cleavage site[38]. Biophysical analysis (tRNA melting profiles and ^{1}H-NMR) revealed that the mutation promoted alternative non-native tRNA conformations that disrupted formation of the canonical tRNA elbow, which is a key structural feature recognized by RNase P [30, 37-39]. These findings showed that tRNA mutations can alter processing by shifting the equilibrium of a pre-tRNA toward conformationally stable structures that are unsuitable substrates for nuclear RNase P.

Structural studies of RNase P complexes with the pre-tRNA have provided a mechanistic explanation for these observations. Analysis of nuclear and mitochondrial RNase P enzymes showed that substrate recognition relies on conserved interactions with the overall tRNA architecture, including contacts with the acceptor arm, T-arm, and tertiary structural elements (either through canonical folding or assistance by MRPP1/2), that position the substrate for

accurate cleavage[39]. Disruption of these structural features can impair enzyme recognition and processing even when the cleavage site sequence is unchanged. Recognition and processing by mitochondrial RNase P may be impaired by mt-tRNA variants that alter local or global mt-tRNA folding, as observed in the nuclear-encoded tRNA example[38]. This results in a dependency for correct RNA folding and conformational stability as a strong determinant of processing efficiency.

Defects in mt-tRNA processing contribute to mitochondrial dysfunction and disease[3,4,12]. Genetic disruption of key processing enzymes highlights the importance of this pathway. For example, knockouts of MRPP3 in mice reduced both 5' and 3' cleavage, impaired mitochondrial ribosome assembly and OXPHOS complex activity[12-14,36]. Knockouts of ELAC2 in skeletal and heart muscles caused premature death in mice due to defective tRNA processing and reduced OXPHOS function[36]. Collectively, these studies demonstrate that precise and coordinated 5' and 3' processing is essential for maintaining mitochondrial gene expression and cellular energy production.

Various mitochondrial diseases have been associated with mutations in mtDNA, many of which affect mt-tRNAs specifically (Fig. 3). These mutations often manifest as neuromuscular disorders such as myopathy, muscular dystrophy, chronic progressive external ophthalmoplegia, and epilepsy. To date, 1,058 mtDNA variants have been reported, with ~40% mapping to tRNA

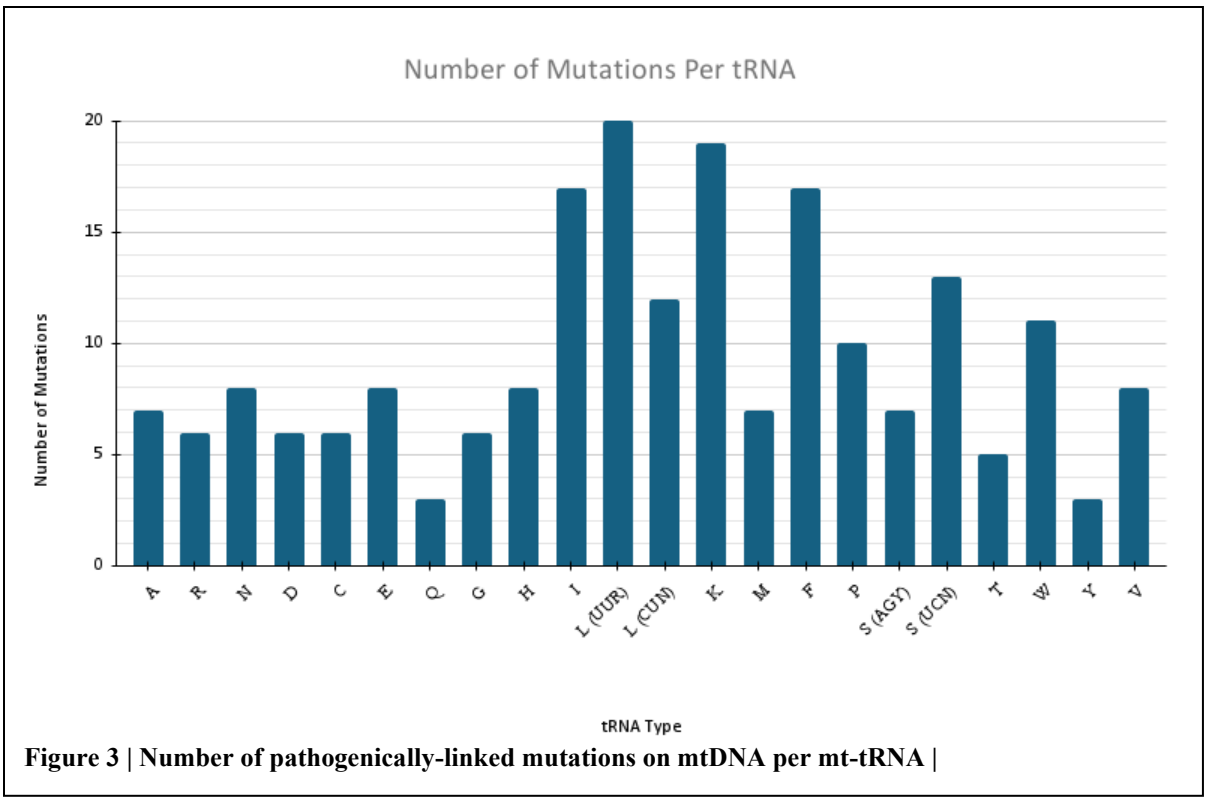

Figure 3 | Number of pathogenically-linked mutations on mtDNA per mt-tRNA |

genes and 60% of those classified as pathogenic, defined as "Two or more independent patient reports; Evolutionary conservation of the nucleotide, Presence of heteroplasmy; correlation of variant with phenotype / segregation of the mutation with the disease within a family; Biochemical defects in OXPHOS complexes; Functional studies showing differential defects segregating with the mutation (cybrid or single fiber studies); Histochemical evidence of a mitochondrial disorder; For fatal or severe phenotypes, the absence or extremely rare occurrence of the variant in large mtDNA sequence databases"[4]. Pathogenic mt-tRNA variants are consistently associated with reduced OXPHOS complex production, and multiple biochemical studies have shown defects in 5′/3′ processing and aminoacylation resulting from these mutations[33,39,40]. These observations establish mt-tRNAs as a major mechanistically relevant source of mitochondrial disease.

Many disease-associated mutations cluster within the acceptor stem region, and the D- and T-loop regions of mt-tRNAs[41-44]. Despite this, the mechanistic relationship between mutation

position and specific defects in tRNA processing remains poorly defined. In particular, no studies have systematically examined how the proximity of a mutation to enzymatic active sites influences both 5' and 3' processing efficiency. Furthermore, while point mutations have been explored in a few recent studies, the impact of deletions in mt-tRNAs has not been systematically characterized. In addition to processing defects, these mutations have also been linked to hypomodification of loss of post-transcriptional modifications, likely due to a disruption of sequence recognition by modifying enzymes[3]. Together, these gaps in knowledge highlight an opportunity for mechanistic studies into how different classes of mt-tRNA mutations disrupt tRNA maturation.

An additional layer of complexity arises from the organization of several mt-tRNAs into clusters within the mitochondrial genome. In these regions, multiple tRNAs are encoded sequentially, such that processing of one tRNA may influence the release and maturation of downstream tRNAs[8]. Clusters on the HSP transcript include $tRNA^{Ile}$-$tRNA^{Met}$ and $tRNA^{His}$-$tRNA^{Ser}$-$tRNA^{Lys}$, while LSP2 drives the synthesis of a $tRNA^{Tyr}$-$tRNA^{Cys}$-$tRNA^{Asn}$-$tRNA^{Ala}$ cluster (Figs. 1A and 4A). The extent to which mutations in an upstream tRNA affect the processing of downstream tRNAs remains unknown.

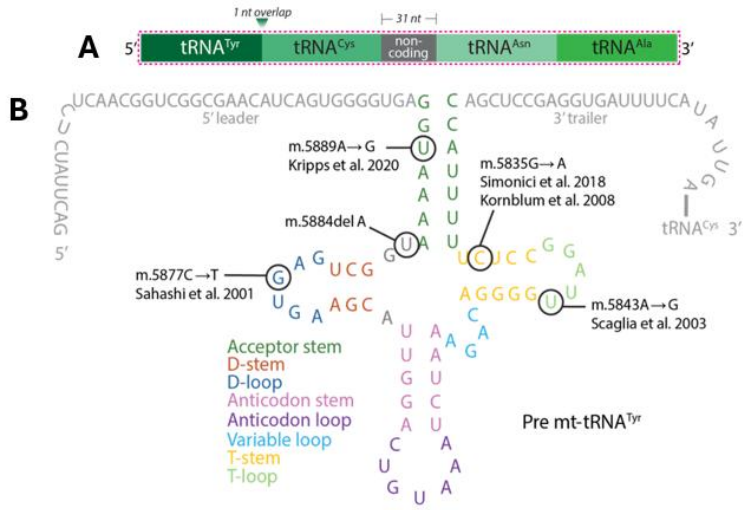

Figure 4 | LSP2 cluster and pre mt-$tRNA^{Tyr}$ secondary structure | (A) Schematic showing the LSP2 cluster containing $tRNA^{Tyr}$-$tRNA^{Cys}$-$tRNA^{Asn}$-$tRNA^{Ala}$ (B) Secondary structure of mt-$tRNA^{Tyr}$ with the structural variations mapped on the schematic.

1.5 Overview of the dissertation

This dissertation addresses key gaps in the field of mitochondrial transcription and RNA processing by investigating three central questions; (1) how mt-tRNA mutations and deletions affect 5' leader and 3' trailer removal, (2) whether processing defects propagate to downstream tRNAs within mt-tRNA clusters, and (3) how mtDNA mutations influence transcriptional pausing within the mt-tRNA genes.

To address the first two questions, I focused on mt-tRNA^{Tyr}, which is the first tRNA in a cluster of tRNAs transcribed from the light strand promoter. This dissertation investigated two disease linked mutations (m.G5835A and m.A5889G), and a single-nucleotide deletion (m.5884delA) located at or near the acceptor stem, and two "benign" variants (m.C5877T and m.T5843C) within the D- and T-loops that contribute to the canonical tertiary tRNA fold (Fig 4B)[40,45-49]. Variants are described using the standard genomic numbering system within the mtDNA.

I found that variants located proximal to the tRNA acceptor stem had the greatest impact on 5' leader cleavage efficiency. In addition, my data support a 5'-to-3' processing model, demonstrating that ELAC2-mediated 3' trailer cleavage does not occur when the 5' leader remains uncleaved, e.g., due to a cleavage-compromising mutation, in line with the proposed steric clash between 5' leader of the pre-tRNA, oriented by MRPP1/2, and the C-terminal region of ELAC2[31]. These findings provide functional *in vitro* validation of structural models and demonstrate, for the first time, how disease-associated mutations disrupt coordinated processing by jointly affecting both MRPP3- and ELAC2-mediated cleavage, revealing a level of mechanistic coupling not captured in prior studies with individual enzymes in isolation[11,31,32].

Furthermore, I demonstrated that defects in processing of an upstream tRNA within a cluster can impair processing of downstream tRNAs. However, this dependency is alleviated when a non-coding sequence separates adjacent tRNAs, indicating that sequential continuity within clusters contributes to coordinated processing. This represents one of the first mechanistic demonstrations that mt-tRNA mutations can propagate processing defects within mt-tRNA clusters through disruption of 5' leader cleavage, unveiling the underlying cleavage defects previously inferred from mt-tRNA levels in cybrid models but not directly examined[50].

To investigate the third question of transcriptional mt-tRNA regulation, I examined mt-tRNA^{Phe}, the first tRNA transcribed from the heavy strand promoter (Fig. 5A). *In vitro* transcription assays using my purified POLRMT revealed a distinct transcriptional pause at position m.T616 within the mt-tRNA^{Phe} transcript (Fig. 5B). I mapped this pause site using RNA sequencing and confirmed this site as a transient transcriptional pause (vs. termination site) by quantifying the fraction of POLRMT molecules at this site as a function of time. The m.T616 position is within the previously discovered "elemental" pause sequence (Fig. 5A)[28]. Introduction of a disease-associated mutation (m.T616C in mtDNA), which clinically presents as severe epilepsy, abolished this pause, as

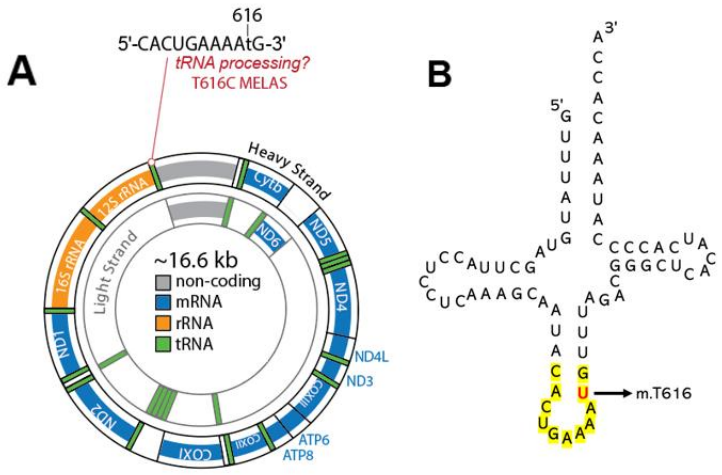

Figure 5 | Location of mt-tRNA^{Phe} on mtDNA and mt-tRNA^{Phe} secondary structure | (A) Map of human mitochondrial genome (mtDNA), with mt-tRNA^{Phe} located and its pausing motif (B) Secondary structure of mt-tRNA^{Phe} with the motif in yellow and the pause site in red.

evidenced by the absence of the corresponding transiently accumulating RNA band, linking sequence variation to altered transcriptional dynamics[51-53].

Together, my work establishes a mechanistic framework connecting mt-tRNA sequence variation to defects in transcriptional pausing, RNA processing, and coordinated tRNA maturation, providing new insight into how disease-associated mutations disrupt the mt-tRNA life cycle.

REFERENCES

1. Moura JP, Oliveira PJ, Urbano AM. Mitochondria: An overview of their origin, genome, architecture, and dynamics. *Biochim Biophys Acta Mol Basis Dis*. 2025 Jun;1871(5):167803. doi: 10.1016/j.bbadis.2025.167803.

2. Suzuki T, Yashiro Y, Kikuchi I, Ishigami Y, Saito H, Matsuzawa I, Okada S, Mito M, Iwasaki S, Ma D, Zhao X, Asano K, Lin H, Kirino Y, Sakaguchi Y, Suzuki T. Complete chemical structures of human mitochondrial tRNAs. Nat Commun. 2020 Aug 28;11(1):4269. doi: 10.1038/s41467-020-18068-6. PMID: 32859890; PMCID: PMC7455718.

3. Suzuki T, Suzuki T. A complete landscape of post-transcriptional modifications in mammalian mitochondrial tRNAs. Nucleic Acids Res. 2014 Jun;42(11):7346-57. doi: 10.1093/nar/gku390. Epub 2014 May 15. PMID: 24831542; PMCID: PMC4066797.

4. MITOMAP: A Human Mitochondrial Genome Database. http://www.mitomap.org, 2023

5. Tan BG, Mutti CD, Shi Y, Xie X, Zhu X, Silva-Pinheiro P, Menger KE, Díaz-Maldonado H, Wei W, Nicholls TJ, Chinnery PF, Minczuk M, Falkenberg M, Gustafsson CM. The human mitochondrial genome contains a second light strand promoter. Mol Cell. 2022 Oct 6;82(19):3646-3660.e9. doi: 10.1016/j.molcel.2022.08.011. Epub 2022 Aug 30. PMID: 36044900.

6. Holzmann J, Frank P, Löffler E, Bennett KL, Gerner C, Rossmanith W. RNase P without RNA: identification and functional reconstitution of the human mitochondrial tRNA processing enzyme. Cell. 2008 Oct 31;135(3):462-74. doi: 10.1016/j.cell.2008.09.013. PMID: 18984158.

7. Vilardo E, Nachbagauer C, Buzet A, Taschner A, Holzmann J, Rossmanith W. A subcomplex of human mitochondrial RNase P is a bifunctional methyltransferase--extensive moonlighting in mitochondrial tRNA biogenesis. Nucleic Acids Res. 2012 Dec;40(22):11583-93. doi: 10.1093/nar/gks910. Epub 2012 Oct 5. *Nucleic Acids Res.* 2018 Nov 16;46(20):11126-11127. doi: 10.1093/nar/gky931. PMID: 23042678; PMCID: PMC3526285.

8. Reinhard L, Sridhara S, Hällberg BM. Structure of the nuclease subunit of human mitochondrial RNase P. *Nucleic Acids Res.* 2015 Jun 23;43(11):5664-72. doi: 10.1093/nar/gkv481. Epub 2015 May 7. PMID: 25953853; PMCID: PMC4477676.

9. Yan H, Zareen N, Levinger L. Naturally occurring mutations in human mitochondrial pre-tRNASer(UCN) can affect the transfer ribonuclease Z cleavage site, processing kinetics, and substrate secondary structure. *J Biol Chem*. 2006;281(7):3926-3935. doi:10.1074/jbc.M509822200

10. Reinhard L, Sridhara S, Hällberg BM. The MRPP1/MRPP2 complex is a tRNA-maturation platform in human mitochondria. *Nucleic Acids Res.* 2017 Dec 1;45(21):12469-12480. doi: 10.1093/nar/gkx902. PMID: 29040705; PMCID: PMC5716156.

11. Vilardo E, Toth U, Hazisllari E, Hartmann RK, Rossmanith W. Cleavage kinetics of human mitochondrial RNase P and contribution of its non-nuclease subunits. *Nucleic Acids Res*. 2023;51(19):10536-10550. doi:10.1093/nar/gkad713

12. Van Haute L, Pearce SF, Powell CA, D'Souza AR, Nicholls TJ, Minczuk M. Mitochondrial transcript maturation and its disorders. *J Inherit Metab Dis.* 2015 Jul;38(4):655-80. doi: 10.1007/s10545-015-9859-z. Epub 2015 May 28. PMID: 26016801; PMCID: PMC4493943.

13. Sen A, Karasik A, Shanmuganathan A, Mirkovic E, Koutmos M, Cox RT. Loss of the mitochondrial protein-only ribonuclease P complex causes aberrant tRNA processing and lethality in Drosophila. *Nucleic Acids Res.* 2016 Jul 27;44(13):6409-22. doi: 10.1093/nar/gkw338. Epub 2016 Apr 30. PMID: 27131785; PMCID: PMC5291253.

14. Rackham O, Busch JD, Matic S, Siira SJ, Kuznetsova I, Atanassov I, Ermer JA, Shearwood AM, Richman TR, Stewart JB, Mourier A, Milenkovic D, Larsson NG, Filipovska A. Hierarchical RNA Processing Is Required for Mitochondrial Ribosome Assembly. *Cell Rep.* 2016 Aug 16;16(7):1874-90. doi: 10.1016/j.celrep.2016.07.031. Epub 2016 Aug 4. PMID: 27498866.

15. Kang JY, Mishanina TV, Landick R, Darst SA. Mechanisms of Transcriptional Pausing in Bacteria. J Mol Biol. 2019 Sep 20;431(20):4007-4029. doi: 10.1016/j.jmb.2019.07.017. Epub 2019 Jul 13. PMID: 31310765; PMCID: PMC6874753.

16. Tan BG, Gustafsson CM, Falkenberg M. Mechanisms and regulation of human mitochondrial transcription. Nat Rev Mol Cell Biol. 2024 Feb;25(2):119-132. doi: 10.1038/s41580-023-00661-4. Epub 2023 Oct 2. PMID: 37783784.

17. Posse V, Gustafsson CM. Human Mitochondrial Transcription Factor B2 Is Required for Promoter Melting during Initiation of Transcription. J Biol Chem. 2017 Feb 17;292(7):2637-2645. doi: 10.1074/jbc.M116.751008. Epub 2016 Dec 27. PMID: 28028173; PMCID: PMC5314162.

18. Bostwick AM, Moya GE, Senti ML, Basu U, Shen J, Patel SS, Dittenhafer-Reed KE. Phosphorylation of mitochondrial transcription factor B2 controls mitochondrial DNA binding and transcription. Biochem Biophys Res Commun. 2020 Jul 30;528(3):580-585. doi: 10.1016/j.bbrc.2020.05.141. Epub 2020 Jun 3. PMID: 32505352; PMCID: PMC9161741.

19. Morozov YI, Temiakov D. Human Mitochondrial Transcription Initiation Complexes Have Similar Topology on the Light and Heavy Strand Promoters. J Biol Chem. 2016 Jun 24;291(26):13432-5. doi: 10.1074/jbc.C116.727966. Epub 2016 May 13. PMID: 27226527; PMCID: PMC4919431.

20. Hillen HS, Morozov YI, Sarfallah A, Temiakov D, Cramer P. Structural Basis of Mitochondrial Transcription Initiation. Cell. 2017 Nov 16;171(5):1072-1081.e10. doi: 10.1016/j.cell.2017.10.036. PMID: 29149603; PMCID: PMC6590061.

21. Zhu X, Xie X, Das H, Tan BG, Shi Y, Al-Behadili A, Peter B, Motori E, Valenzuela S, Posse V, Gustafsson CM, Hällberg BM, Falkenberg M. Non-coding 7S RNA inhibits transcription via mitochondrial RNA polymerase dimerization. Cell. 2022 Jun 23;185(13):2309-2323.e24. doi: 10.1016/j.cell.2022.05.006. Epub 2022 Jun 2. PMID: 35662414.

22. Posse V, Shahzad S, Falkenberg M, Hällberg BM, Gustafsson CM. TEFM is a potent stimulator of mitochondrial transcription elongation in vitro. Nucleic Acids Res. 2015 Mar 11;43(5):2615-24. doi: 10.1093/nar/gkv105. Epub 2015 Feb 17. PMID: 25690892; PMCID: PMC4357710.

23. Yu H, Xue C, Long M, Jia H, Xue G, Du S, Coello Y, Ishibashi T. TEFM Enhances Transcription Elongation by Modifying mtRNAP Pausing Dynamics. Biophys J. 2018 Dec 18;115(12):2295-2300. doi: 10.1016/j.bpj.2018.11.004. Epub 2018 Nov 10. PMID: 30514634; PMCID: PMC6302244.

24. Stephen C, Mishanina TV. Alkaline pH has an unexpected effect on transcriptional pausing during synthesis of the Escherichia coli pH-responsive riboswitch. J Biol Chem. 2022 Sep;298(9):102302. doi: 10.1016/j.jbc.2022.102302. Epub 2022 Aug 4. PMID: 35934054; PMCID: PMC9472077.

25. Mayer A, Landry HM, Churchman LS. Pause & go: from the discovery of RNA polymerase pausing to its functional implications. Curr Opin Cell Biol. 2017 Jun;46:72-80. doi: 10.1016/j.ceb.2017.03.002. Epub 2017 Mar 28. PMID: 28363125; PMCID: PMC5505790.

26. Gressel S, Schwalb B, Cramer P. The pause-initiation limit restricts transcription activation in human cells. Nat Commun. 2019 Aug 9;10(1):3603. doi: 10.1038/s41467-019-11536-8. PMID: 31399571; PMCID: PMC6689055.

27. Dollinger R, Gilmour DS. Regulation of Promoter Proximal Pausing of RNA Polymerase II in Metazoans. J Mol Biol. 2021 Jul 9;433(14):166897. doi: 10.1016/j.jmb.2021.166897. Epub 2021 Feb 25. PMID: 33640324; PMCID: PMC8184617.

28. Hsieh AH, Mishanina TV. Nucleic Acid Sequence Determinants of Transcriptional Pausing by the Human Mitochondrial RNA Polymerase (POLRMT). Biochemistry. 2025 Oct 7;64(19):4081-4090. doi: 10.1021/acs.biochem.5c00236. Epub 2025 Sep 17. PMID: 40958658.

29. Snyder RJ, Shankar U, Delker D, Soerianto W, Burdick JT, Cheung VG, Watts JA. Guanine quadruplexes mediate mitochondrial RNA polymerase pausing. BMC Biol. 2025 May 13;23(1):129. doi: 10.1186/s12915-025-02229-4. PMID: 40361112; PMCID: PMC12076976.

30. Meynier V, Hardwick SW, Catala M, Roske JJ, Oerum S, Chirgadze DY, Barraud P, Yue WW, Luisi BF, Tisné C. Structural basis for human mitochondrial tRNA maturation. *Nat Commun.* 2024 Jun 1;15(1):4683. doi: 10.1038/s41467-024-49132-0. PMID: 38824131; PMCID: PMC11144196.

31. Bhatta, A., Kuhle, B., Yu, R.D. Molecular basis of human nuclear and mitochondrial tRNA 3′ processing. *Nat Struct Mol Biol* **32**, 613–624 (2025). https://doi.org/10.1038/s41594-024-01445-w

32. Valentín Gesé G, Hällberg BM. Structural basis of 3'-tRNA maturation by the human mitochondrial RNase Z complex. *EMBO J.* 2024 Dec;43(24):6573-6590. doi: 10.1038/s44318-024-00297-w. Epub 2024 Nov 8. PMID: 39516281; PMCID: PMC11649783.

33. McShane E, Couvillion M, Ietswaart R, Prakash G, Smalec BM, Soto I, Baxter-Koenigs AR, Choquet K, Churchman LS. A kinetic dichotomy between mitochondrial and nuclear gene expression processes. *Mol Cell.* 2024 Apr 18;84(8):1541-1555.e11. doi: 10.1016/j.molcel.2024.02.028. Epub 2024 Mar 18. PMID: 38503286; PMCID: PMC11236289.

34. Yamagami R, Sieg JP, Assmann SM, Bevilacqua PC. Genome-wide analysis of the *in vivo* tRNA structurome reveals RNA structural and modification dynamics under heat stress. Proc Natl Acad Sci U S A. 2022 Jun 21;119(25):e2201237119. doi: 10.1073/pnas.2201237119. Epub 2022 Jun 13. PMID: 35696576; PMCID: PMC9231505.

35. Siira SJ, Rossetti G, Richman TR, Perks K, Ermer JA, Kuznetsova I, Hughes L, Shearwood AJ, Viola HM, Hool LC, Rackham O, Filipovska A. Concerted regulation of mitochondrial and nuclear non-coding RNAs by a dual-targeted RNase Z. EMBO Rep. 2018 Oct;19(10):e46198. doi: 10.15252/embr.201846198. Epub 2018 Aug 20. PMID: 30126926; PMCID: PMC6172459.

36. Sen A, Karasik A, Shanmuganathan A, Mirkovic E, Koutmos M, Cox RT. Loss of the mitochondrial protein-only ribonuclease P complex causes aberrant tRNA processing and lethality in Drosophila. *Nucleic Acids Res.* 2016 Jul 27;44(13):6409-22. doi: 10.1093/nar/gkw338. Epub 2016 Apr 30. PMID: 27131785; PMCID: PMC5291253.

37. Yuan, Y., & Altman, S. (1995). Substrate recognition by human RNase P: Identification of small, model substrates for the enzyme. *EMBO Journal*, *14*(1), 159-168. https://doi.org/10.1002/j.1460-2075.1995.tb06986.x

38. Lai LB, Lai SM, Szymanski ES, Kapur M, Choi EK, Al-Hashimi HM, Ackerman SL, Gopalan V. Structural basis for impaired 5' processing of a mutant tRNA associated with defects in neuronal homeostasis. *Proc Natl Acad Sci USA.* 2022 Mar 8;119(10):e2119529119. doi: 10.1073/pnas.2119529119. Epub 2022 Mar 1. PMID: 35238631; PMCID: PMC8915964.

39. Bhatta A, Dienemann C, Cramer P, Hillen HS. Structural basis of RNA processing by human mitochondrial RNase P. Nat Struct Mol Biol. 2021 Sep;28(9):713-723. doi:

10.1038/s41594-021-00637-y. Epub 2021 Sep 6. PMID: 34489609; PMCID: PMC8437803.

40. Wittenhagen LM, Kelley SO. Impact of disease-related mitochondrial mutations on tRNA structure and function. *Trends Biochem Sci.* 2003 Nov;28(11):605-11. doi: 10.1016/j.tibs.2003.09.006. PMID: 14607091.

41. Bonnefond L, Florentz C, Giegé R, Rudinger-Thirion J. Decreased aminoacylation in pathology-related mutants of mitochondrial tRNATyr is associated with structural perturbations in tRNA architecture. *RNA*. 2008 Apr;14(4):641-8. doi: 10.1261/rna.938108. Epub 2008 Feb 11. PMID: 18268021; PMCID: PMC2271369.

42. Karasik A, Wilhelm CA, Fierke CA, Koutmos M. Disease-associated mutations in mitochondrial precursor tRNAs affect binding, m1R9 methylation, and tRNA processing by mtRNase P. *RNA*. 2021;27(4):420-432. doi:10.1261/rna.077198.120

43. Meng F, Jia Z, Zheng J, et al. A deafness-associated mitochondrial DNA mutation caused pleiotropic effects on DNA replication and tRNA metabolism. *Nucleic Acids Res*. 2022;50(16):9453-9469. doi:10.1093/nar/gkac720

44. Yan H, Zareen N, Levinger L. Naturally occurring mutations in human mitochondrial pre-tRNASer(UCN) can affect the transfer ribonuclease Z cleavage site, processing kinetics, and substrate secondary structure. *J Biol Chem*. 2006;281(7):3926-3935. doi:10.1074/jbc.M509822200

45. Kripps KA, Friederich MW, Chen T, Larson AA, Mirsky DM, Wang Y, Tanji K, Knight KM, Wong LJ, Van Hove JLK. A novel acceptor stem variant in mitochondrial $tRNA^{Tyr}$ impairs mitochondrial translation and is associated with severe phenotype. *Mol Genet Metab.* 2020 Dec;131(4):398-404. doi: 10.1016/j.ymgme.2020.11.006. Epub 2020 Nov 24. PMID: 33279411; PMCID: PMC7749820.

46. Kornblum C, Zsurka G, Wiesner RJ, Schröder R, Kunz WS. Concerted action of two novel tRNA mtDNA point mutations in chronic progressive external ophthalmoplegia. *Biosci Rep*. 2008;28(2):89-96. doi:10.1042/BSR20080004

47. Simoncini C, Montano V, Alì G, Costa R, Siciliano G, Mancuso M. Proximal Myopathy due to m.5835G>A Mutation in Mitochondrial MT-TY Gene. *Case Rep Neurol Med*. 2018, 8406712. Published 2018 Dec 10. doi:10.1155/2018/8406712

48. Sahashi K, Yoneda M, Ohno K, Tanaka M, Ibi T, Sahashi K. Functional characterisation of mitochondrial tRNA(Tyr) mutation (5877-->GA) associated with familial chronic progressive external ophthalmoplegia. *J Med Genet*. 2001;38(10):703-705. doi:10.1136/jmg.38.10.703

49. Scaglia F, Vogel H, Hawkins EP, Vladutiu GD, Liu LL, Wong LJ. Novel homoplasmic mutation in the mitochondrial tRNATyr gene associated with atypical mitochondrial cytopathy presenting with focal segmental glomerulosclerosis. *Am J Med Genet A*. 2003;123A(2):172-178. doi:10.1002/ajmg.a.20315

50. Meng F, Jia Z, Zheng J, Ji Y, Wang J, Xiao Y, Fu Y, Wang M, Ling F, Guan MX. A deafness-associated mitochondrial DNA mutation caused pleiotropic effects on DNA replication and tRNA metabolism. Nucleic Acids Res. 2022 Sep 9;50(16):9453-9469. doi: 10.1093/nar/gkac720. PMID: 36039763; PMCID: PMC9458427.

51. Ling J, Roy H, Qin D, Rubio MA, Alfonzo JD, Fredrick K, Ibba M. Pathogenic mechanism of a human mitochondrial tRNAPhe mutation associated with myoclonic epilepsy with ragged red fibers syndrome. Proc Natl Acad Sci U S A. 2007 Sep 25;104(39):15299-304. doi: 10.1073/pnas.0704441104. Epub 2007 Sep 18. PMID: 17878308; PMCID: PMC2000536.

52. Xu C, Tong L, Rao J, Ye Q, Chen Y, Zhang Y, Xu J, Mao X, Meng F, Shen H, Lu Z, Cang X, Fu H, Wang S, Gu W, Lai EY, Guan MX, Jiang P, Mao J. Heteroplasmic and homoplasmic m.616T>C in mitochondria tRNAPhe promote isolated chronic kidney disease and hyperuricemia. JCI Insight. 2022 Jun 8;7(11):e157418. doi: 10.1172/jci.insight.157418. PMID: 35472031; PMCID: PMC9220945.

53. Viering D, Schlingmann KP, Hureaux M, Nijenhuis T, Mallett A, Chan MMY, van Beek A, van Eerde AM, Coulibaly JM, Vallet M, Decramer S, Pelletier S, Klaus G, Kömhoff M, Beetz R, Patel C, Shenoy M, Steenbergen EJ, Anderson G, Bongers EMHF, Bergmann C, Panneman D, Rodenburg RJ, Kleta R, Houillier P, Konrad M, Vargas-Poussou R, Knoers NVAM, Bockenhauer D, de Baaij JHF; Genomics England Research Consortium. Gitelman-Like Syndrome Caused by Pathogenic Variants in mtDNA. J Am Soc Nephrol. 2022 Feb;33(2):305-325. doi: 10.1681/ASN.2021050596. Epub 2021 Oct 4. PMID: 34607911; PMCID: PMC8819995.

Pathogenic human mitochondrial tRNA variants impair RNA processing by compromising 5′ leader removal

*Jubilee H. Muñozvilla, Avery Ontiveros, and Tatiana V. Mishanina**

Department of Chemistry and Biochemistry University of California, San Diego, 9500 Gilman Dr, La Jolla, CA 92093

ABSTRACT

Human mitochondrial genome (mtDNA) encodes multiple proteins in the oxidative phosphorylation complexes as well as the ribosomal and transfer RNAs (tRNAs) needed for *in situ* translation. These genes are transcribed from only three promoters, producing polycistronic transcripts that are co-transcriptionally cleaved by mitochondrial RNase enzymes to release majority of individual gene products. tRNAs separate many of these genes and are thought to serve as "punctuation" marks that enable RNase recognition, binding, and hydrolysis of the 5′ "leader" and 3′ "trailer" sequences flanking the tRNA. Mutations in the tRNA genes dominate the mtDNA-linked mitochondrial pathologies; yet a systematic study of the impact of tRNA sequence variation on the RNase-catalyzed processing is lacking. Here, we employed human mitochondrial $tRNA^{Tyr}$ as a model system to dissect the effect of tRNA variants on the *in vitro* 5′ leader and 3′ trailer hydrolysis. We found that nucleotide variations located near the catalytic interfaces – particularly

within or near the tRNA acceptor stem – showed the strongest defects in 5′ processing and prevented release of the downstream tRNA in a tRNA cluster where multiple tRNAs are transcribed in tandem. This work provides mechanistic insight into how mutations disrupt coordinated mitochondrial tRNA processing and establish a framework for predicting variant effects based on their structural position relative to the processing enzymes.

INTRODUCTION

Human mitochondria contain their own DNA (mtDNA), which encodes 13 essential protein subunits of the oxidative phosphorylation (OXPHOS) complexes that drive the synthesis of the majority of cellular adenosine triphosphate (ATP). The mtDNA-encoded genes are transcribed by a single mitochondrial RNA polymerase (POLRMT in humans) from three promoters, each producing a ~16,600 nucleotide-long polycistronic transcript containing protein-coding sequences arranged in tandem (Fig. 1A). Processing of this primary transcript requires precise excision of intervening mitochondrial (mt) tRNAs by the endonucleases RNase P and RNase Z. RNase P consists of three protein subunits: TRMT10C (MRPP1), SDR5C1 (MRPP2), and the endonuclease PRORP (MRPP3), which together mediate hydrolysis of the mt precursor tRNA (pre-tRNA) 5′ leader[1-5]. RNase Z consists of the same MRPP1/2 proteins as in RNase P, plus the ELAC2 endonuclease, which cleaves the pre-tRNA 3′ trailer (Fig. 1B)[4,5]. The MRPP1/2 complex is viewed as a “maturation platform”, positioning the pre-tRNA for reactions with the endonucleases[1,5,6]. Because mt-tRNAs are dispersed throughout the polycistronic transcript, they serve as punctuation marks that release the majority of individual mRNAs and rRNAs when processed. This “tRNA punctuation model” ensures the coordinated maturation of tRNAs, mRNAs, and rRNAs for OXPHOS protein expression within the mitochondrial matrix. The generally accepted stages in an mt-tRNA life cycle includes transcription, 5′ cleavage by RNase P, 3′ cleavage by RNase Z, post- transcriptional addition of the 3′-CCA

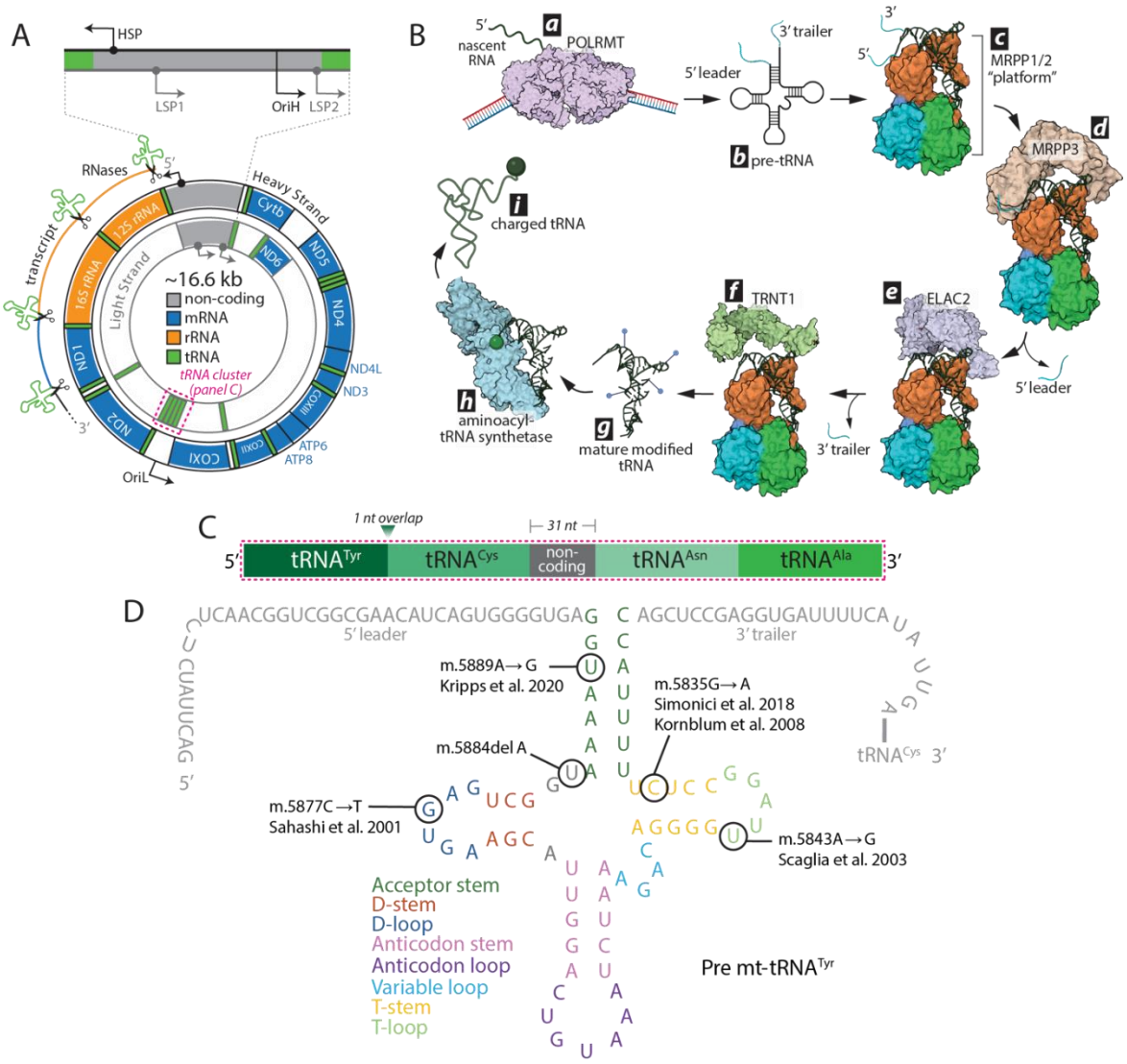

Figure 1 | Mitochondrial tRNA life cycle and the mt-tRNA^{Tyr} variants explored in this study | (A) Map of human mitochondrial genome (mtDNA), with the tRNA^{Tyr} cluster highlighted in magenta. (B) Life cycle of mitochondrial tRNA starting with transcription by human mitochondrial RNA polymerase, POLRMT (*a*), nascent RNA folding into a precursor tRNA containing the 5′ leader and 3′ trailer (*b*), pre-tRNA association with by MRPP1/2 (*c*, PDB ID: 7ONU), 5′ leader processing by MRPP3 (*d*, PDB ID: 7ONU), 3′ trailer processing by ELAC2 (*e*, PDB: 8Z1G), 3′-CCA tail addition by TRNT1 (*f*, PDB ID: 4X4W), tRNA modification by "writer enzymes" (*g*), aminoacylation by the respective tRNA aminoacyl synthetase (*h*, PDB ID: 2PID), and mature mt-tRNA release (*i*). (C) Zoomed view of the light strand tRNA cluster with tRNA^{Tyr} as the pioneer tRNA transcribed. (D) Sequence of mitochondrial pre-tRNA^{Tyr} with the secondary structure elements and sites of the variants investigated in this work.

tail by TRNT1, covalent modifications by "writer" enzymes, and aminoacylation by cognate tRNA synthetases (Fig. 1B)[5,6]. Defects in the above mt-tRNA processing steps have been linked to mitochondrial dysfunction and disease in model systems and patients[7,8]. For example, knockout of MRPP3 in mice reduces both 5′ and 3′ cleavage, impairing mitochondrial ribosome assembly and OXPHOS complex activity[9]. Loss of ELAC2 causes premature death in mice due to defective mt-tRNA processing and reduced OXPHOS function[10]. Collectively, such studies demonstrate that accurate 5′ and 3′ mt-tRNA cleavage is essential for mitochondrial function.

To date, 1,058 mtDNA variants have been reported, with ~40% mapping to tRNA genes and 60% of those classified as pathogenic through a standardized scoring system developed by Clin Gen[11]. In this scoring framework, pathogenicity is determined by assigning weighted points to multiple lines of evidence, such as supported by multiple independent patient reports, evolutionary conservation of the affected nucleotide, heteroplasmy and segregation with disease, biochemical defects in OXPHOS complexes, functional and histochemical evidence of mitochondrial dysfunction, and the rarity or absence of the variant in large mtDNA databases[11]. Pathogenic mt-tRNA variants are associated with reduced OXPHOS complex production, and multiple biochemical studies have shown defects in 5′/3′ processing and aminoacylation due to mt-tRNA mutations[12-14]. No systematic studies have examined the impact of mt-tRNA single-point deletions in mt-DNA.

Although most human mt-tRNAs are separated by rRNA or mRNA genes, several regions of the mtDNA contain "tRNA clusters", where multiple mt-tRNAs are transcribed consecutively (Fig. 1A). The sequential processing of individual tRNAs in tRNA clusters remains poorly understood, and it is unknown if mutations or deletions in the first transcribed mt-tRNA affect downstream mt-tRNA processing. One such cluster is present on the transcript from the light-

strand promoter (LSP) and contains tRNA^{Tyr}-tRNA^{Cys} -tRNA^{Asn} -tRNA^{Ala} (Fig. 1C). Because mt-tRNA^{Tyr} is positioned at the start of this cluster, its processing may act as a "gatekeeper", such that changes in its cleavage efficiency alter downstream maturation events.

Here, we focused on the mt-tRNA^{Tyr} in its native cluster to establish a framework for *in vitro* investigation of disease-linked variants in cluster mt-tRNAs and how they may disrupt sequential processing. We investigated two disease-linked mt-tRNA^{Tyr} variants (m.A5889G[15,11] and m.G5835A[16,17,11]) and a deletion variant (m.5884delA) located at or near the acceptor stem, as well as two "benign" variants (m.C5877T[11,18] and m.A5843G[11,19]) within the D-loop and T-loop (Fig 1D). Benign variants provided a useful contrast, enabling direct comparison of folding and processing defects across variant classes.

Previous studies reported that m.C5877T and m.A5843G, although benign, reduce aminoacylation by tightening the T-loop tRNA^{Tyr} structure, though their effects on 5′/3′ cleavage remain unknown[13]. The m.G5835A variant dramatically reduced steady-state mt-tRNA^{Tyr} levels and aminoacylation (~95%) in patient samples, but effects on processing were not assessed[16]. Thus, it remains unclear whether these pathogenic outcomes originate from early processing defects, misfolding, or downstream steps in tRNA maturation.

In this work, we analyzed the five *in vitro* transcribed pre-mt-tRNA^{Tyr} substrates for any effects of nucleotide sequence variation on the 5′ leader and 3′ trailer cleavage, MRPP1/2 binding, and processing of mt-tRNAs downstream of mt-tRNA^{Tyr} in the cluster. Our findings reveal the majority of examined variants compromise 5′ leader cleavage, which in turn reduces the yield of fully excised mt-tRNA^{Tyr} as well as the downstream mt-tRNA^{Cys} release. Some variants showed poor binding to MRPP1/2, explaining their reduced cleavage. Our work adds to the existing evidence in support of a hierarchical 5′-to-3′ mt-tRNA processing pathway in which MRPP3-

mediated 5′ leader removal must occur before ELAC2 can act on the 3′ trailer, with MRPP1/2 playing an essential role by ensuring that this order is preserved. With these findings, we show that steps in early mt-tRNA processing are governed by 5′ processing and MRPP1/2-mediated pre-tRNA substrate orientation, with variations in the tRNA sequence compromising processing.

MATERIALS AND METHODS

Preparation of RNA substrates

Human mitochondrial DNA was purified from HEK293T cells, and region 5512-7585 (NCBI Reference Sequence: NC_012920.1) was cloned into a pUC19 vector. Variant mtDNA sequences containing either the deletion or mutations on mt-tRNA^{Tyr} within the light strand tRNA "cluster" were commercially synthesized as "E-blocks" by Integrated DNA Technologies and cloned into a pUC19 vector. All DNA sequences encoding the tRNA substrates are listed in Supplementary Table 1. Each plasmid was transformed into *E. coli* HB101 competent cells (Promega) and miniprepped using the ZymoPURE Plasmid Miniprep Kit (Zymo Research). These DNA constructs were used as PCR templates to prepare DNA for *in vitro* transcription. For the PCR, a forward primer was designed to be complementary to the 5′ leader sequence, and a reverse primer complementary to the 3′ trailer sequence. All primers are listed in Supplementary Table 2. The PCR products were gel-purified from a 1% agarose gel and extracted using the Monarch DNA gel extraction kit (New England Biolabs). The purified product was further PCR-amplified with a forward primer complementary to the 5′ leader sequence containing a T7 RNA Polymerase promoter overhang, and a reverse primer complementary to the 3′ trailer sequence. These final PCR-amplified products were cleaned up using the Monarch PCR and DNA clean up kit (New England Biolabs) and used for *in vitro* transcription by T7 RNA Polymerase.

All tRNA substrates used for biochemical analysis were transcribed using the HighScribe T7 Quick High Yield RNA Synthesis kit (New England Biolabs) in a 20 µL transcription reaction containing 0.20 µg of the DNA template, 3.3 mM NTP buffer mix, 2.5 mM DTT, 1 µL of T7 RNA Polymerase mix and incubated at 37 °C for 15 minutes. In the same tube, 70 µL of milliQ Nuclease Free water (ThermoFisher Scientific), 10 µL of Turbo DNase 10x buffer, and 2.5 µL Turbo DNase (ThermoFisher Scientific) were added to the reaction and incubated at 37 °C for an additional 20 minutes to degrade the transcription template DNA. The RNA was purified using the RNA Clean & Concentrator (Zymo Research). The RNA purity was verified on a 7% urea-PAGE gel run for 90 minutes at 100 V, then soaked in 1x Tris-Borate-EDTA buffer (ThermoFisher Scientific) containing 1x SYBR gold nucleic acid gel stain (ThermoFisher Scientific) and visualized on a Gel imaging system (BioRad).

Protein cloning and expression

TRMT10C (MRPP1, UNIPROT: Q7L0Y3), SDR5C1 (MRPP2, UNIPROT: Q99714) and PRORP (MRPP3, UNIPROT: O15091) were synthesized and cloned into pUC57 vectors by Bio Basic with the predicted mitochondrial targeting signals (MTS) of MRPP1 (Δ1-39), MRPP2 (Δ1-11), and MRPP3 (Δ1-45) absent in each construct. Additionally, MRPP1 and MRPP3 contained an N-terminal 6x His-tag followed by a TEV protease cleavage site. MRPP1 and MRPP2 were cloned into a pETDuet-1 vector for co-expression. MRPP3 was also cloned into a pETDuet-1 vector (due to vector availability), with one of the promoters removed from the vector. ELAC2 (UNIPROT: Q9BQ52) was provided by colleagues Dr. Sean Reardon and Shannon Cole from the Mishanina Lab as a plasmid containing the MTS-lacking (Δ1-31) ELAC2 sequence with a SUMO protease cleavable N-terminal 6x His-tag in a pProEXHTB vector. All plasmids were transformed into *E. coli* DH5α cells for colony screening and plasmid propagation. Final expression plasmids

were verified by Sanger sequencing before proceeding with protein expression. All plasmids listed in Supplementary Table 3.

MRPP1/2, MRPP3, and ELAC2 were each transformed into *E. coli* BL21(DE3) CodonPlus-RIPL cells (Promega) and selected for LB agar plates containing 100 µg/ml ampicillin and 34 µg/ml chloramphenicol overnight (12-16 h) at 37 °C. Starter liquid cultures were then prepared by inoculating 4 x 5 mL of LB broth containing 100 µg/ml ampicillin and 34 µg/ml chloramphenicol with one selected colony per 5 mL broth and growing overnight (12-16 h) at 37 °C with shaking. Each 5 mL starting overnight culture was inoculated into 1 L of LB broth containing 100 µg/ml ampicillin and shaken at 200 rpm at 37 °C until the OD_{600} reached 0.6 units (4-6 h). The temperature was then lowered to 16 °C, 0.5 mM (final) IPTG was added to the MRPP1/2 and MRPP3 culture flasks, and 0.15 mM (final) IPTG to the ELAC2 flask to induce expression of each respective protein, and the cultures were shaken overnight (16-20 h) at 16 °C.

Protein purification

HEPES buffer was used for purification of MRPP1/2/3 (pH 7.5) and ELAC2 (pH 8.0) at 4 °C. Cell pellets were harvested and resuspended in the lysis buffer (50 mM HEPES, 500 mM NaC (for MRPP1/2/3) or 300 mM NaCl (for ELAC2) NaCl, 10 mM imidazole, 10% v/v glycerol , 1x Protease Inhibitor Cocktail (PIC: 31.2 µg/ml benzamidine, 0.5 µg/ml chymostatin, 0.5 µg/ml leupeptin, 0.1 µg/ml pepstatin, 1.0 µg/ml aprotinin, and 1.0 µg/ml antipain), 2 mM DTT, 1 mg/ml lysozyme (ThermoFisher Scientific). All protein purification steps were carried out at 4 °C, following the protocol from the Hillen lab as a starting point[2,5,20]. The resuspended cells were lysed by sonication for 20 minutes, 20 seconds off, 20 seconds on, 60% amplitude. Post-lysis, MRPP1/2 lysate was treated with an RNase cocktail (5 U/ml RNase A, 200 U/ml RNase T1, ThermoFisher Scientific), incubating at 4 °C and gently rocking for 2 hours. Each protein overexpression's crude

lysate was centrifuged at 30,187 x *g* for 30 minutes at 4 °C to pellet the cell debris. The supernatant was passed through a 0.45 µM filter before being applied to a 7.5 mL bed volume of Ni-NTA resin (Gold Bio) equilibrated with the respective lysis buffer and rocked at 4 °C (1 h for MRPP1/2, 30 minutes for MRPP3 and ELAC2). The resin was washed with 12 column volumes (CV) of high-salt wash buffer (50 mM HEPES, 1M NaCl, 20 mM imidazole, 10% glycerol, 1x PIC, and 2 mM DTT). Column-bound proteins were eluted with 2 CV of the appropriate elution buffer – for MRPP1/2: 50 mM HEPES, 300 mM NaCl, 400 mM imidazole, 10% glycerol, 1x PIC, and 1.7 mM DTT; for MRPP3: 42.5 mM HEPES, 425 mM NaCl, 317 mM imidazole, 8.5% glycerol, 1x PIC, and 1.7 mM DTT; for ELAC2: 42.5 mM HEPES, 255 mM NaCl, 317 mM imidazole, 8.5% glycerol, 1x PIC, and 1.7 mM DTT. The eluate was dialyzed overnight (16-20 h) against dialysis buffer (50mM HEPES, 200mM NaCl, 10% glycerol, 1x PIC, and 2mM DTT) in the presence of a recombinant His-tagged TEV protease (homemade; approximate molar ratio of 1:25 TEV:MRPP1/2/3) or recombinant ULP1 protease (homemade; approximate molar ratio of 1:500 ULP1:ELAC2). The dialyzed eluate was applied to the 7.5 mL bed volume of Ni-NTA resin equilibrated in each respective dialysis buffer and gently rocked for 20 minutes at 4 °C to allow binding of the cleaved His-tag and His-tagged protease. The untagged protein was eluted and washed with 1 CV of dialysis buffer, then applied to a 5 mL HiTrap heparin column (Cytiva) equilibrated with 3 CV heparin low salt wash buffer (50 mM HEPES, 200 mM NaCl, 10% glycerol, 1x PIC, 2 mM DTT) and washed with 5 CV of the heparin low salt wash buffer. Protein was then eluted with a gradient of 15-50% v/v heparin high salt elution buffer (50 mM HEPES, 1.5 M NaCl, 10% glycerol, 1x PIC, and 2 mM DTT). Fractions containing the protein of interest, identified by SDS-PAGE and Coomassie staining, were pooled and concentrated using Amicon 30K (for MRPP1/2/3) or 50K (for ELAC2) MWCO Centrifugal Filter Devices (ThermoFisher

Scientific) and stored at −80 °C in storage buffer (50 mM HEPES, 150 mM NaCl, 25% glycerol, 1x PIC, and 2 mM DTT).

RNA cleavage assays

All RNase P cleavage assays were carried out in 15 µl reactions containing RNA cleavage assay buffer (25 mM Tris-HCl pH 8.0 at 4 °C, 10 mM $MgCl_2$, 0.1mg ml^{-1} BSA, 70 mM NaCl, 4 mM DTT, 20 µM *S*-adenosine methionine (ThermoFisher Scientific), 1 U/µl Murine RNase inhibitor (ThermoFisher Scientific) and 63 nM pre-$tRNA^{Tyr}$ containing the native 38-nt 5′ leader and 24-nt 3′ trailer (same for the variants). The pre-$tRNA^{Tyr}$ (NCBI Reference Sequence: NC_012920.1, GeneID:4579) was incubated with 650 nM MRPP1/2 at 37 °C for initial protein-RNA binding. After 10 minutes, each endonuclease was added either individually (MRPP3 for 5′ processing or ELAC2 without pre-MRPP1/2 for 3′ processing) or as a combination simultaneously to the reaction at 100 nM each protein final concentration and incubated for 30 minutes at 37°C. For extended substrate assays, such as pre-$tRNA^{Tyr}$-$tRNA^{Cys}$ and pre-$tRNA^{Tyr}$-$tRNA^{Cys}$-$tRNA^{Asn}$, each substrate was pre-incubated with 650 nM MRPP1/2 for 10 minutes at 37 °C, reactions were initiated by the addition of the endonucleases (100 nM each final concentration) and incubated for 20 minutes. To capture additional tRNA released following initial processing, MRPP1/2 was subsequently added to a final concentration of 1.3 µM and reactions were incubated for an additional 10 minutes. MRPP3 and ELAC2 were then supplemented to a final concentration of 200 nM each and reactions were further incubated for 30 minutes. All reactions were quenched by the addition of 15 µL of 2x formamide-urea stop buffer (90 mM Tris-borate buffer, 8 M urea, 47.5 mM EDTA, 50% formamide, and 0.02% of each xylene cyanol and bromophenol blue) and stored at 4°C for up to a week without apparent RNA degradation. The full 30 µL reaction was carefully loaded onto 8 M urea 7% polyacrylamide (bis-acrylamide to acrylamide ratio 1:19) denaturing

gels in 1x Tris-borate-EDTA buffer and run at 100 V for 120 minutes, 130 min (for the pre-tRNA^{Tyr}-tRNA^{Cys}-tRNA^{Asn} substrate), or 115 minutes (for the 5′ leaderless pre-tRNA^{Tyr}). After electrophoresis, gels were stained with 1x SYBR Gold nucleic acid stain, visualized on a gel imaging system (BioRad), and quantified with ImageLab 6.1 software (BioRad). Each experiment was performed in 3-5 replicates, and the obtained data was analyzed using Prism version 10.6.1 (GraphPad) software.

Native polyacrylamide gel electrophoresis (PAGE)

Each pre-tRNA^{Tyr} (2.4 pmol) was unfolded at 95°C for 3 minutes and placed on ice for 5 minutes before adding RNA folding buffer (25 mM HEPES pH 8.0, 7 0mM NaCl and either water or $MgCl_2$ at the indicated final concentrations). After a 30 minute refold at room temperature, samples were mixed 1:1 with 2x native loading dye (1% bromophenol blue, 1% xylene cyanol, 100% glycerol) and run at 4°C on an 8.5% native polyacrylamide gel in 0.5x Tris-borate-EDTA buffer at 80 V, 400 mA for 140 minutes. Gels were then stained with 1x SYBR Green II (ThermoFisher Scientific) and visualized as previously described.

Electrophoretic Mobility Shift Assays (EMSAs)

Each pre-tRNA^{Tyr} (55 nM final) was incubated with MRPP1/2 in varying concentrations in binding buffe r(50 mM Tris-HCl pH 8.0, 100 mM potassium acetate, 2.5 mM magnesium acetate, 1mM DTT, 1x murine RNase inhibitor) for 30 minutes at 37 °C. Glycerol was added to 5% v/v final concentration and each sample was loaded at 4 °C onto an 8.5% native polyacrylamide gel in 0.5x Tris-borate-EDTA buffer and run at 95 V, 400 mA for 106 minutes. Gels were then stained with 1x SYBR Green II (ThermoFisher Scientific) and then visualized and quantified as described. Each experiment was performed in triplicate, and the obtained data was analyzed using

Prism version 10.6.1 (GraphPad) software. Binding curves were fit and the K_d estimated using the specific binding with Hill slope equation:

$$y = (B_{max} * X^h) (K_d^h + X^h)^{-1}$$

where B_{max} is the maximum specific binding, K_d is the mt-tRNA concentration needed to achieve a half-maximum binding at equilibrium, and h is the hill slope which >1.0 and generated a sigmoidal curve if there are multiple binding sites with positive cooperativity.

UV melting experiments

Each pre-$tRNA^{Tyr}$ (500 nM, wt or G5835A) was refolded in RNA refolding buffer using the method mentioned above and then RNA melting buffer (150 mM NaCl, 1 mM $MgCl_2$, and 20 mM sodium cacodylate pH 7) was added. The pre-tRNAs melting was monitored on a Cary 100 UV Spectrophotometer (Agilent). Absorbance was measured at 260 nm as the temperature increased from 25 °C to 92 °C at a rate of 1 °C min^{-1} and T_m values were calculated from first-derivative plots (dA/dT vs T).

Competition assay

Wild-type (wt) pre-$tRNA^{Tyr}$ (40 nM final) was pre-mixed with increasing concentrations of pre-$tRNA^{Tyr}$- $tRNA^{Cys}$ in separate tubes prior to the addition of processing proteins, and reactions were carried out in a total volume of 15 µL as described above. All reactions were quenched by the addition of 15 µL of 2x formamide-urea stop buffer. After electrophoresis, gels were stained with 1x SYBR Gold nucleic acid stain and visualized and quantified as described above. Each experiment was performed in triplicate, and the obtained data was analyzed using Prism version 10.6.1 (GraphPad) software.

RESULTS

Pathogenically linked variants of the human mitochondrial tRNA^{Tyr} impair 5′ leader processing with minimal effect on 3′ trailer processing.

To reconstitute human mitochondrial pre-tRNA processing *in vitro*, we recombinantly expressed and purified MRPP3 and ELAC2 individually and MRPP1/2 as a complex and *in vitro* transcribed the pre-tRNA^{Tyr} substrates (Fig. S1), each containing the native 38-nucleotide (nt) 5′ leader and the native 24-nt 3′ trailer. We analyzed the 5′-end processing by first forming an MRPP1/2-pre-tRNA complex and then adding the 5′ endonuclease MRPP3. MRPP3 is has been documented to require the presence of MRPP1/2 binding to carry out RNA cleavage[2,3,20,21]. Initial analysis of 5′ cleavage products revealed a significant reduction in cleavage activity in the A5889G, 5884delA, and G5835A pre-tRNA^{Tyr} variants, some reduced cleavage in A5843G, and wild-type (wt) pre-tRNA^{Tyr}-like cleavage efficiency in the C5877T variant (Fig. 2A).

To monitor the 3′ trailer hydrolysis, ELAC2 was added alone to the 5′ leader containing pre-tRNA substrates, as previous structural work by the Hillen lab showed that the 5′ leader of the MRPP1/2-bound pre-tRNA creates a steric clash with ELAC2, thereby preventing 3′ processing in the presence of the 5′ leader[5]. Analysis of 3′ cleavage patterns by ELAC2 in this context revealed generally similar processing efficiencies between wt pre-tRNA^{Tyr} and the variant substrates (Fig. 2B), although A5889G and 5884delA exhibited reproducible trends toward miscleavage, defined here as cleavage within sites of the pre-tRNA other than the cognate 3′ cleavage site (Figs. 2B and S2A).

To verify ELAC2 activity in the context of a fully assembled RNase Z complex, we carried out the 3′ hydrolysis reactions using 5′ leaderless pre-tRNA^{Tyr} substrates pre-bound to the MRPP1/2 platform. We observed similar 3′ cleavage trends across pre-tRNA^{Tyr} variants (Fig. S2B

and S2C). Interestingly, the 5′ leaderless substrate cleaved with ELAC2 alone, i.e., in the absence of MRPP1/2, also resulted in reproducible miscleaved products (Fig. S2B and S2D).

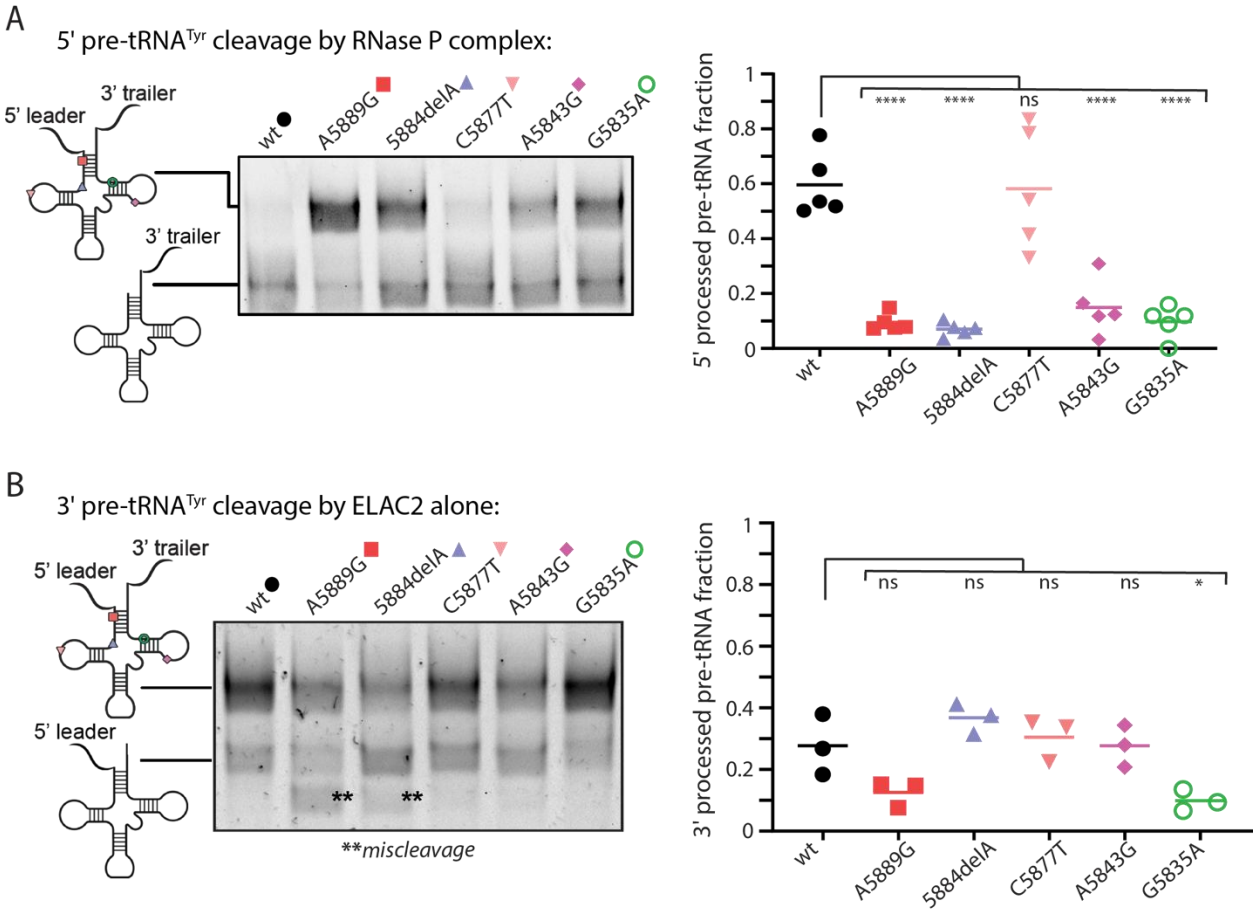

Figure 2 | Sequence variants of mt-tRNA^{Tyr} impair 5′ leader processing by RNase P but not 3′ trailer processing by ELAC2 alone | (A) *In vitro* cleavage gel showing RNase P-catalyzed 5′ leader processing differences for the wild-type (wt) vs variant tRNA^{Tyr} precursors. The 5′ processed tRNA product fraction was quantified and plotted. (B) *In vitro* cleavage gel showing differences in 3′ trailer removal by ELAC2 alone on the wt vs variant tRNA^{Tyr}. The 3′ processed tRNA fraction was quantified and plotted. A one-way ANOVA was used for statistical analysis (****adjusted *p*-value <0.0001, *adjusted *p*-value 0.0203).

Full tRNA excision out of a polycistronic transcript is governed by the efficiency of 5′ leader processing

With the processing enzymes showing varying cleavage efficiencies and patterns across the pre-tRNA^{Tyr} variants, we next sought to assay cleavage when both endonucleases (MRPP3 and ELAC2) were present to replicate a physiological scenario. We assayed the one-pot 5′ and 3′

cleavage of both the wt pre-tRNA^{Tyr} and disease-associated variants by first combing the pre-tRNA substrate containing both the 5′ leader and 3′ trailer with MRPP1/2 and then adding MRPP3 and ELAC2 simultaneously. The resulting cleavage pattern closely resembled the 5′-only cleavage profile generated by RNase P (Fig. 3A, compare to Fig. 2A), with cleavage reduced in A5889G,

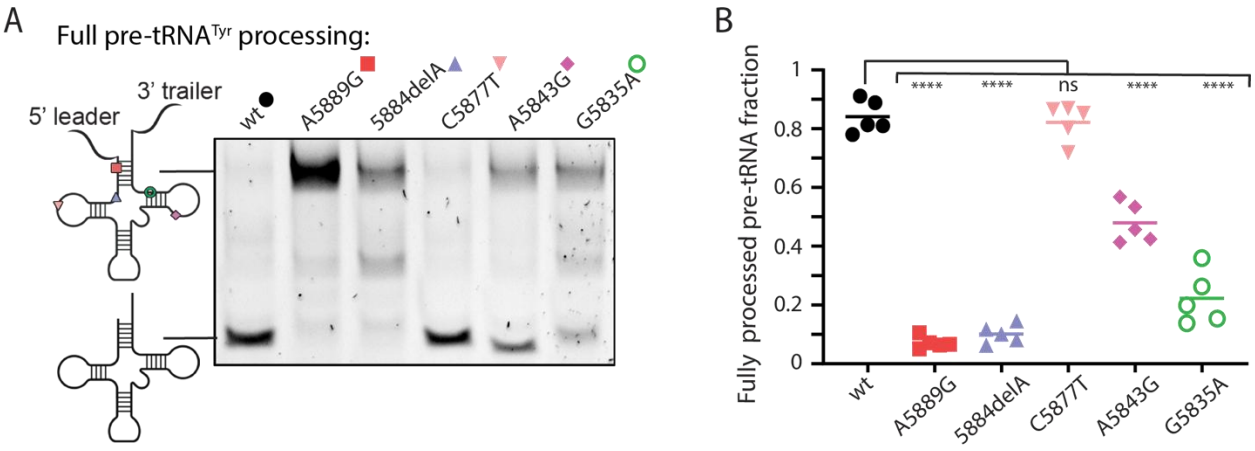

Figure 3 | Sequence variants of mt-tRNA^{Tyr} compromise complete 5′ and 3′ cleavage by RNase P and RNase Z | (A) *In vitro* cleavage gel showing processing differences of the 5′ leader and 3′ trailer for the wt vs variant tRNA^{Tyr} precursors by RNase P and RNase Z. (B) The fraction of tRNA product without the 5′ leader and 3′ trailer was quantified and plotted. A one-way ANOVA was used for statistical analysis (****adjusted *p*-value <0.0001).

5884delA, A5843G, and G5835A and unchanged in the C5877T variant. When we tested different protein combinations with the wt pre-tRNA substrate containing both the 5′ leader and 3′ trailer, we observed that ELAC2 alone hydrolyzed some of the pre-tRNA (Fig. S3, lanes 3 and 6; consistent with Fig. 2B wt lane), whereas no cleavage of the 3′ trailer by ELAC2 occurred when the tRNA precursor was pre-bound by MRPP1/2 (Fig. S3, lane 7), in line with the inhibitory effect of MRPP1/2 on the ELAC2 enzymatic activity in the presence of the 5′ leader. In contrast, the presence of the complete RNase P complex capable of efficiently removing the 5′ leader (Fig. S3, lane 2) enabled ELAC2 to hydrolyze the 3′ trailer and yield a fully processed mt-tRNA^{Tyr} (Fig. S3, lanes 4 and 8; Fig. 2A wt lane). Together, these data support the ordered 5′ leader first-then 3′ trailer processing of a precursor mt-tRNA.

Disease-associated sequence variations lower pre-tRNA^{Tyr} affinity for MRPP1/2

To gain insight into what step(s) in pre-tRNA processing the RNA sequence alterations impose their effect, we used electrophoretic mobility shift assay (EMSA) to qualitatively assess MRPP1/2-RNA binding. For consistency with the RNase-catalyzed cleavage experiments above, we used pre-tRNA^{Tyr} substrates containing the 5′ leader and 3′ trailer. Protein-bound RNA was quantified with increasing MRPP1/2 concentration, plotted and fitted to approximate K_d values using a Hill-slope model (Fig. 4, see Methods). The measured wt pre-tRNA^{Tyr} K_d (~300 nM) was consistent

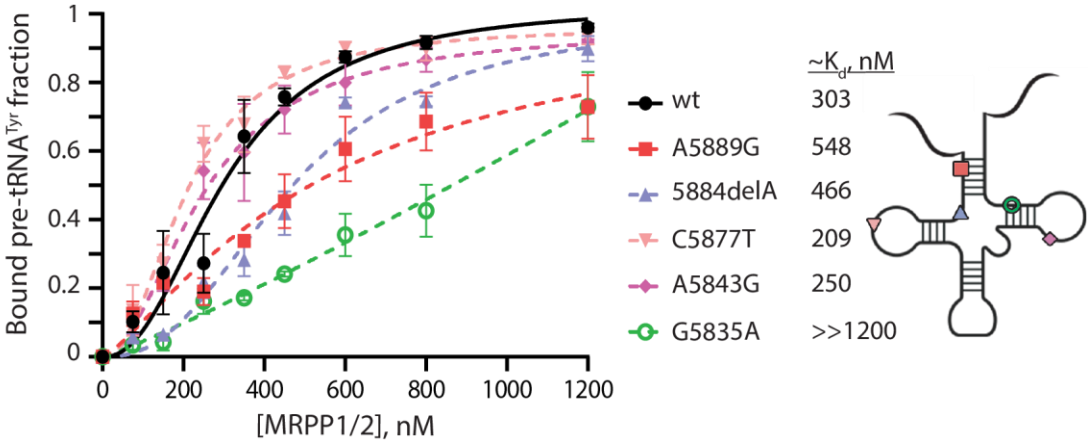

Figure 4 | Mutations and a deletion in mt-tRNA^{Tyr} alter binding affinity for MRPP1/2 | Quantitative analysis of pre-tRNAs bound by MRPP1/2. Each symbol represents the mean from three replicates with error bars showing the standard deviation. Protein-RNA dissociation constants (K_d) was calculated in GraphPad Prism using a Hill-slope model (see Methods). Representative uncropped gel images are in Figure S7.

with previously reported values determined by fluorescent anisotropy[5]. The C5877T and A5843G pre-tRNA^{Tyr} variants exhibited binding affinities akin to the wt pre-tRNA^{Tyr}. The A5889G and 5884delA variants showed moderately increased K_d values indicative of weaker binding, whereas the G5835A mutant displayed a substantially higher K_d that exceeded the MRPP1/2 concentration range tested, suggesting significantly impaired binding.

To assess whether variant pre-tRNAs assumed alternative conformations that may explain compromised association with MRPP1/2, we analyzed wt pre-tRNA^{Tyr} and variant pre-tRNAs by native PAGE. The wt pre-tRNA^{Tyr} displayed two predominant conformers, as evident from the two gel bands, and several variants showed a similar migration pattern (Fig. S4A). To further investigate the basis for the starkly weaker binding of the G5835A pre-tRNA^{Tyr} mutant to MRPP1/2, we performed thermal denaturation experiments comparing the stability of wt pre-tRNA^{Tyr} and G5835A pre-tRNA^{Tyr}. At lower temperatures (~35-45 ºC), a slight shift in the first transition, associated with tertiary structural elements unfolding unfolding[21], was observed. The second transition, corresponding to secondary structure melting, showed minimal differences between wt pre-tRNA^{Tyr} and the G5835A mutant in first-derivative plots (Fig. S4B), ~60 ºC and 62 ºC respectively, consistent with previous UV melting data showing reduced peak amplitude of the derivative maxima in mutant pre-tRNAs[21]. This pattern persisted at higher temperatures (~70-90 ºC). We next examined whether Mg^{2+} concentration in solution influenced pre-tRNA conformational states, given that Mg^{2+} plays a critical role in stabilizing tertiary architecture in cytosolic tRNAs via a site-specific coordination[22]. Native gel analysis of the wt pre-tRNA^{Tyr} and the G5835A mutant performed at 0-10 mM Mg^{2+} showed similar migration patterns, with two dominant conformers observed once again across all divalent metal ion conditions (Fig. S4C).

An open question in the field is when in the pre-tRNA life cycle MRPP1/2 releases the tRNA with current models proposing that MRPP1/2 remains bound to the tRNA for 5′ leader and 3′ trailer hydrolysis, as well as 3′ CCA tail addition[5,6]. Because the A5843G pre-tRNA^{Tyr} variant bound MRPP1/2 with a similar relative affinity to the wt pre-tRNA^{Tyr} (Fig. 4), yet showed decreased cleavage (Figs. 2 and 3), we tested whether the A5843G mutant tRNA precursor could act as an MRPP1/2 “sponge” to sequester this protein complex and consequently impair wt pre-

tRNA^{Tyr} processing. To model increasing mtDNA mutant loads (heteroplasmy) under physiologically relevant conditions, we performed 5′ cleavage assays using a substrate mixture of a constant amount of the wt pre-tRNA^{Tyr} and increasing concentration of the A5843G mutant. Processing of the 5′ leader remained unaffected by the presence of the A5834G pre-tRNA^{Tyr}, even when the mutant concentration exceeded that of the wt pre-tRNA^{Tyr} (Fig. S4D and S4E).

Release of mature mt-tRNA^{Cys} from the tRNA cluster is dependent on its 5′-proximal mt-tRNA^{Tyr} processing

Because tRNA^{Tyr} and tRNA^{Cys} are transcribed in tandem on the light strand of mtDNA and overlap by one nucleotide (Fig. 1C), we wondered whether the tRNA^{Cys} processing depends on the successful processing of the preceding tRNA^{Tyr}. To address this, we *in vitro* transcribed extended pre-tRNA substrates consisting of the tRNA^{Tyr} sequence with its native 38-nt 5′ leader, the full tRNA^{Cys} and its native 48-nt 3′ trailer, and performed the same 5′ and 3′ cleavage assays as with the stand-alone pre-tRNA^{Tyr} (Fig. 3). The tRNA^{Tyr} variants that showed reduced cleavage on isolated pre-tRNA^{Tyr} substrates also displayed substantially decreased release of mature tRNA^{Tyr} and tRNA^{Cys} in the extended constructs (Fig. 5).

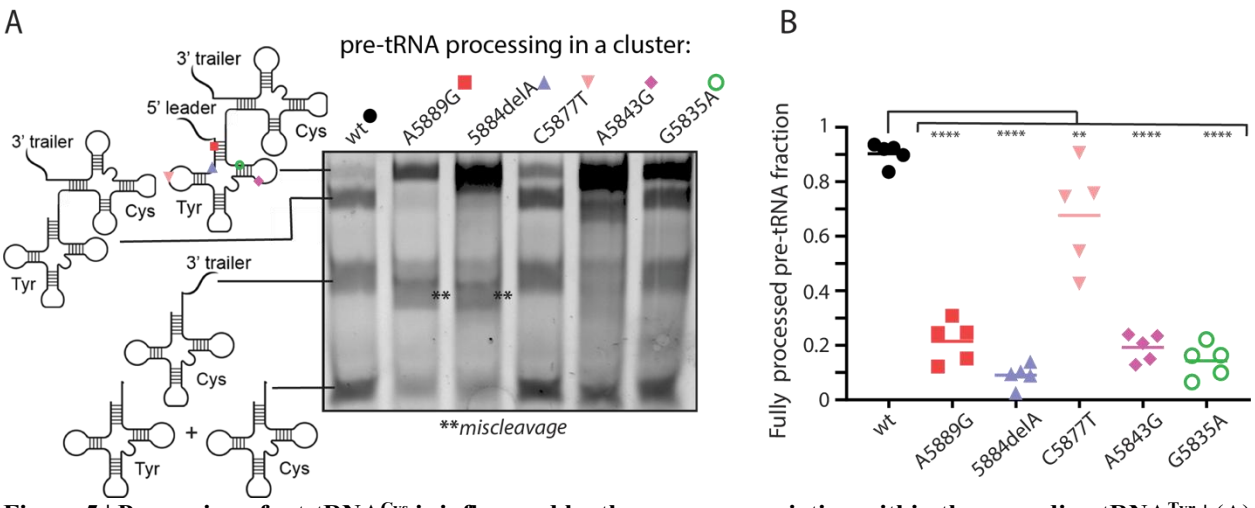

Figure 5 | Processing of mt-tRNA^{Cys} is influenced by the sequence variation within the preceding tRNA^{Tyr} | (A) *In vitro* cleavage gel showing differences in processing of the 5′ leader and 3′ trailer on the wt vs tRNA^{Tyr} precursors containing the tRNA^{Tyr}-tRNA^{Cys} extended sequence. ** denotes miscleaved products within the tRNA^{Tyr}. (B) The fraction of tRNA product without the 5′ leader and 3′ trailer was quantified and plotted. A one-way ANOVA was used for statistical analysis (****adjusted *p*-value <0.0001, ** adjusted *p*-value 0.0031).

We next examined the processing of the tRNA^{Tyr}-tRNA^{Cys} -tRNA^{Asn} cluster, as these tRNAs belong to the same light-strand transcript. A 31-nt noncoding region separates tRNA^{Cys} and tRNA^{Asn} (Fig. 1C) the tRNA^{Asn} processing, thus may not rely on the tRNA^{Cys} release, which itself in turn depends on its 5′-adjacent tRNA^{Tyr} processing. Previous work from the Guan lab using mitochondrial cybrids demonstrated that a tRNA^{Cys} mutation decreased mature tRNA^{Cys} as well as tRNA^{Tyr}, while tRNA^{Asn} levels remained unchanged[23]. Consistent with these observations, tRNA^{Asn} was efficiently excised from the extended tRNA^{Tyr}-tRNA^{Cys}-tRNA^{Asn} transcript in our assays (Fig. S5).

DISCUSSION

Human mitochondrial pre-tRNA sequence variants and their effect on the early stages of the tRNA life cycle

Recent advances in visualizing high-resolution 3D structures of the mitochondrial RNase P and RNase Z complexes engaged with a tRNA precursor have beautifully illuminated how these enzymes recognize and cleave pre-tRNA substrates[5,6]. The impact of nucleotide variation within

the pre-tRNAs on these processing steps, however, remains poorly understood. 60% of mutations, deletions and insertions in mt-tRNAs are associated with mitochondrial dysfunction, yet a systematic understanding of how these sequence changes influence the 5′ and 3′ processing of the tRNA is lacking. Earlier studies demonstrated that some individual variants perturb either 5′ or 3′ cleavage[21,23,24], but little is known about dual-end processing, the effects of deletions, or how processing of one tRNA influences excision of adjacent tRNAs within the same transcript. Here, we expand upon these prior findings by defining how specific variations within human mt-tRNA^{Tyr} alter enzyme recognition, cleavage efficiency, and downstream maturation within the multi-tRNA transcriptional unit.

Some human mt-tRNAs are transcribed as a cluster without separation by rRNA or mRNA. In the light-strand cluster containing tRNA^{Tyr}-tRNA^{Cys}-tRNA^{Asn}-tRNA^{Ala}, tRNA^{Tyr} processing may regulate downstream maturation of the sequential mt-tRNA release (Fig. 1C). Several disease-associated sequence variants of mt-tRNA^{Tyr} have been linked to disorders including myopathy, neurological deterioration, and chronic progressive external ophthalmoplegia[15-19] (Fig. 1D). However, the mechanistic connection between early tRNA transcript processing and these disease phenotypes has remained unclear. Our analysis provides evidence that the impact of these variants depends on their location within the mt-tRNA and proximity to enzyme interaction surfaces, offering a framework for understanding how early processing alterations may contribute to mitochondrial disease. Here we show how the specific nucleotide substitutions – along with a single-nucleotide deletion – within the mt-tRNA^{Tyr} negatively influence its 5′ leader processing by RNase P, with minimal effects on the 3′ trailer processing by RNase Z. The A5889G and 5884del, both located in or proximal to the tRNA acceptor stem, produced the largest reduction in 5′ cleavage, likely due to their proximity to the MRPP3 catalytic site (Figs. 2 and 6). A previous

study found that the A4269G mutation in the acceptor stem of human mt-tRNA^{Ile} decreased 5′ processing by disrupting the base-pairing at the base of the acceptor stem[22]. Similarly, the A5889G

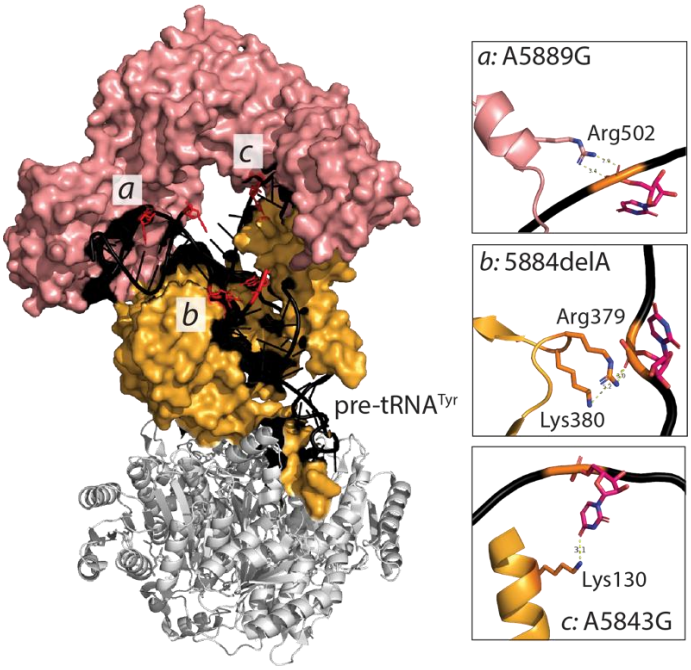

Figure 6 | Interactions of the tRNA^{Tyr} substrate with RNase P | 3D structure and interactions (black patches) of mitochondrial pre-tRNA^{Tyr} within the mitochondrial RNase P complex (MRPP1 gold; MRPP2 gray; MRPP3 endonuclease salmon pink. PDB ID: 7ONU). Protein-RNA interactions for the representative variants with impaired 5′ leader cleavage are shown in the insets. Majority of protein interactions are with the phosphate-sugar backbone, except for m.A5843 (uracil in the RNA) where MRPP1 lysine and the carbonyl of the uracil ring form base-specific hydrogen bonding interactions (inset *c*).

substitution may disrupt base-pairing in the pre-tRNA^{Tyr}, influencing how MRPP3 engages with the substrate. RNAfold simulations show that the A5889G centroid structure – the average structure from all potential structures – disrupts acceptor-stem base pairs and widens the overall tRNA architecture, in contrast to the cloverleaf structure of the wt pre-tRNA^{Tyr} (Figs. S6A and S6B). Consistent with the secondary structure predictions, the A5889G variant displays nearly a two-fold increase in its K_d for MRPP1/2 relative to the wt pre-tRNA^{Tyr} (Fig. 4), indicating weaker association with the MRPP1/2 processing platform. The Koutmos lab observed similar

compromised MRPP1/2 binding for their pre-tRNA^{Ile} and pre-tRNA^{Leu} containing mutations in the acceptor stem[21].

The 5884delA deletion shortens the distance between the acceptor stem and the D-stem, potentially creating a more constricted substrate that hinders access of MRPP3 to the 5′ leader (Fig. S6C). MRPP1/2 binding to this variant is also impaired, though to a lesser extent than in A5889G (Fig. 4). This may be because the anticodon region, which MRPP1/2 engages with most extensively, remains largely intact in 5884delA, whereas A5889G disrupts interactions more globally (Figs. 6 and S6C).

With the C5877T mutation located in the D-loop, the cleavage efficiency of its 5′ leader and binding to MRPP1/2 closely matched wt pre-tRNA^{Tyr} (Figs. 2, 4, S7A and S7D). Consistent with these observations, the predicted secondary structure shows only minimal changes due to this substitution (Fig. S6A and S6D). A previous study using chemical and enzymatic probing, however, showed that this nucleotide substitution contributes to the structural destabilization of the tRNA D-arm and a 40-fold reduction in aminoacylation[13]. This residue may participate in transient tertiary interactions, potentially corresponding to the weaker, less stable conformer detected in our native gels and does not have direct interactions with the MRPP1/2 or endonuclease surface residues (Figs. S4A, S6, and S7D).

The A5843G mutation in the T-loop was also characterized by Bonnefond et al. for aminoacylation and showed only a modest (2-fold) reduction in the tRNA^{Tyr} charging with an amino acid[13]. The predicted secondary structure closely resembles that of the wt pre-tRNA^{Tyr}, which is consistent with its near-wild-type pre-tRNA^{Tyr} binding to MRPP1/2 (Figs. 4 and S7E). Nevertheless, the 5′ cleavage efficiency of this mutant by MRPP3 was lower than for the wt pre-tRNA^{Tyr}, possibly due to altered interactions between the mutated T-loop region and non-catalytic

surfaces of MRPP1/2 or MRPP3. The T-loop is positioned closer to these enzyme interfaces than the D-loop, having interactions with both MRPP1/2 and each endonuclease, which could explain the drop in 5′ processing (Fig. 6). Our competition assays showed that the A5843G pre-tRNA^{Tyr} substrate does not inhibit 5′ cleavage of the wt pre-tRNA^{Tyr} even at elevated concentrations of the mutant competitor (Figs. S4D and S4E), suggesting that this variant would likely impact physiology only at high mutant mt-DNA levels, consistent with the >70% heteroplasmy reported in patients[20]. Notably, this variant is not classified as pathogenic according to criteria such as conservation, heteroplasmy, segregation, biochemical defects, and cybrid evidence[11].

The final mutation, G5835A, located in the T-stem, affected both the 3′ trailer processing and 5′ leader cleavage – unlike all other variants, which primarily compromised 5′ leader processing (Fig. 2). This variant showed severe defects in binding to MRPP1/2 (Figs. 4 and S7F), consistent with the near absence of cleavage. Patient cell lines harboring this mutation lacked mature and aminoacylated mt-tRNA^{Tyr}, in line with our biochemical *in vitro* findings where this variant fails to be processed out of the polycistronic transcript[16]. RNAfold predicts a large unpaired region following the D-loop, which may destabilize or break hydrogen-bonding interactions (Fig. S6F). Thermal denaturation analyses showed that although the first melting transition of the G5835A variant (~60 °C) was similar to the wt pre-tRNA^{Tyr}, the maximum of the first-derivative curve was markedly lower, suggesting an altered structural ensemble with reduced stabilizing interactions (Fig. S4B). At higher temperatures, resolution of transitions became more difficult, likely due to the presence of two structural conformers, visible on native gels that unfold differently (Fig. S4C). The ~2 °C difference in melting temperature for the first curve resembles observations from a T-stem mt-tRNA^{Cys} variant and parallels behavior seen in mt-tRNA^{Ile} and mt-tRNA^{Ser} mutants, where melting temperatures remain similar but the derivative maxima shift[21,23].

Interestingly, the nucleotides do not appear to have apparent interactions with MRPP1/2, MRPP3, or ELAC2 (Fig. 6). Definitive determination of the structural differences imposed by the G5835A $tRNA^{Tyr}$ mutation will require future RNA structure-probing experiments.

The role of MRPP1/2 in the sequential 5′-to-3′ mitochondrial pre-tRNA processing pathway

Our data suggest a model where full maturation of mt-tRNAs depends primarily on successful 5′ processing. This idea is consistent with observations from a study that knocked out MRPP3 in mice, which resulted in reduced 5′ and 3′ mt-tRNA cleavage and led to defects in the mitochondrial ribosome assembly and OXPHOS activity[9]. Structural studies from the Hillen lab also indicate that the 5′ leader creates a steric clash within the ELAC2 active site when MRPP1/2 is bound to the pre-tRNA, implying that RNase P-mediated 5′ cleavage is required *before* ELAC2 can properly engage with the substrate[5]. This does not mean that ELAC2 cannot function independently as we also observed 3′ cleavage when ELAC2 acted alone, without the MRPP1/2 maturation platform (Fig. 2B). This aligns with findings from the Churchman lab showing that some mt-RNAs possess 3′ adenylated tails even when 5′ leaders remain unprocessed[14]. Nonetheless, we observed MRPP1/2 inhibition of ELAC2 catalysis when the 5′ leader was present (Fig. S3B). Together, these studies indicate that ELAC2 has independent catalytic activity, but MRPP1/2 dictates the correct order of cleavage events.

We additionally observed miscleavage by ELAC2 in wt pre-$tRNA^{Tyr}$ when MRPP1/2 was absent (Fig. S2A, S2B, and S2D). ELAC2 is known to have broad substrate tolerance, but its accuracy on mt-RNA substrates is less understood – particularly because many mt-tRNAs cannot form the canonical tertiary "elbow" architectures due to lacking key nucleotides in the D-loop and T-loop[14]. Prior studies suggested that mitochondrial RNase P components help orient non-canonical substrates for cleavage, and our data support this idea as miscleavage was detected when

ELAC2 acted alone but disappeared when MRPP1/2 was included or when the 5′ leader was removed (Fig. 2B, Fig. S2A, Fig. S3B)[2,3,5,6,25]. Moreover, the miscleavage detected on the wt pre-tRNA^{Tyr} was not observed in full 5′ leader and 3′ trailer removal assays, further reinforcing the sequential model of mt-tRNA maturation (Fig. S2C).

Processing of downstream mt-tRNA^{Cys} affected by mt-tRNA^{Tyr} variants

Our extended-substrate processing assays reveal that mt-tRNA^{Cys} processing depends strongly on the successful excision of the upstream mt-tRNA^{Tyr} (Fig. 5). This is perhaps expected as tRNA^{Tyr} and tRNA^{Cys} overlap by one nucleotide, meaning release of tRNA^{Cys} requires accurate and timely tRNA^{Tyr} 3′ cleavage. Such a model is supported by a prior study which showed using mitochondrial cybrids that the m.C5783T mutation on the T-stem of tRNA^{Cys} reduced mature levels of both tRNA^{Cys} and tRNA^{Tyr}, likely as a direct consequence of impaired tRNA^{Cys} 3′ processing[23].

To extend the tRNA cluster further, we examined tRNA^{Tyr}-tRNA^{Cys}-tRNA^{Asn} processing. Variants that impaired cleavage of the tRNA^{Tyr}-tRNA^{Cys} portion did not significantly impact release of tRNA^{Asn}. This is consistent with the presence of a 31-nt non-coding region between tRNA^{Cys} and tRNA^{Asn}, allowing RNase P to cleave the 5′ end of tRNA^{Asn} independently of tRNA^{Cys} release. Prior studies showed that tRNA^{Asn} can be processed by RNase P or ELAC2 alone and that tRNA^{Ala} – which follows tRNA^{Asn} – can be cleaved by MRPP3 independently of MRPP1/2[5,26]. Notably, tRNA^{Asn} and tRNA^{Ala} are among the few mt-tRNAs predicted to adopt canonical cytosolic-like tertiary structures, as they retain the nucleotide features required for the classical D-T loop tertiary fold[5]. Meng and Jia similarly observed normal tRNA^{Asn} abundance in m.C5783T tRNA^{Cys} mutation-containing cybrids[23]. Together, the published results and our current work suggest that downstream RNA processing defects are likely only when a tRNA relies directly on

the release of its upstream neighbor. If no such dependency exists (such as having a non-coding spacer), processing proceeds normally as long as the relevant enzymes can recognize the pre-tRNA substrate.

CONCLUSIONS

We found that mutations and a single-nucleotide deletion within the precursor tRNA can impair mitochondrial tRNA processing, often by altering local structure in ways that reduce MRPP3, ELAC2, or MRPP1/2 accessibility and binding. These defects likely arise from local changes in base-pairing or overall pre-tRNA conformation, each of which can disrupt recognition by the RNA processing machinery. Our work also supports a key role for MRPP1/2 in maintaining RNA processing order in human mitochondria. Variants in the pre-tRNA^{Tyr} acceptor stem produced some of the strongest defects, with further investigation needed to fully distinguish contributions from binding vs catalytic positioning. Moreover, the question of whether multiple-nucleotide deletions disrupt processing to the same extent as single-nucleotide deletions remains to be explored. Finally, our data shows that mutations in and upstream mt-tRNA can affect processing of downstream tRNAs in a tRNA cluster, but only when the downstream mt-tRNA relies directly on accurate 3′ processing of the upstream tRNA, e.g. due to sequence overlap. This principle may explain why some disease-associate variants disrupt only a subset of tRNAs within a polycistronic transcript, helping to connect molecular processing defects with patient phenotypes.

ASSOCIATED CONTENT

Supporting Information

Purification gels for Preparation of the recombinant human RNase P and RNase Z and tRNA Substrates; 3′ miscleavage by ELAC2 on full-length and leaderless pre-tRNA^{Tyr} gel image and plotted graphs; Wild-type pre-tRNATyr cleavage in the presence different protein combinations gel images; Variant effects on tRNA conformation and competitive inhibition of 5′ leader Removal with native PAGE gel images, UV-Vis RNA melting-curve, and plotted processed 5` wt pre-tRNA^{Tyr}; Release of tRNA^{Asn} from the tRNA^{Tyr}-tRNA^{Cys}-tRNA^{Asn} cluster gel image and band quantitation plotted; RNAfold centroid structure models of the wild-type and variant tRNA^{Tyr}; Representative EMSA gels for wt and variant pre-tRNA^{Tyr}; Full gel images for biological replicates for individual 5`and 3` processed tRNA^{Tyr}; Full gel images for biological replicates for dual 5`and 3` processed tRNA^{Tyr}; Full gel images for biological replicates for dual 5`and 3` processed tRNA^{Tyr}-tRNA^{Cys}; (PDF)

Table of tRNA DNA templates; Table of primers; Table of plasmids (XLSX)

Accession codes

TRMT10C (MRPP1, UNIPROT: Q7L0Y3)

SDR5C1 (MRPP2, UNIPROT: Q99714)

PRORP (MRPP3, UNIPROT: O15091

ELAC2 (UNIPROT: Q9BQ52)

AUTHOR INFORMATION

Corresponding Author

*Address correspondence to: tmishanina@ucsd.edu

Author Contributions

The manuscript was written through contributions of all authors. All authors have given approval to the final version of the manuscript. J.H.M., conceptualization; J.H.M., methodology; J.H.M. and A.O., investigation; J.H.M., formal analysis; J.H.M., visualization; J.H.M., writing-initial draft; J.H.M., and T.V.M, writing-review and editing; T.V.M, supervision; T.V.M., funding acquisition.

Funding Sources

This work was supported by the National Institutes of Health [NIGMS ESI grant R35GM142785], UCSD institutional funds to T.V.M., National Institutes of Health Molecular Biophysics Training Grant (T32 GM008326) and American Epilepsy Society BRIDGE award (#30330424) to J.H.M.

Notes

The authors declare no competing financial interests.

Acknowledgements

Chapter 2, in part, has been submitted for publication of the material as it may appear in Journal of Biological Chemistry, 2026, Munozvilla, Jubilee; Ontiveros, Avery; Mishanina, Tatiana, ASBMB Journals, 2026. The dissertation author was the primary researcher and author of this paper.

We would like to thank Dr. Susan Ackerman for her valuable insights in project development and direction. We would also like to thank Dr. Phil Ordoukhanian (Scripps Research Institute) for his training and guidance on the use of the Cary 100 Spectrophotometer. We would like to thank Dr. Elizabeth Komives for her encouragement. We would like to thank and acknowledge Linh Tran and Aaron Bagaoisan for their support and early-stage assistance for this

project. We are grateful to Jonathan Eger for assistance with figure preparation. We greatly appreciate Yuntong Ou and Shannon Cole for the assistance with various components such as gel staining and providing protocols that aided us in this work. We are also greatly appreciative of Dr. Mukesh Mahajan, Dr. An Hsieh, Dr. Sean Reardon, and Dr. Ravish Sharma for their protocol refinement suggestion and intellectual advice and feedback. Thank you to the rest of the Mishanina research group for their feedback and encouragement.

ABBREVIATIONS

OXPHOS, oxidative phosphorylation; mtDNA, mitochondrial DNA; ATP, adenosine triphosphate; POLRMT, human mitochondrial RNA polymerase; mRNA, messenger RNA; rRNA, ribosomal RNA; tRNA, transfer RNA, MT, mitochondrial; MRPP1, Mitochondrial RNase P protein 1 (TRMT10C, tRNA methyltransferase 10C); MRPP2, Mitochondrial RNase P protein 2 (SDR5C1, Succinate dehydrogenase complex assembly factor 1); MRPP3, Mitochondrial RNase P protein 3 (PRORP, Protein-only RNase P); ELAC2, ElaC ribonuclease Z 2; RNase P, MRPP1/2/3; RNase Z, MRPP1/2 & ELAC2; MTS, mitochondrial targeting signal; PIC, protease inhibitor cocktail;

REFERENCES

1. Holzmann J, Frank P, Löffler E, Bennett KL, Gerner C, Rossmanith W. RNase P without RNA: identification and functional reconstitution of the human mitochondrial tRNA processing enzyme. Cell. 2008 Oct 31;135(3):462-74. doi: 10.1016/j.cell.2008.09.013. PMID: 18984158.

2. Reinhard L, Sridhara S, Hällberg BM. Structure of the nuclease subunit of human mitochondrial RNase P. *Nucleic Acids Res.* 2015 Jun 23;43(11):5664-72. doi: 10.1093/nar/gkv481. Epub 2015 May 7. PMID: 25953853; PMCID: PMC4477676.

3. Vilardo E, Nachbagauer C, Buzet A, Taschner A, Holzmann J, Rossmanith W. A subcomplex of human mitochondrial RNase P is a bifunctional methyltransferase--extensive moonlighting in mitochondrial tRNA biogenesis. Nucleic Acids Res. 2012 Dec;40(22):11583-93. doi: 10.1093/nar/gks910. Epub 2012 Oct 5. *Nucleic Acids Res.* 2018

Nov 16;46(20):11126-11127. doi: 10.1093/nar/gky931. PMID: 23042678; PMCID: PMC3526285.

4. Meynier V, Hardwick SW, Catala M, Roske JJ, Oerum S, Chirgadze DY, Barraud P, Yue WW, Luisi BF, Tisné C. Structural basis for human mitochondrial tRNA maturation. *Nat Commun.* 2024 Jun 1;15(1):4683. doi: 10.1038/s41467-024-49132-0. PMID: 38824131; PMCID: PMC11144196.

5. Bhatta, A., Kuhle, B., Yu, R.D. *et al.* Molecular basis of human nuclear and mitochondrial tRNA 3′ processing. *Nat Struct Mol Biol* **32**, 613–624 (2025). https://doi.org/10.1038/s41594-024-01445-w

6. Valentín Gesé G, Hällberg BM. Structural basis of 3'-tRNA maturation by the human mitochondrial RNase Z complex. *EMBO J.* 2024 Dec;43(24):6573-6590. doi: 10.1038/s44318-024-00297-w. Epub 2024 Nov 8. PMID: 39516281; PMCID: PMC11649783.

7. Van Haute L, Pearce SF, Powell CA, D'Souza AR, Nicholls TJ, Minczuk M. Mitochondrial transcript maturation and its disorders. *J Inherit Metab Dis.* 2015 Jul;38(4):655-80. doi: 10.1007/s10545-015-9859-z. Epub 2015 May 28. PMID: 26016801; PMCID: PMC4493943.

8. Sen A, Karasik A, Shanmuganathan A, Mirkovic E, Koutmos M, Cox RT. Loss of the mitochondrial protein-only ribonuclease P complex causes aberrant tRNA processing and lethality in Drosophila. *Nucleic Acids Res.* 2016 Jul 27;44(13):6409-22. doi: 10.1093/nar/gkw338. Epub 2016 Apr 30. PMID: 27131785; PMCID: PMC5291253.

9. Rackham O, Busch JD, Matic S, Siira SJ, Kuznetsova I, Atanassov I, Ermer JA, Shearwood AM, Richman TR, Stewart JB, Mourier A, Milenkovic D, Larsson NG, Filipovska A. Hierarchical RNA Processing Is Required for Mitochondrial Ribosome Assembly. *Cell Rep.* 2016 Aug 16;16(7):1874-90. doi: 10.1016/j.celrep.2016.07.031. Epub 2016 Aug 4. PMID: 27498866.

10. Siira SJ, Rossetti G, Richman TR, Perks K, Ermer JA, Kuznetsova I, Hughes L, Shearwood AJ, Viola HM, Hool LC, Rackham O, Filipovska A. Concerted regulation of mitochondrial and nuclear non-coding RNAs by a dual-targeted RNase Z. *EMBO Rep.* 2018 Oct;19(10):e46198. doi: 10.15252/embr.201846198. Epub 2018 Aug 20. PMID: 30126926; PMCID: PMC6172459.

11. MITOMAP: A Human Mitochondrial Genome Database. http://www.mitomap.org, 2023

12. Wittenhagen LM, Kelley SO. Impact of disease-related mitochondrial mutations on tRNA structure and function. *Trends Biochem Sci.* 2003 Nov;28(11):605-11. doi: 10.1016/j.tibs.2003.09.006. PMID: 14607091.

13. Bonnefond L, Florentz C, Giegé R, Rudinger-Thirion J. Decreased aminoacylation in pathology-related mutants of mitochondrial tRNATyr is associated with structural

perturbations in tRNA architecture. *RNA*. 2008 Apr;14(4):641-8. doi: 10.1261/rna.938108. Epub 2008 Feb 11. PMID: 18268021; PMCID: PMC2271369.

14. McShane E, Couvillion M, Ietswaart R, Prakash G, Smalec BM, Soto I, Baxter-Koenigs AR, Choquet K, Churchman LS. A kinetic dichotomy between mitochondrial and nuclear gene expression processes. *Mol Cell.* 2024 Apr 18;84(8):1541-1555.e11. doi: 10.1016/j.molcel.2024.02.028. Epub 2024 Mar 18. PMID: 38503286; PMCID: PMC11236289.

15. Kripps KA, Friederich MW, Chen T, Larson AA, Mirsky DM, Wang Y, Tanji K, Knight KM, Wong LJ, Van Hove JLK. A novel acceptor stem variant in mitochondrial $tRNA^{Tyr}$ impairs mitochondrial translation and is associated with severe phenotype. *Mol Genet Metab.* 2020 Dec;131(4):398-404. doi: 10.1016/j.ymgme.2020.11.006. Epub 2020 Nov 24. PMID: 33279411; PMCID: PMC7749820.

16. Kornblum C, Zsurka G, Wiesner RJ, Schröder R, Kunz WS. Concerted action of two novel tRNA mtDNA point mutations in chronic progressive external ophthalmoplegia. *Biosci Rep*. 2008;28(2):89-96. doi:10.1042/BSR20080004

17. Simoncini C, Montano V, Alì G, Costa R, Siciliano G, Mancuso M. Proximal Myopathy due to m.5835G>A Mutation in Mitochondrial MT-TY Gene. *Case Rep Neurol Med*. 2018, 8406712. Published 2018 Dec 10. doi:10.1155/2018/8406712

18. Sahashi K, Yoneda M, Ohno K, Tanaka M, Ibi T, Sahashi K. Functional characterisation of mitochondrial tRNA(Tyr) mutation (5877-->GA) associated with familial chronic progressive external ophthalmoplegia. *J Med Genet*. 2001;38(10):703-705. doi:10.1136/jmg.38.10.703

19. Scaglia F, Vogel H, Hawkins EP, Vladutiu GD, Liu LL, Wong LJ. Novel homoplasmic mutation in the mitochondrial tRNATyr gene associated with atypical mitochondrial cytopathy presenting with focal segmental glomerulosclerosis. *Am J Med Genet A*. 2003;123A(2):172-178. doi:10.1002/ajmg.a.20315

20. Bhatta A, Dienemann C, Cramer P, Hillen HS. Structural basis of RNA processing by human mitochondrial RNase P. *Nat Struct Mol Biol*. 2021;28(9):713-723. doi:10.1038/s41594-021-00637-y

21. Karasik A, Wilhelm CA, Fierke CA, Koutmos M. Disease-associated mutations in mitochondrial precursor tRNAs affect binding, m1R9 methylation, and tRNA processing by mtRNase P. *RNA*. 2021;27(4):420-432. doi:10.1261/rna.077198.120

22. Lai LB, Lai SM, Szymanski ES, Kapur M, Choi EK, Al-Hashimi HM, Ackerman SL, Gopalan V. Structural basis for impaired 5' processing of a mutant tRNA associated with defects in neuronal homeostasis. *Proc Natl Acad Sci USA.* 2022 Mar 8;119(10):e2119529119. doi: 10.1073/pnas.2119529119. Epub 2022 Mar 1. PMID: 35238631; PMCID: PMC8915964.

23. Meng F, Jia Z, Zheng J, et al. A deafness-associated mitochondrial DNA mutation caused pleiotropic effects on DNA replication and tRNA metabolism. *Nucleic Acids Res*. 2022;50(16):9453-9469. doi:10.1093/nar/gkac720

24. Yan H, Zareen N, Levinger L. Naturally occurring mutations in human mitochondrial pre-tRNASer(UCN) can affect the transfer ribonuclease Z cleavage site, processing kinetics, and substrate secondary structure. *J Biol Chem*. 2006;281(7):3926-3935. doi:10.1074/jbc.M509822200

25. Reinhard L, Sridhara S, Hällberg BM. The MRPP1/MRPP2 complex is a tRNA-maturation platform in human mitochondria. *Nucleic Acids Res.* 2017 Dec 1;45(21):12469-12480. doi: 10.1093/nar/gkx902. PMID: 29040705; PMCID: PMC5716156.

26. Vilardo E, Toth U, Hazisllari E, Hartmann RK, Rossmanith W. Cleavage kinetics of human mitochondrial RNase P and contribution of its non-nuclease subunits. *Nucleic Acids Res*. 2023;51(19):10536-10550. doi:10.1093/nar/gkad713

Chapter 3 Expression and Purification of Recombinant Human Mitochondrial RNA Polymerase (POLRMT)

bio-protocol

Open Access

Published: Dec 05, 2023

Expression and Purification of Recombinant Human Mitochondrial RNA Polymerase (POLRMT) and the Initiation Factors TFAM and TFB2M

An H. Hsieh[1, §], Sean D. Reardon[1], Jubilee H. Munozvilla-Cabellon[1], Jiayu Shen[2], Smita S. Patel[2] and Tatiana V. Mishanina[1,*]

[1]Department of Chemistry and Biochemistry, University of California San Diego, La Jolla, CA, USA
[2]Department of Biochemistry and Molecular Biology, Rutgers University, Robert Wood Johnson Medical School, Piscataway, NJ, USA
*For correspondence: tmishanina@ucsd.edu
[§]Technical contact

Abstract

Human mitochondrial DNA (mtDNA) encodes several components of oxidative phosphorylation responsible for the bulk of cellular energy production. The mtDNA is transcribed by a dedicated human mitochondrial RNA polymerase (POLRMT) that is structurally distinct from its nuclear counterparts, instead closely resembling the single-subunit viral RNA polymerases (e.g., T7 RNA polymerase). The initiation of transcription by POLRMT is aided by two initiation factors: transcription factor A, mitochondrial (TFAM), and transcription factor B2, mitochondrial (TFB2M). Although many details of human mitochondrial transcription initiation have been elucidated with in vitro biochemical and structural studies, much remains to be addressed relating to the mechanism and regulation of transcription. Studies of such mechanisms require reliable, high-yield, and high-purity methods for protein production, and this protocol provides the level of detail and troubleshooting tips that are necessary for a novice to generate meaningful amounts of proteins for experimental work. The current protocol describes how to purify recombinant POLRMT, TFAM, and TFB2M from *Escherichia coli* using techniques such as affinity column chromatography (Ni^{2+} and heparin), how to remove the solubility tags with TEV protease and recover untagged proteins of interest, and how to overcome commonly encountered challenges in obtaining high yield of each protein.

Key features

- This protocol builds upon purification methods developed by Patel lab (Ramachandran et al., 2017) and others with greater detail than previously published works.
- The protocol requires several days to complete as various steps are designed to be performed overnight.
- The recombinantly purified proteins have been successfully used for in vitro transcription experiments, allowing for finer control of experimental components in a minimalistic system.

Keywords: POLRMT, TFAM, TFB2M, Protein purification, Bacterial protein expression, Ni-NTA, Maltose binding protein (MBP) fusion protein purification, TEV protease, Heparin

This protocol is used in: J. Biol. Chem. (2023), DOI: 10.1016/j.jbc.2022.101815

Cite as: Hsieh, A. H. et al. (2023). Expression and Purification of Recombinant Human Mitochondrial RNA Polymerase (POLRMT) and the Initiation Factors TFAM and TFB2M. Bio-protocol 13(23): e4892. DOI: 10.21769/BioProtoc.4892

Background

The mitochondrial RNA polymerase (POLRMT) is a DNA-dependent RNA polymerase (RNAP) that transcribes the human mitochondrial DNA (mtDNA), which encodes several protein components of the complexes that carry out oxidative phosphorylation. POLRMT is structurally similar to other single-subunit RNAPs such as T7 phage RNAP (Schwinghammer et al., 2013; Sultana et al., 2017), and current models suggest that POLRMT transcribes short RNA primers used in mtDNA replication initiation (Tan et al., 2022). Considering the central role of POLRMT in cellular metabolism and maintenance of mtDNA, it is not surprising that mutations associated with mitochondrial dysfunction map to POLRMT, such as respiratory chain defects, hypotonia, and global developmental delays (Oláhová et al., 2021).

To start transcription de novo from a promoter sequence, POLRMT requires two initiation factors: transcription factor A (TFAM) and transcription factor B2 (TFB2M), which aid the melting of the promoter sequence and the formation of a stable initiation complex (Hillen et al., 2017; Ramachandran et al., 2017). TFAM is also the mtDNA packaging protein that compacts the mtDNA into structures called nucleoids. While too much TFAM can prevent proteins involved in transcription and other processes from accessing the mtDNA, TFAM is required to bend the upstream promoter region to recruit POLRMT to the promoter site; the underlying mechanisms of this process are yet to be worked out. Published work suggests that post-translational modifications (PTMs) to TFAM, such as acetylation or phosphorylation, do not compromise its function as a transcription factor but make it easier for POLRMT to remove TFAM from DNA, thus increasing transcription processivity through TFAM-compacted DNA (Reardon and Mishanina, 2022).

This protocol describes in detail how to isolate recombinant POLRMT, TFAM, and TFB2M from *Escherichia coli* in high purity and how to overcome the challenges in achieving high protein yield. These protocols build upon the procedures developed in the Patel lab and others (Yakubovskaya et al., 2014; Ramachandran et al., 2017) and describe the steps in greater detail than in any previously published work to provide access to these resources to a wider community. The resulting proteins can be used to reconstitute human mitochondrial transcription on promoter sequences in vitro, as in prior biochemical and structural studies (Bird et al., 2018; Tan et al., 2022). These proteins can be post-translationally modified to probe the impact of PTMs on their function to fine-tune mitochondrial transcription output (Reardon and Mishanina, 2022). Finally, the protocols can also be applied to express and purify mutant proteins to study the underlying basis of mutations associated with mitochondrial dysfunction.

Materials and reagents

1. 4× Laemmli sample buffer (Bio-Rad, catalog number: 1610747)
2. 10× Tris/Glycine/SDS (Bio-Rad, catalog number: 1610732)
3. Dithiothreitol (DTT) (Fisher BioReagents, catalog number: BP172-5), see Recipes for preparation
4. Ethanol (EtOH) (Fisher Scientific, catalog number: 2818500)
5. Glycerol (Fisher Scientific, catalog number: BP229-1)
6. HiTrap heparin column (GE Healthcare, catalog number: 17-0407-03)
7. Hydrochloric acid (HCl) (Fisher Scientific, catalog number: LC149502)
8. Imidazole (molecular biology grade, > 99%) (Fisher Scientific, catalog number: O3196-500)
9. Isopropyl-β-D-1-thiogalactopyranoside (IPTG) (Fisher Scientific, catalog number: BP1755100), see Recipes for preparation
10. LB agar, Miller (Fisher Scientific, catalog number: BP1425-2)
11. LB broth (LB), Miller, granulated (Fisher Scientific, catalog number: BP9723-2)
12. Lysozyme (Fisher Scientific, catalog number: BP535-5)
13. Precision Plus Protein™ All Blue Prestained Protein Standards (Bio-Rad, catalog number: 1610373)
14. Protease inhibitor cocktail (PIC) powder (used in this protocol as 1,000× stock and prepared following instructions online: https://www.sigmaaldrich.com/US/en/product/sigma/p2714) (Sigma-Aldrich, catalog number: P2714-1BTL)
15. Sodium hydroxide (NaOH) pellets (Fisher Scientific, catalog number: S318-500)

16. β-mercaptoethanol (BME) (Fisher Scientific, catalog number: AC125472500)

Part I: POLRMT purification materials and reagents
1. Amicon Ultra-15 centrifugal filter units (50K MWCO, 15 mL) (Millipore Sigma, catalog number: UFC905024)
2. Ammonium sulfate (AS) (Fisher Scientific, catalog number: A702-3)
3. Ampicillin (Fisher Scientific, catalog number: BP1760-25), see Recipes for preparation
4. Cytiva Capto™ DEAE chromatography media (Fisher Scientific, catalog number: 45-002-960) or, if using an FPLC, HiTrap DEAE Fast Flow (Cytiva, catalog number: 17-5154-01)
5. HisTrap FPLC column (Cytiva, catalog number: 17-3712-06)
6. Polyethyleneimine (PEI), MN 60,000 50% (Fisher Scientific, catalog number: AC178571000), see Recipes for preparation
7. Poly-Prep® chromatography columns (Bio-Rad, catalog number: 7311550)
8. Sodium chloride (NaCl) (Fisher Scientific, catalog number: BP358-212, CAS number: 7647-14-5)
9. Tris base (Fisher BioReagents, catalog number BP152-1)
10. Tween 20 (Fisher BioReagents, catalog number: BP337-100)

Part II: TFAM purification materials and reagents
1. 1 kb DNA ladder (NEB, catalog number: N3232S)
2. 4-(2-hydroxyethyl)-1-piperazineethanesulfonic acid (HEPES) (Fisher Scientific, catalog number: BP310-1)
3. Amicon Ultra-15 centrifugal filter units (3K MWCO, 15 mL) (Millipore Sigma, catalog number: UFC900324)
4. Ethidium bromide solution, 10 mg/mL (Bio-Rad, catalog number: 1610433)
5. HisPur Ni-NTA resin (Thermo Scientific, catalog number: 88222)
6. Kanamycin (Fisher Scientific, catalog number: 611290050), see Recipes for preparation
7. Potassium chloride (KCl) (molecular biology grade) (Fisher Scientific, catalog number: P217-3)
8. Sodium chloride (Fisher Scientific, catalog number: BP358-212, CAS number: 7647-14-5)

Part III: TFB2M purification materials and reagents
1. 4-(2-hydroxyethyl)-1-piperazineethanesulfonic acid (HEPES) (Fisher Scientific, catalog number: BP310-1)
2. Amicon Ultra-4 centrifugal filter units (10K MWCO, 4 mL) (Millipore Sigma, catalog number: UFC801008)
3. HisPur Ni-NTA resin (Thermo Scientific, catalog number: 88222)
4. Kanamycin (Fisher Scientific, catalog number: 611290050), see Recipes for preparation
5. Potassium chloride (KCl) (Fisher Scientific, catalog number: P217-3)
6. Potassium hydroxide (KOH) (Fisher Scientific, catalog number: P250 500)

Biological materials

Plasmids available upon request
1. *Escherichia coli* (*E. coli*) BL21-CodonPlus (DE3)-RIPL competent cells (Agilent, catalog number: 230280) or *E. coli* BL21-CodonPlus (DE3)-RIL competent cells (Agilent, catalog number: 230245)
2. Optional: *E. coli* ArcticExpress (DE3) competent cells (Agilent, catalog number: 230192)
3. Tobacco Etch Virus (TEV) protease (Kapust et al., 2001; Raran-Kurussi et al., 2017)
4. POLRMT construct in pPROEXHTb. It contains residues 43–1230 [lacking its N-terminal mitochondrial targeting sequence (MTS)] with an N-terminal hexahistidine 6x-His-tag
5. TFAM construct in pPROEXHTb. It contains residues 43–246 (lacking its N-terminal MTS) with an N-terminal 6x-His-tag and a TEV protease site
6. TFB2M construct in pT7TEV-HMBP4. It contains residues 20–398 with an N-terminal 6x-His-tag, maltose binding protein (MBP) tag, and a TEV protease site

Solutions

See Recipes for all solutions.

Part I: POLRMT purification
1. 5% Polyethylenimine (PEI) solution pH 7.0
2. POLRMT Lysis Buffer
3. POLRMT HisTrap Buffer A
4. POLRMT HisTrap Buffer B
5. POLRMT Heparin No Salt Buffer
6. POLRMT Heparin Buffer A
7. POLRMT Heparin Buffer B

Part II: TFAM purification and activity test
1. TFAM Lysis Buffer
2. TFAM Ni-NTA Buffer A
3. TFAM Ni-NTA Buffer B
4. TFAM TEV Cleavage Buffer
5. TFAM Heparin Buffer A
6. TFAM Heparin Buffer B
7. TFAM Storage Buffer (2×)
8. 10× TFAM Binding Buffer
9. TFAM Electrophoretic Mobility Shift Assay (EMSA) Buffer

Part III: TFB2M Purification
1. TFB2M Lysis Buffer
2. TFB2M Ni-NTA Buffer A
3. TFB2M Ni-NTA Buffer B
4. TFB2M TEV Cleavage Buffer
5. TFB2M No Salt Heparin Buffer
6. TFB2M Heparin Buffer A
7. TFB2M Heparin Buffer B

Recipes

Common stock solutions
Note: Sterilize all stocks by filtering through a 0.22 μm syringe filter, aliquot into 1 mL portions, and store at -20 °C.

1. 1 M IPTG Stock
   2.38 g of IPTG
   Dissolve in Milli-Q water and bring the final volume up to 10 mL.
   *Add 200 μL of 1 M IPTG per 1 L of cell culture for a final concentration of 0.2 mM IPTG.

2. Amp stock (100 mg/mL)
   1 g of ampicillin
   Dissolve in Milli-Q water and bring the final volume up to 10 mL.

3. Kan stock (25 mg/mL)
   0.25 g of kanamycin
   Dissolve in Milli-Q water and bring the final volume up to 10 mL.

4. 1 M DTT Stock

1.54 g of DTT
Dissolve in Milli-Q water and bring the final volume up to 10 mL.

Part I: POLRMT Purification

Note: All buffers (except for 5% PEI) are adjusted to pH 7.9 with HCl or NaOH, sterilized with a 0.22 μm filter, and stored at 4 °C. Add BME to the Lysis and HisTrap purification buffers and DTT to the HiTrap heparin purification buffers right before use. Prepare cold, filtered Milli-Q H_2O and 20% EtOH to wash and store the FPLC columns after use.

1. **5% PEI solution**

Reagent (stock concentration)	Final concentration	Quantity
PEI (50%)	5%	10 mL
Milli-Q H_2O	n/a	90 mL
Total		**100 mL**

Adjust pH to 7.0 with HCl when the solution is cold or on ice. No need to filter.

2. **POLRMT Lysis Buffer**

Reagent (stock concentration)	Final concentration	Quantity
Tris-HCl (1 M, pH 7.9)	40 mM	10 mL
NaCl (3 M)	400 mM	33.3 mL
Glycerol (100%)	15% v/v	37.5 mL
Tween 20 (100%)	0.1% v/v	0.25 mL
EDTA (500 mM)	1 mM	0.5 mL
BME* (14.3 M)	5 mM	See Note
Lysozyme*	1 mg/mL	See Note
PIC (1,000×)*	1×	See Note
Milli-Q H_2O	n/a	168 mL
Total		**250 mL**

**Add right before use. Pour 50 mL of the buffer into a conical tube and then add these components (5 mg of lysozyme, 17.5 μL of BME, and 50 μL of PIC) to the tube instead of the entire bottle of buffer. PIC was prepared following instructions online and is used as 1,000× stock: https://www.sigmaaldrich.com/US/en/product/sigma/p2714.*

3. **POLRMT HisTrap Buffer A**

Reagent (stock concentration)	Final concentration	Quantity
Tris-HCl (1 M, pH 7.9)	40 mM	40 mL
NaCl (3 M)	300 mM	100 mL
Glycerol (100%)	15% v/v	150 mL
Tween 20 (100%)	0.1% v/v	1 mL
Imidazole	20 mM	1.36 g
BME* (14.3 M)	5 mM	350 μL
Milli-Q H_2O	n/a	707 mL
Total		**1,000 mL**

*Add BME right before use.

4. **POLRMT HisTrap Buffer B**

Reagent (stock concentration)	Final concentration	Quantity
Tris-HCl (1 M, pH 7.9)	40 mM	20 mL
NaCl (3 M)	300 mM	50 mL
Glycerol (100%)	15% v/v	75 mL
Tween 20 (100%)	0.1% v/v	0.5 mL

Imidazole	500 mM	17.02 g
BME* (14.3 M)	5 mM	175 µL
Milli-Q H_2O	n/a	353 mL
Total		**500 mL**

*Add BME right before use.

5. **POLRMT Heparin No Salt Buffer**

Reagent (stock concentration)	Final concentration	Quantity
Tris-HCl (1 M, pH 7.9)	40 mM	4 mL
NaCl (3 M)	0 mM	n/a
Glycerol (100%)	15% v/v	15 mL
Tween 20 (100%)	0.1% v/v	0.1 mL
EDTA (500 mM)	1 mM	0.2 mL
DTT* (1 M)	1 mM	100 µL
Milli-Q H_2O	n/a	81.6 mL
Total		**100 mL**

This buffer is used to adjust the salt concentration of the elution from the HisTrap column. *Add DTT right before use.

6. **POLRMT Heparin Buffer A**

Reagent (Stock concentration)	Final concentration	Quantity
Tris-HCl (1 M, pH 7.9)	40 mM	40 mL
NaCl (3 M)	150 mM	50 mL
Glycerol (100%)	15% v/v	150 mL
Tween 20 (100%)	0.1% v/v	1 mL
EDTA (500 mM)	1 mM	2 mL
DTT* (1 M)	1 mM	1,000 µL
Milli-Q H_2O	n/a	756 mL
Total		**1,000 mL**

*Add DTT right before use.

7. **POLRMT Heparin Buffer B**

Reagent (Stock concentration)	Final concentration	Quantity
Tris-HCl (1 M, pH 7.9)	40 mM	20 mL
NaCl (3 M)	1,000 mM	167 mL
Glycerol (100%)	15% v/v	75 mL
Tween 20 (100%)	0.1% v/v	0.5 mL
EDTA (500 mM)	1 mM	1 mL
DTT* (1 M)	1 mM	500 µL
Milli-Q H_2O	n/a	236 mL
Total		**500 mL**

*Add DTT right before use.

Part II: TFAM purification

Note: All buffers are adjusted to pH 7.5 with HCl or NaOH, sterilized with a 0.22 µm filter, and stored at 4 °C. Prepare cold, filtered Milli-Q H_2O and 20% EtOH to wash and store the FPLC columns after use.

1. **TFAM Lysis Buffer**

Reagent (stock concentration)	Final concentration	Quantity
Tris-HCl (1 M, pH 7.5)	20 mM	4 mL
NaCl (3 M)	200 mM	13.33 mL
Glycerol (100%)	15% v/v	30 mL

Imidazole	10 mM	0.136 g
BME* (14.3 M)	5 mM	See Note
Lysozyme*	1 mg/mL	See Note
Protease inhibitor cocktail* (1,000×)	1×	See Note
Milli-Q H_2O	n/a	152.47 mL
Total		**200 mL**

*Add right before use. We only need 50 mL of the buffer in a conical tube; then, add these components (5 mg of lysozyme, 17.5 µL of BME, and 50 µL of PIC) to the tube instead of the entire bottle of buffer.

2. **TFAM Ni-NTA Buffer A***

Reagent (stock concentration)	Final concentration	Quantity
Tris-HCl (1 M, pH 7.5)	20 mM	20 mL
NaCl (3 M)	200 mM	66.65 mL
Glycerol (100%)	15% v/v	150 mL
Imidazole	10 mM	0.681 g
BME* (14.3 M)	5 mM	350 µL
Milli-Q H_2O	n/a	762.35 mL
Total		**1,000 mL**

*This buffer is the same as the TFAM Lysis Buffer without lysozyme and PIC. Add BME right before use.

3. **TFAM Ni-NTA Buffer B**

Reagent (stock concentration)	Final concentration	Quantity
Tris-HCl (1 M, pH 7.5)	20 mM	20 mL
NaCl (3 M)	200 mM	66.65 mL
Glycerol (100%)	15% v/v	150 mL
Imidazole	500 mM	34.04 g
BME* (14.3 M)	5 mM	350 µL
Milli-Q H_2O	n/a	762.35 mL
Total		**1,000 mL**

*Add BME right before use.

4. **TFAM TEV Cleavage Buffer**

Reagent (stock concentration)	Final concentration	Quantity
Tris-HCl (1 M, pH 7.5)	20 mM	40 mL
NaCl (3 M)	300 mM	200 mL
Glycerol (100%)	15% v/v	300 mL
BME* (14.3 M)	5 mM	700 µL
Milli-Q H_2O	n/a	1,459 mL
Total		**2,000 mL**

*Add BME right before use.

5. **TFAM Heparin Buffer A**

Reagent (stock concentration)	Final concentration	Quantity
Tris-HCl (1 M, pH 7.5)	20 mM	20 mL
NaCl (3 M)	200 mM	66.67 mL
Glycerol (100%)	15% v/v	150 mL
DTT* (1 M)	1 mM	1,000 µL
Milli-Q H_2O	n/a	762.33 mL
Total		**1,000 mL**

*Add DTT right before use.

6. **TFAM Heparin Buffer B**

Reagent (stock concentration)	Final concentration	Quantity
Tris-HCl (1 M, pH 7.5)	30 mM	30 mL
NaCl (3 M)	1500 mM	500 mL
Glycerol (100%)	15% v/v	150 mL
DTT* (1 M)	1 mM	1,000 µL
Milli-Q H_2O	n/a	319 mL
Total		**1,000 mL**

*Add DTT right before use.

7. **TFAM Storage Buffer (2×)**

Reagent (stock concentration)	Final concentration	Quantity
Tris-HCl (1 M, pH 7.5)	80 mM	16 mL
NaCl (3 M)	200 mM	13.33 mL
DTT* (1 M)	2 mM	400 µL
Milli-Q H_2O	n/a	170.27 mL
Total		**200 mL**

*Add DTT right before use.

8. **10× TFAM Binding Buffer**
   500 mM Tris-HCl pH 8.0
   1 M KCl
   50 mM $MgCl_2$
   1 mM DTT (add right before use)

9. **TFAM EMSA Running Buffer**
   50 mM Tris-acetate pH 8.0
   2.5 mM EDTA

Part III: TFB2M purification

Note: All buffers are adjusted to pH 8.0 with HCl or KOH, sterilized with a 0.22 µm filter, and stored at 4 °C. Use BME for the Lysis and HisTrap buffers and DTT for the HiTrap Heparin column and Storage buffers. Prepare cold, filtered Milli-Q H_2O and 20% EtOH to wash and store the FPLC columns after use.

1. **TFB2M Lysis Buffer**

Reagent (stock concentration)	Final concentration	Quantity
HEPES-KOH (1 M, pH 8.0)	20 mM	6 mL
KCl (3 M)	1 M	100 mL
Glycerol (100%)	5% v/v	15 mL
Imidazole	10 mM	0.204 g
BME* (14.3 M)	5 mM	See Note
Lysozyme*	1 mg/mL	See Note
Protease inhibitor cocktail* (PIC, 1,000×)	1×	See Note
Milli-Q H_2O	n/a	179 mL
Total		**300 mL**

*Add right before use. We only need 50 mL of the buffer in a conical tube; then, add these components (5 mg of lysozyme, 17.5 µL of BME, and 50 µL of PIC) to the tube instead of the entire bottle of buffer.

2. **TFB2M Ni-NTA Buffer A**

Reagent (stock concentration)	Final concentration	Quantity
HEPES-KOH (1 M, pH 8.0)	20 mM	20 mL
KCl (3 M)	300 mM	100 mL

Glycerol (100%)	5% v/v	50 mL
Imidazole	20 mM	1.36 g
BME* (14.3 M)	5 mM	350 µL
Milli-Q H_2O	n/a	830 mL
Total		**1,000 mL**

*Add BME right before use.

3. **TFB2M Ni-NTA Buffer B**

Reagent (stock concentration)	Final concentration	Quantity
HEPES-KOH (1 M, pH 8.0)	20 mM	10 mL
KCl (3 M)	300 mM	50 mL
Glycerol (100%)	5% v/v	25 mL
Imidazole	500 mM	17.02 g
BME* (14.3 M)	5 mM	175 µL
Milli-Q H_2O	n/a	415 mL
Total		**500 mL**

*Add BME right before use.

4. **TFB2M TEV Cleavage Buffer**

Reagent (stock concentration)	Final concentration	Quantity
HEPES-KOH (1 M, pH 8.0)	20 mM	40 mL
KCl (3 M)	300 mM	200 mL
Glycerol (100%)	5% v/v	100 mL
BME (14.3 M) *	5 mM	699.3 µL
Milli-Q H_2O	n/a	1,659.3 mL
Total		**2,000 mL**

*Add BME right before use.

5. **TFB2M No Salt Heparin Buffer**

Reagent (stock concentration)	Final concentration	Quantity
HEPES-KOH (1 M, pH 8.0)	20 mM	4 mL
Glycerol (100%)	5% v/v	10 mL
EDTA (500 mM)	1 mM	0.4 mL
DTT (1 M) *	1 mM	0.2 mL
Milli-Q H_2O	n/a	185.4 mL
Total		**200 mL**

*Add DTT right before use.

6. **TFB2M Heparin Buffer A**

Reagent (stock concentration)	Final concentration	Quantity
HEPES-KOH (1 M, pH 8)	20 mM	20 mL
KCl (3 M)	200 mM	66.67 mL
Glycerol (100%)	5% v/v	50 mL
EDTA (500 mM)	1 mM	2 mL
DTT (1 M) *	1 mM	1 mL
Milli-Q H_2O	n/a	860.33 mL
Total		**1,000 mL**

*Add DTT right before use.

7. **TFB2M Heparin Buffer B**

Reagent (stock concentration)	Final concentration	Quantity
HEPES-KOH (1 M, pH 8.0)	20 mM	10 mL
KCl (3 M)	1.5 M	250 mL
Glycerol (100%)	5% v/v	25 mL
EDTA (500 mM)	1 mM	1 mL
DTT (1 M) *	1 mM	0.5 mL
Milli-Q H_2O	n/a	213.5 mL
Total		**500 mL**

*Add DTT right before use.

SDS-PAGE sample recipes

Note: These recipes make 20 µL of each SDS-PAGE sample. Boil samples for 5 min at 95 °C before running and load 9–12 µL per lane. All POLRMT samples can be run on 8%–10% SDS-PAGE. For TFAM and TFB2M, 10%–12% SDS-PAGE would be suitable. We run the gels in 1× Tris/Glycine/SDS buffer and stain with Coomassie.

1. Uninduced, induced, pellet, lysate, PEI pellet, PEI supernatant, AS pellet, Ni-NTA or HisTrap flowthrough, and wash samples
   1.5 µL of sample or scrape a small amount of pellet directly into the microfuge tube
   13.5 µL of Milli-Q water
   5 µL of 4× Laemmli buffer

2. Ni-NTA Elution samples, AS supernatant
   7.5 µL of sample or small piece of pellet
   7.5 µL of Milli-Q water
   5 µL of 4× Laemmli buffer

3. TEV-cleaved sample, HisTrap, and Heparin column fractions
   Note: Load as much as possible (at least 12 µL per lane) to visualize very diluted samples
   10 µL of sample or small piece of pellet
   5 µL of Milli-Q water
   5 µL of 4× Laemmli buffer

Laboratory supplies

1. 17 mm × 100 mm culture tubes, 14 mL (VWR, catalog number: 60818-689)
2. BD disposable syringe, 50 mL (Fisher Scientific, catalog number: 13-689-8)
3. Biotix 10 µL tips (Fisher Scientific, catalog number: 12-111-021)
4. Fernsbach culture flasks, 2.8 L (Fisher Scientific, catalog number: 09-552-39)
5. Membrane filters, 0.22 µm pore size, 47 mm diameter (Fisher Scientific, catalog number: 09-719-2B)
6. Petri dishes (Fisher Scientific, catalog number: FB0875713)
7. Pipette tips, microfuge tubes, and low-retention tubes (Genesee Scientific, catalog numbers: 24-282, 23-150RL, 23-165RL, 28-103, 22-281LR)
8. Serological pipettes, 5, 10, and 25 mL (VWR, catalog numbers: 75816-094, 75816-100, 75816-090)
9. Syringe filters (0.22 µm pore size, 25 mm diameter) (VWR, catalog number: 76479-024)

Equipment

1. 1 L centrifuge bottles with sealing closure (Thermo Scientific, catalog number: 31411006)
2. 4 L capacity centrifuge (Thermo Scientific, Sorvall LYNX 4000 Superspeed Centrifuge, catalog number:

75006580)
3. Benchtop centrifuges (Eppendorf, 5910 R, 5425)
4. Benchtop incubator shaker (Eppendorf, model: New Brunswick Benchtop Incubator Shaker I24)
5. BioSpectrometer Basic (Eppendorf)
6. Dialysis tubing, 14,000 MWCO (Sigma-Aldrich, catalog number: D9777-100FT)
7. Fast protein liquid chromatography (FPLC) system (Bio-Rad, NGC Quest 10 Chromatography System, catalog number: 7880001)
8. Gel imager (Bio-Rad, model: Gel Doc EZ Imager)
9. Glass column for Ni-NTA resin (Bio-Rad, Econo-Column Chromatography Column, catalog number: 7371512)
10. Hot plate stirrer (VWR, catalog number: 97042-674)
11. Magnetic stir bar (Fisher Scientific, catalog number: 14-513-51)
12. Reusable bottle top filter unit (Thermo Scientific, Nalgene, catalog number: DS0320-2533)
13. SDS-PAGE running system (Bio-Rad, Mini-PROTEAN Tetra System)
14. Sonicator (Qsonica, CL-18 Sonicator Probe)

Software and datasets

1. Bio-Rad Image Lab (https://www.bio-rad.com/en-us/product/image-lab-software?ID=KRE6P5E8Z)
2. ImageJ version 1.53e (https://imagej.net/ij/index.html)

Procedure

Part I: POLRMT Purification

A. Overexpression of recombinant POLRMT in *E. coli*

1. Transform the plasmid into BL21-CodonPlus (DE3)-RIPL and plate on LB agar plates containing ampicillin (or the appropriate antibiotic). Incubate inverted overnight at 37 °C.
   Note: This transformation can also be done with BL21-CodonPlus-RIL. This step can be skipped if glycerol stocks of cells carrying the POLRMT-coding plasmid have been made previously.
2. Get an autoclaved flask with 50 mL of autoclaved LB media and add 50 µL of Amp stock (100 mg/mL, see Recipes).
3. Pick five separate colonies from the plate with a sterile pipette tip or stick for inoculation (or add a small piece of glycerol stock).
4. Once inoculated, start incubating the cultures in the afternoon around 5 pm at 28 °C and shake overnight (14–17 h) at 200 rpm (see General note 2 for temperature and oversaturation of cells).
5. In four flasks (2.8 L Fernsbach culture flasks), prepare 1 L each of autoclaved LB media and add 1 mL of Amp stock per liter of media.
6. Add 10 mL of inoculum per liter of LB media with ampicillin (see General note 3 for how to make glycerol stocks).
7. Incubate the inoculated flasks at 37 °C with shaking at 200 rpm. Check cell density by measuring the OD_{600} after 3–4 h to see if it is between 0.4 and 0.6.
8. Once in the above OD range, lower the shaker temperature to 18 °C. Withdraw a 1 mL sample (label as "Uninduced") into a microfuge tube and tape it on the side of the flask to let it continue shaking.
9. Cool down the flasks to 18 °C from 30 min to 1 h before adding IPTG (0.2 mM final concentration) to induce POLRMT expression. To do this, add 200 µL of 1 M IPTG stock (see Recipes) per 1 L of LB (see General note 4 for cooling flasks).
10. Continue growing overnight (16–20 h) at 18 °C at 200 rpm.
11. Withdraw a 1 mL sample at the end of the induction period ("Induced") and remove the "Uninduced"

sample tube off the side of the flask (see Recipes for SDS-PAGE samples). Run out samples on a 10% SDS-PAGE gel and Coomassie stain to visualize POLRMT overexpression.

12. Harvest the cells by centrifugation at 2,991× *g* for 30 min at 4 °C in 1 L centrifuge bottles.
13. Safely dispose of the supernatant with 10% bleach and scrape the pellets into a 50 mL conical tube. Store the combined pellet at -80 °C (flash freezing is not necessary) or proceed with the next step.

B. Lysis of POLRMT overexpression pellet by sonication

Note: All steps below should be done at 4 °C or on ice unless noted otherwise.

1. Thaw the pellet by putting the tube in tap water. Scrape out the cells with a spatula into a metal beaker and add 50 mL of cold Lysis Buffer with BME, lysozyme, and PIC. **Optional:** Stir on a stir plate with a stir bar at 4 °C for 1 h to let the lysozyme break down cells.
2. Put the beaker in an ice bucket and sonicate cell suspension for 30 min at 4 °C (30 s on and off, 60% amplitude). Check that the suspension has become less viscous and slightly darker at this point.
3. Centrifuge the suspension at 30,000× *g* for 1 h at 4 °C.
4. Pour supernatant ("Lysate") into a cold beaker on ice and record the volume.
5. Take samples to run on an SDS-PAGE gel: Pellet and Lysate (see Recipes). There will be more POLRMT in the pellet than in the lysate, but we will use the soluble POLRMT in the lysate for purification (Figure 1B).

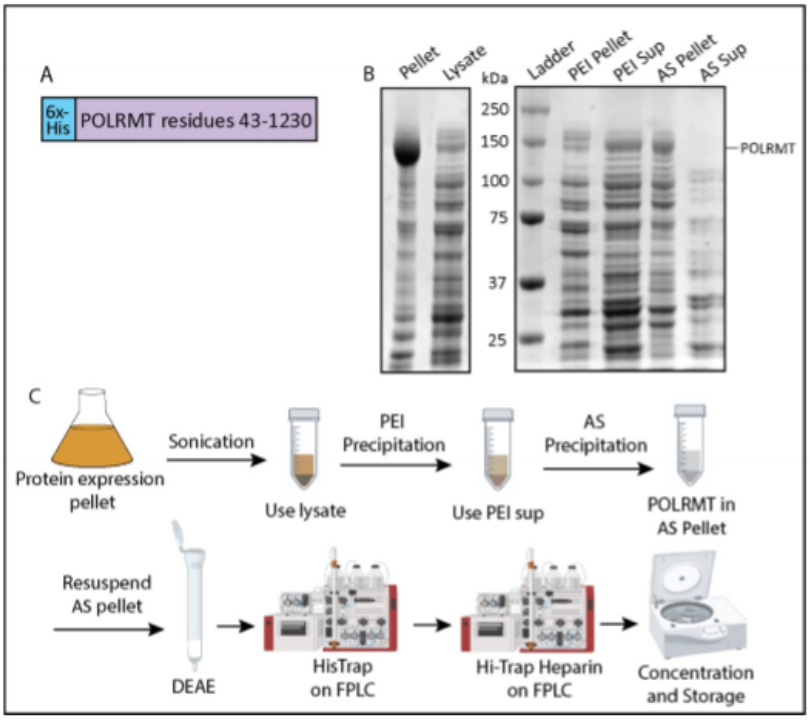

Figure 1. Mitochondrial RNA polymerase (POLRMT) purification flowchart and polyethyleneimine (PEI) and ammonium sulfate (AS) precipitation. (A) Expression construct containing the nucleotide sequence for POLRMT residues 43–1,230 (Uniprot: O00411) and an N-terminal 6x-His-tag. (B) 10%

SDS-PAGE analysis of samples from the sonication step, PEI precipitation, and AS precipitation steps. (C) Schematic of POLRMT purification including sonication, PEI precipitation, AS precipitation, a DEAE column, a HisTrap column, a HiTrap heparin column, and concentration.

C. POLRMT PEI precipitation

1. With the lysate in a cold glass beaker on ice or at 4 °C, add a stir bar and check that it gently stirs the solution while on a stir plate.
2. Slowly add cold 5% PEI (see Recipes) dropwise into the lysate to get 0.3% PEI final concentration. To calculate how much 5% PEI we need, find 6% of the volume of the lysate:
   _____ mL of 5% PEI to be added = _____ mL of lysate × 0.06
3. Cover the top of the beaker with aluminum foil and keep stirring gently at 4 °C for an additional 30 min.
4. Centrifuge at 30,000× *g* for 10 min at 4 °C.
5. Take out samples for gel analysis [PEI pellet, PEI supernatant (see Recipes)] and run them out on a 10% SDS-PAGE gel. POLRMT should be in the supernatant (Figure 1B).

D. POLRMT AS precipitation

1. Add AS powder slowly (for a period of 30 min) to the supernatant to get 55% saturation.
   For example, 55% saturation of 100 mL of lysate requires 35.1 g of AS.
   _____mL lysate × 3.51 g/mL = _____ grams AS to be added
2. Cover the top of the beaker with aluminum foil and gently stir at 4 °C for 1 h (or overnight) to dissolve AS and precipitate proteins.
3. Centrifuge at 30,000× *g* for 10 min at 4 °C. The POLRMT protein is in the pellet.
4. Take out samples for gel analysis: AS pellet, AS supernatant (see Recipes). On an SDS-PAGE gel, you should see POLRMT (~140 kDa) in the AS pellet and not in the AS supernatant (Figure 1B).
5. Record the weight of the pellet in grams and store it at -80 °C.
   Pause point: The AS pellet can be stored for a few months before moving on to FPLC purification.

E. POLRMT DEAE gravity column and overnight HisTrap column

Note: One column volume (CV) corresponds to 5 mL for the HisTrap column (Cytiva). The DEAE gravity column can be replaced by using a HiTrap DEAE Fast Flow column (Cytiva) attached in tandem with the HisTrap column.

1. Start by attaching the 5 mL HisTrap column and loading POLRMT HisTrap buffers (see Recipes) onto the FPLC.
2. Wash and equilibrate the column (2 mL/min for five CV each of filtered Milli-Q water, HisTrap Buffer B, and then HisTrap Buffer A).
3. Resuspend the AS pellet in the HisTrap Buffer A by adding 4 mL of cold buffer per gram of pellet. Stir gently until dissolved.
   Note: The following steps with the DEAE column can be done at room temperature as long as all the buffers are cold and the samples are kept on ice.
4. Prepare the DEAE by placing 10 mL of the DEAE resin suspension into a clean gravity column. Once the resin settles, you should get approximately 5 mL of bed resin.
5. Wash the DEAE with 5× bed volume of cold filtered water and cold HisTrap Buffer A.
   Note: This DEAE column can be washed with water and stored in 20% EtOH for reuse.
6. With the stopper on the gravity column closed, pour the dissolved AS pellet into the column and gently stir with a spatula. **Optional:** Incubate for 15 min at 4 °C with gentle rocking.
7. Elute into a clean container on ice and then add 10 mL of HisTrap Buffer A to ensure all POLRMT is washed out.
8. Filter the eluent with a 0.22 µm syringe filter and prepare to load it on the HisTrap column on the FPLC. Use these settings for the FPLC run while monitoring eluent absorbance at 280 nm (A_{280}) and collect all

flowthrough/eluent for a later SDS-PAGE analysis (Figure 2B):

- Sample application: 0.3 mL/min (for running overnight).
- Column wash with Buffer A: 0.5 mL/min (for running overnight). Wash the column until the A_{280} trace returns to baseline (approximately five CV or 25 mL). After reaching baseline, continue to wash for at least 20 mL.
- Protein elution: 1 mL/min, collect 5 mL fractions.
  Elution program:
  0–50% Buffer B gradient for 40 CV (200 mL). **Optional:** Wash the column with Buffer B. No need to collect samples from these steps.
  70% Buffer B for five CV (25 mL)
  100% Buffer B for five CV (25 mL)
- Wash the column with five CV of water and five CV of 20% EtOH (use a lower flow rate of 1 mL/min) and store the columns.

Note: POLRMT elutes in a small broad peak and is very dilute. Do not let the fractions sit for longer than one day, as the more concentrated fractions of POLRMT will start precipitating (see General note 5).

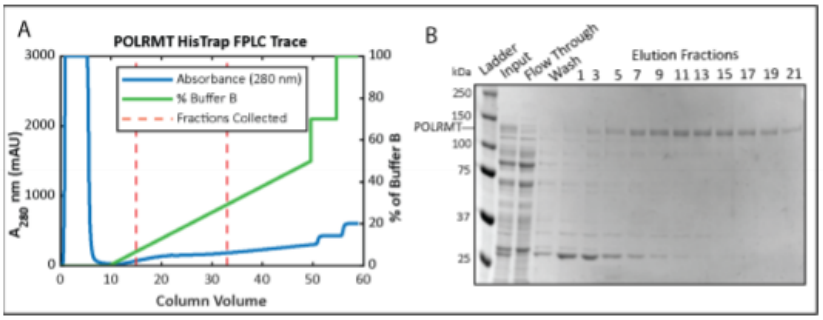

Figure 2. Mitochondrial RNA polymerase (POLRMT) HisTrap chromatography (A) Chromatogram for the elution phase of the HisTrap column run on the FPLC and (B) 8% SDS-PAGE analysis of the collected fractions.

9. Take out samples of the HisTrap fractions and run them on a 10% SDS-PAGE gel alongside a protein ladder. POLRMT appears around 140 kDa on an SDS-PAGE gel and is more concentrated roughly around fractions #4–22 (Figure 2B). (To save time, start preparing the filters and concentrate while the gel is running; see step below.)
10. Equilibrate two 50K MWCO Amicon filters at 4,000× *g* and 4 °C.
11. Concentrate POLRMT by centrifuging the Amicon filtration units at 1,900× *g*. Pipette solution gently every 5–10 min to avoid precipitation. Stop when the total volume becomes less than 25 mL (see General note 6 about this concentration step).
12. Add an equal volume of No Salt Heparin Buffer to the concentrate to bring the final NaCl concentration to 150 mM (see General note 7).

F. POLRMT overnight HiTrap heparin column

1. Wash and equilibrate the 5 mL HiTrap heparin column in Buffer A on the FPLC (2 mL/min for five CV each of filtered Milli-Q water, Heparin Buffer B, and then Heparin Buffer A).
2. Load your protein sample that has been diluted with the No Salt Heparin buffer.
3. Run the following FPLC program:
   - Sample application: 0.3 mL/min (for running overnight).

- Column wash with Buffer A: 0.5 mL/min (for running overnight). Wash the column until the A_{280} trace returns to baseline (approximately five CV or 25 mL). After reaching baseline, continue to wash for at least 20 mL.
- Protein elution: 2 mL/min, collect 3 mL fractions.
  0–50% Buffer B gradient for 20 CV (100 mL).
  55% Buffer B for five CV or 25 mL (POLRMT elutes here!).
  70% Buffer B for five CV or 25 mL.
  100% Buffer B for five CV or 25 mL.
- Wash the column with five CV of water and five CV of 20% EtOH (use a lower flow rate of 1 mL/min) for storage of the columns.

G. Concentration and storage of POLRMT

1. Run a 10% SDS-PAGE gel of the fractions (see Recipes) and pool together the fractions with POLRMT (Figure 3B).

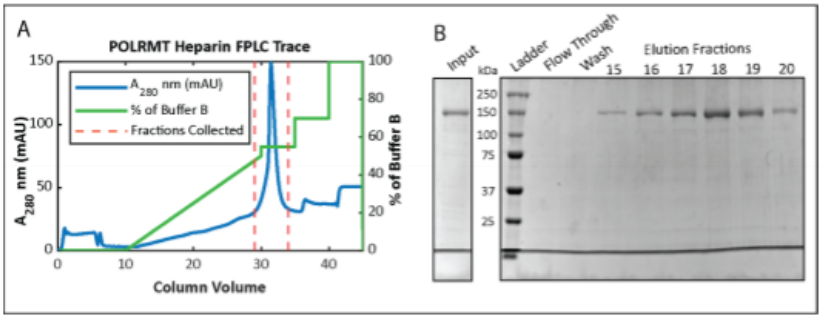

Figure 3. Mitochondrial RNA polymerase (POLRMT) HiTrap Heparin chromatography (A) Chromatogram for the elution phase of the HiTrap Heparin column run on the FPLC and (B) 10% SDS-PAGE analysis of the collected fractions.

2. Equilibrate the membrane of a 50K MWCO Amicon filtration unit with 150 mM NaCl Heparin Buffer by spinning in the centrifuge for 5 min. Add pooled POLRMT fractions to the unit.
3. Start centrifuging at 2,500× *g* at 4 °C and gradually decrease the speed to 1,300× *g*, pipetting gently from the bottom of the membrane and checking concentration frequently until at least 7 µM. POLRMT will easily precipitate out, so if you notice precipitate forming or if the concentration in the solution is not increasing, stop concentrating (see General note 8).
4. Measure and calculate protein concentration using these parameters by the Protparam tool (https://web.expasy.org/protparam/):
   6x-His-POLRMT: 137.7 kDa or 137,700 mg/mole
   Molar extinction coefficient: 143,700 L $(cm*M)^{-1}$ (assuming all cys reduced)
   Abs 0.1% = 1.043 (assuming all cys reduced)
5. Add sterile glycerol to get a final concentration of 25% glycerol.
6. Aliquot 10 µL into low-retention tubes, flash freeze in liquid nitrogen, and store at -80 °C.

Part II: TFAM purification

A. Overexpression of recombinant TFAM in *E. coli*

1. Transform BL21-CodonPlus(DE3)-RIPL cells using ~200 ng of ProEX_Htb_TFAM plasmid and plate on LB agar plates containing ampicillin. Incubate inverted overnight at 37 °C.
2. Grow 5 × 5 mL starter cultures overnight in LB supplemented with ampicillin, one colony per tube.
3. In the morning, spin down the 5 mL starter cultures at 2,782× *g* for 6 min and pour off the media. Carefully resuspend the cells in a total of 1 mL of LB, transferring the 1 mL to resuspend all the cells from the five tubes.
4. Add ampicillin to LB media (1 mL of 100 mg/mL ampicillin stock per 1 L of LB). Evenly split the 1 mL cell suspension between the 1 L LB flasks.
5. Incubate at 37 °C at 200 rpm. Check the OD_{600} after 4–5 h to see if it is between 0.4 and 0.6.
6. Once in the above OD range, withdraw a 1 mL sample ("uninduced") into a microfuge tube, tape the tube on the side of the flask, and lower the shaker temperature to 16 °C.
7. Cool down the flasks before inducing with IPTG (0.2 mM final concentration; add 200 µL of 1 M IPTG stock per 1 L of LB).
8. Continue shaking overnight at 16 °C (~16–20 h) at 200 rpm.
9. Take a sample at the end of the induction period ("Induced") and run it alongside the "Uninduced" sample (see Recipes) on an SDS-PAGE gel to visualize protein expression.
10. Harvest the cells by centrifuging at 2,991× *g* for 15 min at 4 °C.
11. Dispose of the supernatant and scrape the pellets into a 50 mL conical tube. Store the combined pellet at -80 °C or proceed with the cell lysis.

B. Cell lysis: lysozyme treatment and sonication

Note: All steps below should be done at 4 °C or on ice unless noted otherwise.

1. Thaw cells if frozen. Add 40 mL of TFAM Lysis Buffer (with lysozyme, BME, and PIC; see Recipes) to the pellet (10 mL of lysis buffer per liter of expressed culture) and resuspend the pellet until homogenous.
2. Incubate for 1 h at 4 °C.
3. Sonicate cell suspension for 20 min at 4 °C (20 s on and off, 60% amplitude).
4. Centrifuge at 30,000× *g* for 1 h at 4 °C.
5. Save ~10 µL of "Cell Pellet" and "Lysate" samples (see Recipes) for SDS-PAGE gel analysis.

C. TFAM Ni-NTA resin #1

Note: This is Ni-NTA by centrifugation method at 4 °C.

1. Prepare a 5 mL Ni-NTA resin bed in a 50 mL conical tube according to the manufacturer's instruction and wash three times with Ni-NTA Buffer A by resuspending the resin in the buffer, spinning it down at 363 × *g* for 3 min at 4 °C, carefully decanting the buffer, and repeating the process.
2. Add the supernatant and incubate overnight at 4 °C with gentle agitation.
3. Spin down the resin, collect the supernatant as "Sample Application" into a conical tube, and begin resin washing steps by adding 5 mL of Ni-NTA Buffer A to the resin, gently mixing, and spinning the sample at 1,932× *g* at 4 °C.
4. Collect the supernatant as "Wash 1" and repeat washes to wash #10.
5. Beginning with wash #10, check the absorbance of the sample at 280 nm and continue the washes until the absorbance is close to 0.
6. Elute the proteins by adding 5 mL of Ni-NTA Buffer B and spinning as before. Collect the sample as "Elution 1" and repeat this 3–5 times, keeping "Elution" supernatants separate.
7. Run a 10% or 12% SDS-PAGE gel with collected samples from the cell lysis, sample application, washing, and elution (see Recipes). A TFAM band just above 25 kDa should be obvious but some contaminants will

still be present (Figure 4B).

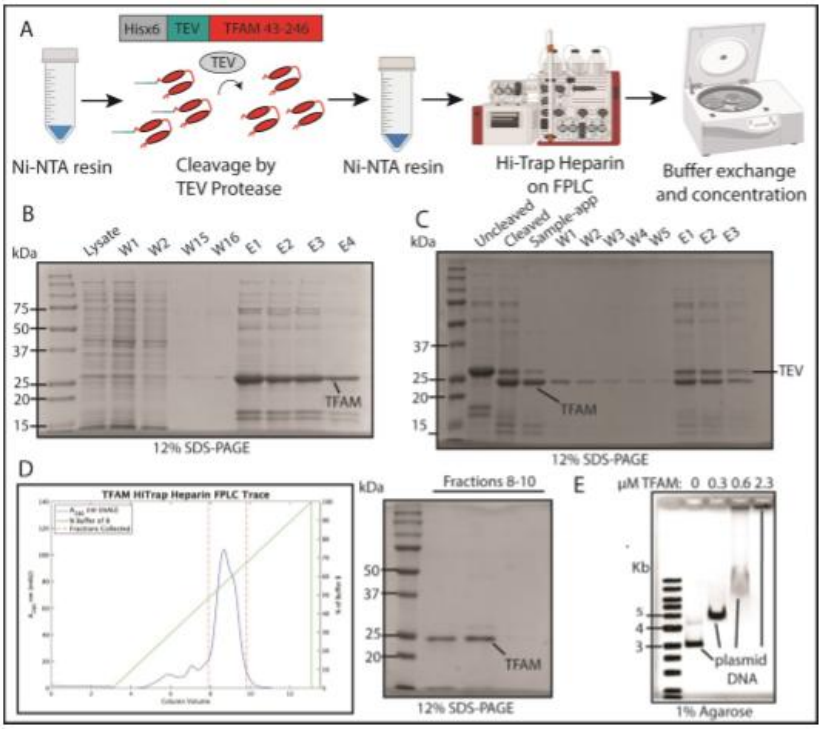

Figure 4. Transcription factor A, mitochondrial (TFAM) purification flowchart, Ni-NTA and HiTrap Heparin chromatography, and TFAM DNA-compaction test (A) Schematic of TFAM purification including Ni-NTA Resin purification, cleavage by TEV protease, a second Ni-NTA resin step, a HiTrap Heparin column, and concentration. (B) 12% SDS-PAGE analysis of Ni-NTA #1 results including washes (W) and elution steps (E). (C) 12% SDS-PAGE analysis of TEV protease cleavage of TFAM and Ni-NTA resin step. (D) Chromatogram for the elution phase of the HiTrap Heparin column run on the FPLC and the SDS-PAGE analysis of the collected fractions. (E) Electrophoretic mobility shift assay (EMSA) to test TFAM ability to compact plasmid DNA.

D. Dialysis and TEV cleavage of the His tag on TFAM

1. Add 2 L of ice-cold TFAM TEV Cleavage Buffer to a large beaker.
2. Place the elution samples with significant TFAM content into dialysis tubing and add TEV protease at a 1:30 TEV:TFAM protein molar ratio. (Estimate TFAM content using the absorbance of the pooled elution samples at 280 nm. See step G for protein mass and extinction coefficient.)
3. Allow the sample to dialyze in Cleavage Buffer and cleave overnight at 4 °C with gentle stirring.
4. Check the success of TEV cleavage on a 12% SDS-PAGE gel by comparing the sample before and after dialysis. If cleavage is complete, continue to the next step. If not, add more TEV protease and continue dialysis (Figure 4C).
   Note: The version of TEV protease used in our lab is ~26 kDa in size. This means it will look a lot like uncleaved TFAM on the SDS-PAGE gel.

E. TFAM Ni-NTA resin #2

1. Prepare a 5 mL resin bed of Ni-NTA resin as before (see step C1).
2. Add the dialyzed sample to the resin and incubate overnight at 4 °C as before with gentle agitation.
3. Spin down the resin as before (1,932× *g* at 4 °C) and collect the supernatant ["Sample application" (this will have the TEV-cleaved, now untagged TFAM)].
4. Add 5 mL of Ni-NTA Buffer B to the resin, mix, and spin to collect "Elution 1." You want to collect this to be sure the TEV protease was bound by the Ni resin.
5. Repeat the elution 2–3 times.
6. Run a 10% or 12% SDS-PAGE gel to be sure that TFAM is in the "Sample application" (Figure 2C).

F. TFAM concentration and HiTrap heparin column

Note: An alternative to the first concentration step is to adjust the salt concentration by adding a version of the Ni-NTA Buffer A without any salt. Adjust the salt to <200 mM for use on the HiTrap heparin column.

1. Wash and equilibrate the 5 mL HiTrap heparin column (Cytiva) on the FPLC with five CV of heparin Buffer B and then Buffer A.
2. Add elution fractions from Ni-NTA resin #2 to a 50 mL conical tube and begin buffer exchanging the sample by adding it in 15 mL volumes to a 3K MWCO Amicon filter and spinning at 3,434× *g* at 4 °C. Stop concentrating when the buffer exchange sample is down to 2 mL.
3. When the entire protein sample has been added and spun down to approximately 2 mL, fill the 3K MWCO Amicon filter with Heparin Buffer A and continue to spin. Continue to add Heparin Buffer A and spin until ~30 mL has flown through the filter and you are left with 2–3 mL. This lowers the salt concentration from 300 mM to 200 mM to ensure binding to the HiTrap Heparin column.
4. Load the buffer-exchanged protein sample onto the prepared HiTrap Heparin column.
5. Run using these settings:
   - Sample application: 1.0 mL/min.
   - Column wash: 1.0 mL/min until A_{280} reaches ~0.
   - Elution: 2.5 mL/min with 2 mL fractions.
     0–100% Buffer B gradient over 10 CV (50 mL).
   - Wash the column with five CV of water and five CV of 20% EtOH (1 mL/min) for storage.

G. Concentration and storage of TFAM

1. Run a 10% or 12% SDS-PAGE gel of the fractions and pool together the fractions with TFAM (Figure 4D)
2. Concentrate as before using a fresh 3K MWCO Amicon filter.
3. When all the pooled fractions have been concentrated to a small volume (0.5–1 mL), add 2× Storage Buffer to fill the filter and continue to centrifuge. Repeat this process to pass two full volumes of Storage Buffer through the filter to exchange the buffer. Stop when the second full pass of 2× Storage buffer has reached ~2 mL and begin measuring the absorbance at 280 nm for TFAM concentration while continuing to centrifuge.
4. Measure and calculate protein concentration using these parameters from the protein sequence by the Protparam tool (https://web.expasy.org/protparam/):
   TFAM after TEV cleavage: 24.4 kDa or 24,400 mg/mole.
   Molar extinction coefficient: 35,410 L $(cm*M)^{-1}$ (assuming all cys reduced).
   Abs 0.1% = 1.45 (assuming all cys reduced).
5. When the desired concentration has been reached (100–200 mM), move the sample from the Amicon filter to a conical tube and add an equal volume of filtered 50% glycerol for a final concentration of 25% glycerol.
6. Aliquot 20 mL per tube, flash freeze, and store at -80 °C.

H. Testing TFAM DNA-compaction activity with electrophoretic mobility shift assay (EMSA)

Note: To know if the purified TFAM is active, it is best to run an electrophoretic mobility shift assay. TFAM can bind DNA non-specifically, so any plasmid DNA can be used. If the bands shift upwards in the assay, the TFAM is active and will work with transcription assays. In our assays, we use the Puc19 plasmid.

1. Prepare a 1% agarose EMSA gel using TFAM EMSA Running Buffer
2. Prepare reactions with 1× TFAM Binding Buffer, add ~200 ng of plasmid DNA, and add TFAM in increasing amounts to the plasmid. These reactions are typically done in total volumes of 20–30 mL.
3. Incubate samples at 37 °C for 30 min.
4. Add filtered glycerol to 10% in the samples and load onto the EMSA gel along with a 1 kb DNA ladder.
5. Run the EMSA gel at 70 V for 65 min at room temperature in TFAM EMSA Running Buffer.
6. Stain the gel with gentle agitation using ethidium bromide for 30 min at room temperature and image using UV light on a Bio-Rad Gel Doc EZ Imager system or equivalent (Figure 4E).

Part III: TFB2M purification

A. Expression of TFB2M

1. Transform the plasmid containing TFB2M (Figure 5) into BL21-CodonPlus (DE3)-RIPL and spread on Kan-containing (25 µg/mL, see Recipes) plates. Incubate inverted overnight at 37 °C.
   Note: The transformation step can be skipped if glycerol stocks have been previously made. E. coli *strain ArcticExpress (DE3) could also be used for transformation.*

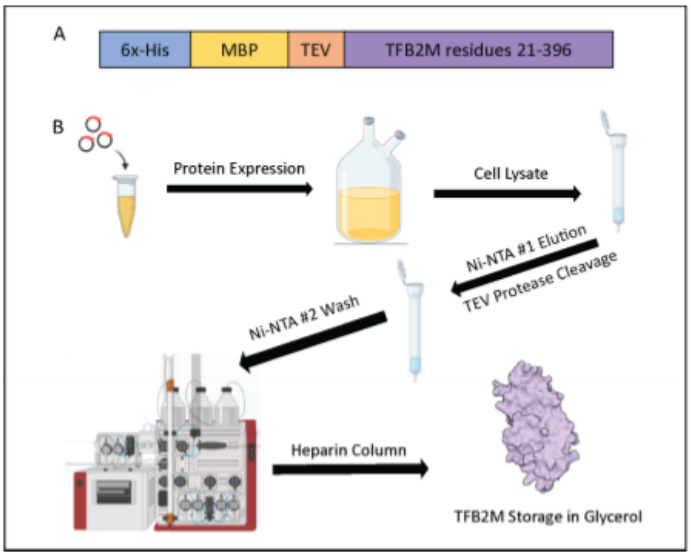

Figure 5. Transcription factor B2, mitochondrial (TFB2M) purification flowchart (A) Expression construct containing the nucleotide sequence for TFB2M, corresponding to residues 21–396 (Uniprot: Q9H5Q4). This plasmid has an N-terminal 6x-His-tagged Maltose-binding protein (MBP) solubility tag connected to TFB2M with a TEV-cleavage site. (B) Schematic of TFB2M purification including protein expression, Ni-NTA #1 Resin purification, cleavage by TEV protease, Ni-NTA #2 Resin step, a HiTrap Heparin column, and concentration.

2. Add five colonies or a small chunk of the frozen glycerol stock to 5–10 mL of LB culture with Kan (25 µg/mL). Grow overnight while shaking at 28–37 °C; avoid letting the starter culture become oversaturated (see General note 2 for POLRMT purification).
3. In the morning, add primary culture (2.5–5 mL) to 1 L of LB culture.
4. Grow at 37 °C at 200 rpm until OD_{600} reaches 0.7–0.8 (approximately 3–5 h).
5. Once in the OD range, cool down the shaker to 14 °C and withdraw a 1 mL sample ("uninduced") before inducing the rest of the culture with 0.2 mM final IPTG (refer to Recipes). Continue to shake for 16–20 h at 14 °C.
6. Take a 1 mL sample ("Induced") at the end of the induction period to run on an SDS-PAGE gel.
7. Harvest the cells by centrifuging at 2,991× *g* for 15 min at 4 °C.
8. Store cell pellet at -80 °C.

B. Sonication

Note: All steps below should be done at 4 °C or on ice unless noted otherwise.

1. Add 40 mL of Lysis Buffer (with lysozyme, BME, and PIC, see Recipes) to 4 L-worth of cell pellet (10 mL of lysis buffer per liter of expressed culture) and stir the pellet at 4 °C for 1 h.
2. In the cold room, sonicate for 20 min at 60% amplitude, 30 s on and off.
3. Centrifuge at 30,000× *g* for 1 h at 4 °C to remove cell debris.

C. Ni-NTA Resin #1

1. Set up a gravity column by clamping it onto a stand and pipette 10 mL of Ni-NTA resin solution into the column to get 5 mL bed volume.
2. Wash the resin with filtered, cold Milli-Q water three times and then wash once to equilibrate with your Ni Buffer A.
   Note: The volume of each wash should be five times the bed volume of the resin.
3. Pour the cell lysate onto Ni-NTA resin and gently stir with a metal spatula to promote the binding of your His-tagged protein. Securely close the column/vial and rock gently for 1 h at 4 °C.
4. Clamp the column again on the stand and collect your sample application flowthrough. Label the sample as "Ni flowthrough" for SDS-PAGE.
5. Prepare the following mixtures of Buffer A and B to perform the wash and elution steps:
   One CV = 5 mL bed resin.
   Wash 1, 2, and 3: 0% B, five CV: prepare three tubes containing 50 mL of Buffer A each.
   Wash 4: 5% B, five CV: one tube containing 47.5 mL of Buffer A and 2.5 mL of Buffer B.
   Elution 1: 40% B, two CV: one tube containing 6 mL of Buffer A and 4 mL of Buffer B.
   Elution 2: 50% B, two CV: one tube containing 5 mL of Buffer A and 5 mL of Buffer B.
   Elution 3: 100% B, two CV: one tube with 10 mL of Buffer B.
   Keep them on ice or at 4 °C before use.
   Note: The washes and elution can be done at room temperature if all the buffers are cold and samples are kept on ice. Avoid drying out the resin.
6. Wash the resin with Wash 1. Collect and label the flowthrough as "W1."
7. Repeat with Wash 2 and Wash 3.
8. Wash a final time with Wash 4 (which contains 5% v/v of Buffer B in Buffer A). Save the flowthrough as "W4."
9. Elute TFB2M with Elution 1. Collect and label the elution as "E1."
10. Repeat with Elution 2 and 3.
11. Pool elution 1, 2, and 3 together and estimate the protein concentration with the spectrophotometer:
    6x-His-MBP-TFB2M: 87.7 kDa or 87,691 mg/mole.
    Molar extinction coefficient: 117,230 L $(cm \cdot M)^{-1}$ (assuming all cys reduced).
    Abs 0.1% = 0.00134 (assuming all cys reduced).

D. Overnight TEV cleavage

1. Estimate the amount of TFB2M using the absorbance of the pooled elution samples at 280 nm:
   Amount of total TFB2M (spectrometer reading) =_____mg/mL
   Total volume = ____ mL
   Total amount of protein = ____mg (assume it is all TFB2M)
   We need a molar ratio of 1:25 TEV:TFB2M
   Amount of TEV to be added =_____mg
   Concentration of your TEV protease stock = _____mg/mL
   Volume of TEV to be added = _____mL.
2. Add 2 L of ice-cold TEV Cleavage Dialysis Buffer to a large beaker with a large stir bar.
3. Add TEV to the same tube as your Ni-resin eluted TFB2M, gently mix, and then transfer into the dialysis tubing (see General note 9).
4. Allow the sample to dialyze in the TEV Cleavage Buffer for 19–20 h overnight at 4 °C with gentle stirring.
5. Check the completion of TEV cleavage of TFB2M on a 10% or 12% SDS-PAGE gel by comparing the TFB2M band size before (~88 kDa) and after dialysis (~43 kDa). If cleavage is complete, continue to the next step. If not, add more TEV protease and continue dialysis (Figure 6).
   Note: The MBP tag (42 kDa) will be similar in size to TFB2M, and the band may be more intense. The version of purified TEV protease used in our lab is approximately 26 kDa in size.

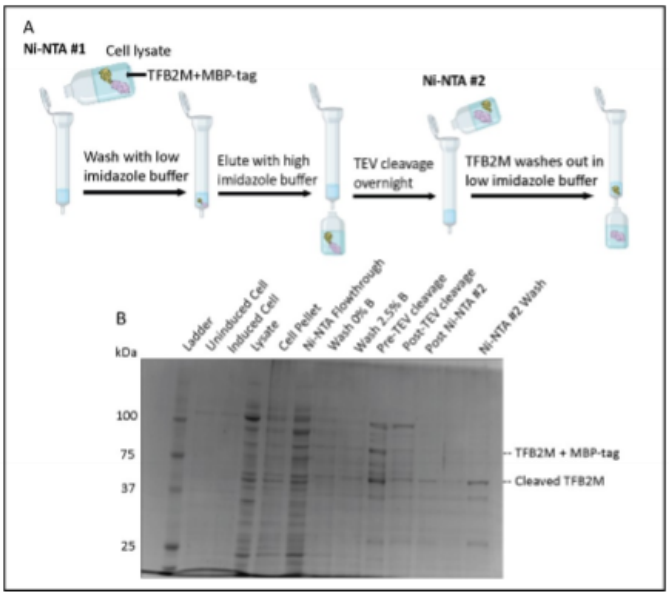

Figure 6. Transcription factor B2, mitochondrial (TFB2M) Ni-NTA chromatography. (A) Flowchart of the Ni-NTA #1, TEV cleavage, and Ni-NTA #2 steps. (B) SDS-PAGE of TFB2M expression, the first Ni-NTA purification step, the TEV cleavage process, and TFB2M presence in Ni-NTA #2 wash.

E. Ni-NTA Resin #2

Note: This is to remove His-tagged TEV protease and other contaminants from the cleaved TFB2M, which is now missing its His-tag. TFB2M will be in the flowthrough instead of the elution (Figure 6A).

1. Using the same Ni-NTA column from the previous step, wash the column with 5× bed volume of Buffer B to remove all the bound proteins, and then wash with Buffer A to equilibrate the column.
2. Before applying your cleaved TFB2M sample onto the Ni-NTA resin, add Buffer B to the TFB2M solution to bring the imidazole concentration to 20 mM (matching that in Buffer A):
   (20 mM imidazole needed) (____ mL of cleaved TFB2M sample) = (500 mM imidazole in Buffer B) (x mL Buffer B needed)
   Note: Introducing a small (20 mM) amount of imidazole ensures that most of TFB2M does not bind to the resin. The other protein contaminants like the His-MBP-tag and His-tagged TEV protease will stay bound to the Ni-NTA.
3. Add the sample to the Ni resin and rock gently for 30 min at 4 °C.
4. Collect the flowthrough (or "wash") containing TFB2M and run a 10% or 12% SDS-PAGE gel to be sure that TFB2M is present in the flowthrough (Figure 6B).
   Note: What remains bound to the column are the His-MBP tag and His-tagged TEV protease. Be aware that the His-MBP tag is similar in size to untagged TFB2M (approximately 42 kDa), and its band is often more intense on a gel.

F. Overnight heparin column

1. Wash and equilibrate a 5 mL HiTrap heparin column (Cytiva) on the FPLC.
2. Dilute the TFB2M sample (currently in 300 mM KCl buffer) with the No Salt Heparin Buffer to get a final salt concentration between 75 and 150 mM KCl.
   Note: The lower the salt, the more TFB2M binds to the heparin column. Do not concentrate TFB2M before loading it on the column or it will precipitate out.
3. Run using these settings:
   Note: One column volume (CV) is 5 mL for the HiTrap Heparin column (Cytiva).
   - Sample application: 1 mL/min.
   - Column wash: 0.5 mL/min (for running overnight) for five CV.
   - Protein elution: 0.5 mL/min, collect 2 mL fractions. Elution program:
     0–70% gradient for 10 CV (50 mL total)
     100% for one CV
   - Wash the column with five CV of water and five CV of 20% EtOH (1 mL/min) for storage.
4. Collect fractions and run a sample on a 10%–12% SDS-PAGE to determine which fractions contain TFB2M (Figure 7B).

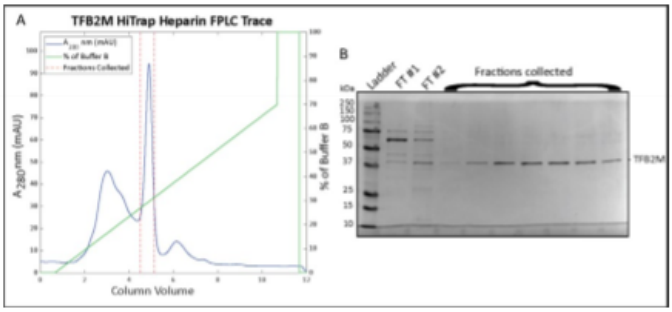

Figure 7. Transcription factor B2, mitochondrial (TFB2M) HiTrap Heparin chromatography. (A) Chromatogram for the elution phase of the HiTrap Heparin column run on the FPLC and (B) a 12% SDS-PAGE analysis of the collected fractions.

G. TFB2M concentration

1. Pool together the fractions containing TFB2M.
2. Equilibrate a 10K MWCO Amicon membrane in a centrifuge for 5 min with the Heparin Buffer A.
3. Start centrifuging the TFB2M sample at 2,500× *g* and gradually decrease the speed to 1,300× *g* if precipitate starts forming. Stop the centrifuge every 10 min and gently pipette TFB2M solution up and down with a pipette to mix. If you notice precipitate forming or if the concentration in the solution is not increasing, stop concentrating.
4. Measure and calculate the protein concentration using these parameters from the protein sequence by the Protparam tool (https://web.expasy.org/protparam/):
   TFB2M after TEV cleavage: 43.405 kDa or 43,405 mg/mole.
   Molar extinction coefficient: 49,390 L $(cm \cdot M)^{-1}$ (assuming all cys reduced).
   Abs 0.1% = 1.138 (assuming all cys reduced).
5. Add sterile glycerol to get a final concentration of 25%, aliquot 15 µL into low-retention tubes, flash freeze in liquid nitrogen, and store at -80 °C (see General note 10 for estimating salt concentration in TFB2M samples).

Data analysis

To assess the purity of the proteins, run the purified samples on an SDS-PAGE gel (see Figure 8A below). Protein band intensity can be analyzed using Bio-Rad Image Lab and ImageJ software.

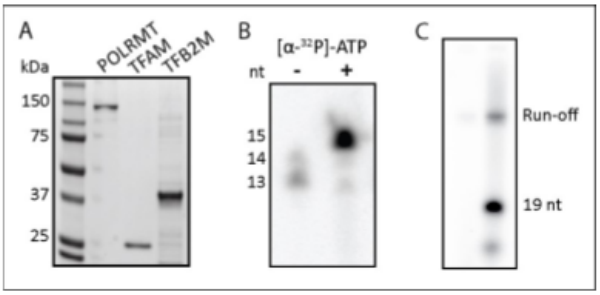

Figure 8. Validation of POLRMT, TFAM, and TFB2M purification. (A) SDS-PAGE analysis of purified POLRMT, TFAM, and TFB2M. (B) Validation of POLRMT activity on a nucleic acid scaffold. The size of a weakly radiolabeled RNA was increased by POLRMT-catalyzed incorporation of [a-^{32}P]NTP to produce a 15-nt RNA. (C) TFB2M activity was validated in a promoter (LSP)-initiated transcription assay. The reaction was stopped at 19 nt with the incorporation of 3'-dCTP. The two lanes are the same sample loaded in increasing amounts.

To evaluate the expression of the proteins, a western blot can be run using an anti-His antibody. POLRMT can be identified this way after the purification as it still retains its His-tag. For TFAM and TFB2M, which will lack their His-tag after purification, performing the TFAM functional assay described above and performing an in vitro transcription assay will confirm the activity of the proteins.

Validation of protocol

1. The protocol was used to purify the POLRMT, TFAM, and TFB2M used for an in vitro transcription initiation assay in Figure 5D of our paper (Reardon and Mishanina, 2022).

2. POLRMT activity was validated by performing an in vitro transcription assay (Figure 8B) on a nucleic acid scaffold designed by Schwinghammer et al., 2013 (Supplementary Figure 1 in the paper). This assay indicated that POLRMT was able to add the incoming nucleotide to the starting RNA.
3. TFB2M activity was validated by performing an in vitro transcription initiation assay (Figure 8C) following the protocol by Ramachandran et al., 2017 (Figure 1 in the paper). The template contained the light strand promoter (LSP) sequence of mtDNA, which requires TFB2M and TFAM for transcription to occur.

General notes and troubleshooting

1. This protocol describes how to lyse cells with a sonicator, but a French press could be used instead. Similarly, a peristaltic pump could be used to generate buffer gradients instead of an FPLC.
2. For POLRMT expression: the goal is to prevent oversaturation of the cells. The lower the temperature, the longer the colonies can be left growing overnight, so any temperature between 25 °C and 37 °C will work. If colonies are oversaturated, the growth will be extremely slow, most likely because the leaky expression of POLRMT is toxic to *E. coli* cells.
3. Glycerol stocks could also be prepared at this time by storing 1 mL of the inoculum in 25% glycerol at -80 °C. We usually vortex 500 µL of inoculum with 500 µL of 50% sterile glycerol before freezing.
4. Lower temperatures will slow down translation and promote proper folding of the protein. To cool down the flasks, we leave them shaking on the incubator while they cool or put the flasks in large buckets of ice. The OD_{600} can be checked again but inducing in the range of 0.6–1.0 works fine.
5. We have tried to change the method to get more concentrated POLRMT in fewer fractions, but POLRMT ended up precipitating out very quickly, so it is not recommended.
6. We concentrate the HisTrap elution in the Amicon filter down to 25 mL (step 10) because 50 mL is a convenient volume that we can load onto our Bio-Rad NGC FPLC via a sample pump. If your system can handle a larger loading volume, you can add an equal volume of the No Salt Heparin buffer and skip the concentration step.
7. Because the HisTrap Buffer B has 300 mM NaCl, we need to bring the salt concentration down to the same as in the Heparin Buffer A to have POLRMT bind to the Heparin column. The Heparin column does not greatly increase purity but removes endogenous bound nucleic acids from the protein.
8. Previous attempts at buffer exchange resulted in increased POLRMT precipitation and are thus not recommended. We usually concentrate POLRMT to 6 or 7 µM before we start losing protein to precipitation.
9. The goal of the dialysis is to remove imidazole from the buffer, which inhibits TEV protease activity. It is also important to keep the salt concentration above 300 mM KCl to prevent TEV protease from crashing out. There is no EDTA in the TEV buffer because EDTA inhibits TEV activity.
10. Optional for downstream transcription experiments where salt concentration could be an issue: we can estimate the salt concentration of the purified TFB2M by the % Buffer B line at the time of TFB2M elution on the FPLC trace and calculate based on the known salt concentrations of Buffers A and B:
    % of buffer B: _____
    % of buffer A: 100% - % buffer B = ____
    Volume of that fraction collected: ____mL
    Volume of buffer B: Vol of fraction * % buffer B = _____mL
    Volume of buffer A: Vol of fraction * % buffer A = _____mL
    Moles of B = Vol Buffer B (1.5 mol)/(1,000 mL)=x mol KCl
    Moles of A = Vol Buffer A (0.200 mol)/(1,00 0mL)= x mol KCl
    Salt concentration of fraction = (Moles A+Moles B)/(Volume of fraction collected (mL)) × (1,000 mL)/(1 L) = x M salt concentration

Acknowledgments

We greatly appreciate Dr. Smita Patel (Rutgers University) and her lab members for providing the expression

Acknowledgements

Chapter 3, in full, is a reprint of the material as it appears in BioProtocol, 2023, Hsieh, An; Reardon, Sean; Munozvilla-Cabellon, Jubilee; Shen, Jiayu; Patel, Smita; Mishanina, Tatiana. The dissertation author was the co-investigator and co-author of this paper.

plasmids for POLRMT and TFAM and the protocols used in this work. We would like to thank Dr. Miguel Garcia-Diaz (Stony Brook University) for providing the expression plasmid for TFB2M. This work was supported by UCSD institutional support, Yinan Wang Memorial Chancellor's Endowed Junior Faculty Fellowship, and R35GM142785 to T.V.M., R35GM118086 to S.S.P.; NIH Molecular Biophysics Training Grant (T32 GM008326) to A.H.H. and J.H.M-C.; NIH Multi-Scale Analysis of Biological Structure and Function Training Grant (T32 EB009380) to S.D.R. This protocol was adapted from and validated in previous works (Ramachandran et al., 2017; Reardon and Mishanina, 2022).

Competing interests

The authors declare no competing interests.

References

Bird, J. G., Basu, U., Kuster, D., Ramachandran, A., Grudzien-Nogalska, E., Towheed, A., Wallace, D. C., Kiledjian, M., Temiakov, D., Patel, S. S., et al. (2018). Highly efficient 5' capping of mitochondrial RNA with NAD+ and NADH by yeast and human mitochondrial RNA polymerase. *eLife* 7: e42179.

Hillen, H. S., Morozov, Y. I., Sarfallah, A., Temiakov, D. and Cramer, P. (2017). Structural Basis of Mitochondrial Transcription Initiation. *Cell* 171(5): 1072–1081.e10.

Kapust, R. B., Tözsér, J., Fox, J. D., Anderson, D., Cherry, S., Copeland, T. D. and Waugh, D. S. (2001). Tobacco etch virus protease: mechanism of autolysis and rational design of stable mutants with wild-type catalytic proficiency. *Protein Eng. Des. Sel.* 14(12): 993–1000.

Oláhová, M., Peter, B., Szilagyi, Z., Diaz-Maldonado, H., Singh, M., Sommerville, E. W., Blakely, E. L., Collier, J. J., Hoberg, E., Stránecký, V., et al. (2021). POLRMT mutations impair mitochondrial transcription causing neurological disease. *Nat. Commun.* 12(1): e1038/s41467-021-21279-0.

Ramachandran, A., Basu, U., Sultana, S., Nandakumar, D. and Patel, S. S. (2017). Human mitochondrial transcription factors TFAM and TFB2M work synergistically in promoter melting during transcription initiation. *Nucleic Acids Res.* 45(2): 861–874.

Raran-Kurussi, S., Cherry, S., Zhang, D., Waugh, D. S. (2017). Removal of Affinity Tags with TEV Protease. In: Burgess-Brown, N. (Ed.) *Heterologous Gene Expression in E. coli* (pp. 221–230). Methods in Molecular Biology. Humana Press, New York, NY.

Reardon, S. D. and Mishanina, T. V. (2022). Phosphorylation and acetylation of mitochondrial transcription factor A promote transcription processivity without compromising initiation or DNA compaction. *J. Biol. Chem.* 298(4): 101815.

Schwinghammer, K., Cheung, A. C. M., Morozov, Y. I., Agaronyan, K., Temiakov, D. and Cramer, P. (2013). Structure of human mitochondrial RNA polymerase elongation complex. *Nat. Struct. Mol. Biol.* 20(11): 1298–1303.

Sultana, S., Solotchi, M., Ramachandran, A. and Patel, S. S. (2017). Transcriptional fidelities of human mitochondrial POLRMT, yeast mitochondrial Rpo41, and phage T7 single-subunit RNA polymerases. *J. Biol. Chem.* 292(44): 18145–18160.

Tan, B. G., Mutti, C. D., Shi, Y., Xie, X., Zhu, X., Silva-Pinheiro, P., Menger, K. E., Díaz-Maldonado, H., Wei, W., Nicholls, T. J., et al. (2022). The human mitochondrial genome contains a second light strand promoter. *Mol. Cell* 82(19): 3646–3660.e9.

Yakubovskaya, E., Guja, K. E., Eng, E. T., Choi, W. S., Mejia, E., Beglov, D., Lukin, M., Kozakov, D. and Garcia-Diaz, M. (2014). Organization of the human mitochondrial transcription initiation complex. *Nucleic Acids Res.* 42(6): 4100–4112.

Chapter 4 Transcriptional Pausing during the Synthesis of Mitochondrial tRNA^{Phe}

In this chapter, I describe foundational unpublished findings on mitochondrial transcriptional pausing, the effect on pausing of a disease-linked mutation within the mitochondrial tRNA^{Phe} coding sequence, and outline troubleshooting strategies and outcomes to support future continuation of this work.

4.1 Introduction

Over 80% of individuals with mitochondrial diseases like MELAS (Mitochondrial Encephalopathy, Lactic Acidosis, and Stroke-like episodes) harbor mutations within their mt-tRNAs, yet the molecular mechanisms by which these mutations lead to mitochondrial dysfunction remain poorly understood[1-5]. Defining how disease-linked mt-tRNA mutations disrupt mitochondrial gene expression is critical for understanding and potentially combatting mitochondrial disease pathology.

Mitochondrial genes are transcribed by a single-subunit mitochondrial RNA polymerase (POLRMT in humans) which is structurally divergent to multi-subunit bacterial and eukaryotic RNA polymerases[6-8]. In bacterial and eukaryotic systems, transcriptional pausing or stalling has been observed to facilitate ribosome binding and RNA folding[9-13]. However,transcriptional pausing in mitochondrial systems remains poorly understood. Previous work by Dr. An Hsieh, in

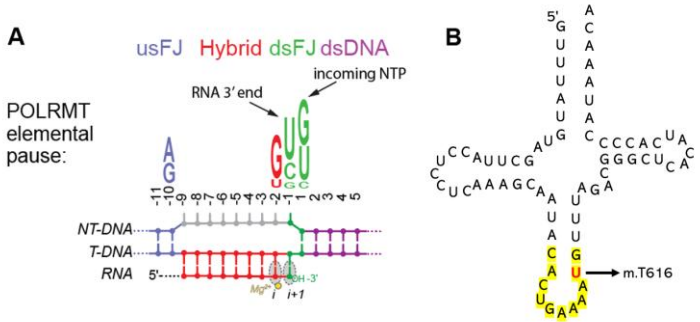

Figure 1 | POLRMT elemental consensus pause and mt-tRNA^{Phe} structure | (A) The previously published POLRMT pause motif demonstrated on a scaffold template. (B) Secondary structure of himan mt-tRNA^{Phe}, where the m.T616C mutation site is colored red, and the residues located within the pause motif are highlighted in yellow.

the Mishanina lab, identified a consensus sequence motif (Fig. 1A) within mtDNA that drives POLRMT to pause (5'-R_{-10}NNNNNNNGT$_{-1}G_{+1}$-3', where -1 is the 3' nascent RNA nucleotide in the POLRMT active site, +1 is the incoming NTP to be added to the nascent RNA, R is A or G, and N is any base[8]. In addition, an mtDNA genome-wide analysis of 12 precision run-on sequencing (PRO-seq) data sets from 4 different human cells (including primary cells) revealed over 400 POLRMT pauses across mtDNA, with most of these occurrences in light strand transcripts[9,14]. A potential reason for the larger pause abundance on these light strand transcripts could be the much higher prevalence of guanine-quadruplexes (G-quadruplexes) within the nascent RNA forming upstream of and in close proximity to the actively transcribing POLRMT, which may act as a structural barrier temporarily holding POLRMT back[9,14]. Nascent RNA structure is well-documented to modulate pausing by multi-subunit RNAPs[15-17]. Dr. Hsieh's studies showing high sensitivity of POLRMT pausing to the transcribed sequence inspired me to investigate whether variations in the mt-tRNA coding stretches of mtDNA may alter transcriptional pausing.

In this Chapter, I investigated a disease-associated mutation (m.T616C) located within mitochondrial phenylalanine tRNA (mt-tRNA^{Phe}, (NCBI Reference Sequence: NC_012920.1, GeneID:4558, Fig. 1B). I found that this mutation localized to the 3' nucleotide of the nascent RNA at a POLRMT pause site, disrupting POLRMT recognition of the pause. This compromised pausing may be altering RNA folding and modification, thereby impairing downstream processing and function.

4.2 Attempt at an *in vitro* promoter-initiated transcription

Human mtDNA (NCBI Reference Sequence: NC_012920.1) was isolated from HEK293T cells to generate template DNA containing the heavy strand promoter (HSP) followed by the mt-

$tRNA^{Phe}$ sequence, mirroring the native genomic arrangement in mt-DNA. After sequence verification, the templates were purified to ensure consistency across experiments.

Using POLRMT and transcription factors TFB2M and TFAM detailed in Chapter 3, I assembled the initiation complex *in vitro* and attempted to perform *de novo*-initiated transcription assays in the presence of an α-phosphate radiolabeled NTP to visualize POLRMT pauses. The resulting RNA products were analyzed on denaturing gels to locate bands that accumulate and gradually diminish over transcription time, indicative of a pause site. My initial experiments showed a radioactive run-off "product" migrating between 147-160 bp, larger than the expected full-length 105-nucleotide transcript (data not shown). A series of control experiments, including protease treatment, phenol RNA extraction, and heat protein denaturation, failed to alter the band's position. These results suggest that the anomalous band reflects an alternative nucleic acid product rather than a protein-bound complex of my desired full-length RNA. I further investigated this species by altering the cross-linking ratios of the gel, which improved resolution of nucleic acid species, but did not change this band's migration. Coincidentally, Dr. An Hsieh, in the lab at the time, determined that POLRMT can "label" the ends of a linear piece of DNA by incorporating an [α-^{32}P] NTP, by an unknown mechanism, suggesting that my band was likely the radiolabeled DNA, rather than RNA[8]. Due to these limitations in promoter-based assays, I transitioned to an established scaffold-based transcription system, which utilizes a pre-assembled DNA-RNA scaffold to skip *de novo* transcription initiation altogether and interrogate pausing during RNA elongation directly.

4.3 Scaffold-based studies of transcriptional pausing on mitochondrial tRNA^{Phe}

Initial experiments using physiological NTP concentrations (1.5 mM CTP, 1.5 mM GTP, 4 mM ATP, 100 µM UTP, final) resulted in rapid production of the run-off product, preventing resolution of intermediate transcript lengths. Reducing NTP concentration tenfold (150 µM CTP, 150 µM GTP, 400 µM ATP, 10 µM UTP, final) slowed transcription sufficiently to observe RNA extension over time, although signal intensity remained low. To optimize detection sensitivity, radiolabeled ATP levels were adjusted empirically, increasing or decreasing input based on observed signal intensity.

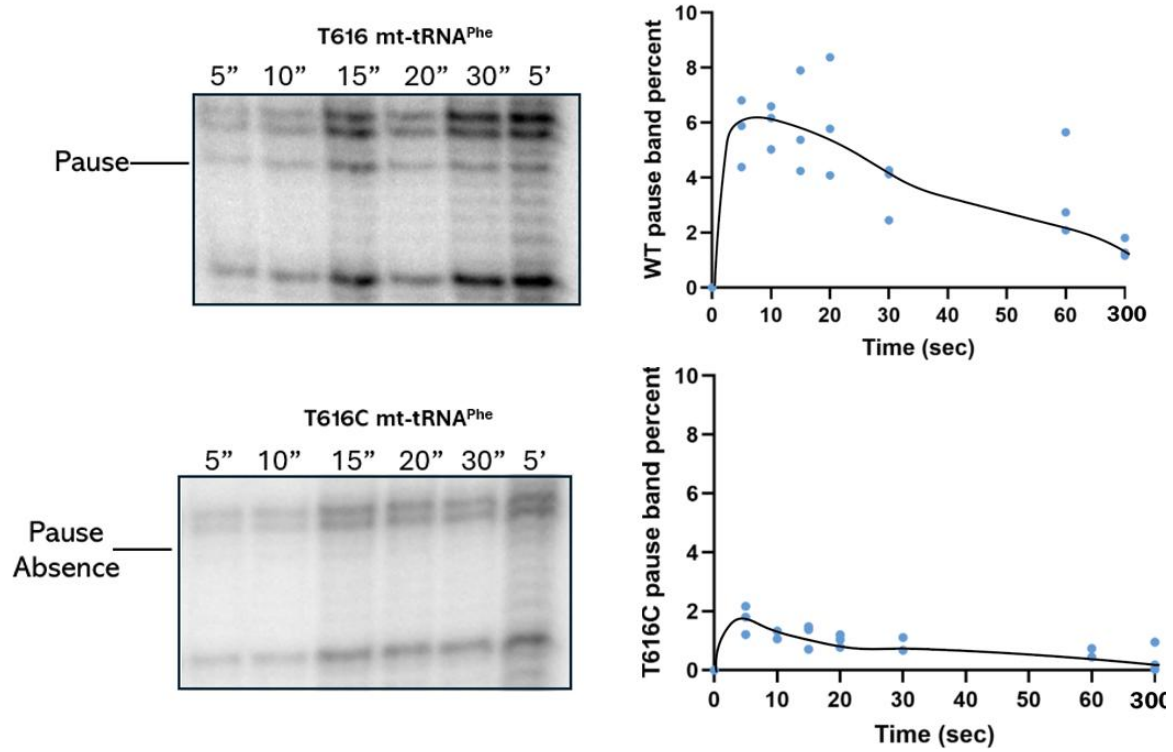

Figure 2 | Comparing pausing activity of m.T616 vs m.T616C | (A) 12% 8MUrea-acrylamide gel showing time-course assay of m.T616 and a plotted graph of quantified band intensity percent over time. Three replicates for each sample are plotted with a representative curve of the average plot.. (B) 12% 8MUrea-acrylamide gel showing time-course assay of m.T616C and plotted graph of quantified band intensity percent over time. Three replicates for each sample are plotted with a representative curve of the average plot.

Using recombinantly prepared POLRMT as detailed in Chapter 3 and synthetic DNA scaffolds encoding tRNA^{Phe} (NCBI Reference Sequence: NC_012920.1, GeneID: 4558), *in vitro*

transcription assays revealed a distinct and reproducible transcriptional pause during elongation (Fig. 2A). With an RNA sequencing ladder prepared in house on the same DNA transcription template but in the presence of chain-terminating 3'-deoxyNTPs, I mapped the pause site to position m.T616 on the mt-tRNA^{Phe} transcript. Quantification of the pause-associated RNA band intensity as a fraction of total signal in the lane over time demonstrated accumulation and subsequent decay at this position, consistent with transient pausing behavior (Fig. 2A).

This pause site sequence contains the elements of the consensus pause signal motif previously identified in mitochondrial transcription (Fig. 1A), specifically a 3' UMP and an incoming GTP. In addition, these results validate scaffold-based transcription as a reliable system for resolving POLRMT pausing on mt-tRNA sequences.

4.4 The effects of mitochondrial-disease related mutation on transcriptional pausing

Previous literature reported that the m.T616C mutation is associated with MELAS and clinically presents as severe epilepsy[18-20]. Additionally, the corresponding uridine at this position is typically modified into a pseudouridine, a modification which may be necessary for a biologically functional tRNA structure[2]. This may suggest that sequence variation may play a role in disrupting transcriptional pausing, post-transcriptional modification, and tRNA structure.

Introduction of the m.T616C mutation into the transcription template reproducibly resulted in an abolishment of the observed paused, as indicated by the absence of the corresponding pause RNA band on the gel (Fig. 2B). This finding demonstrates that disease-associated mutations can directly compromise transcriptional pausing, linking sequence variation to altered transcriptional dynamics. These observations suggest that transcriptional pausing may represent an early regulatory checkpoint in the mt-tRNA life cycle that is disrupted by disease-associated mutations.

4.5 Conclusion and Final Thoughts

I demonstrated that disease-associated mutations within mt-tRNA^{Phe} can abolish transcriptional pausing, supporting a sequence dependent mechanism for POLRMT pausing. These findings extend previous work on pausing motifs and reveal that disease-linked mutations can disrupt mt-tRNA life cycle at an earlier stage than previously appreciated.

In addition, I established and documented a scaffold-based transcription system for analyzing POLRMT pausing on mt-tRNAs, providing a foundation for future mechanistic studies. Together, this work identifies transcriptional pausing as critical and previously underexplored regulatory step in mitochondrial RNA biology, linking sequence variation to downstream defects in RNA processing and function.

Acknowledgements

Chapter 4 contains unpublished material. The dissertation author was the primary author of this chapter.

REFERENCES

1. Suzuki T, Yashiro Y, Kikuchi I, Ishigami Y, Saito H, Matsuzawa I, Okada S, Mito M, Iwasaki S, Ma D, Zhao X, Asano K, Lin H, Kirino Y, Sakaguchi Y, Suzuki T. Complete chemical structures of human mitochondrial tRNAs. Nat Commun. 2020 Aug 28;11(1):4269. doi: 10.1038/s41467-020-18068-6. PMID: 32859890; PMCID: PMC7455718.

2. Suzuki T, Suzuki T. A complete landscape of post-transcriptional modifications in mammalian mitochondrial tRNAs. Nucleic Acids Res. 2014 Jun;42(11):7346-57. doi: 10.1093/nar/gku390. Epub 2014 May 15. PMID: 24831542; PMCID: PMC4066797.

3. MITOMAP: A Human Mitochondrial Genome Database. http://www.mitomap.org, 2023

4. Van Haute L, Pearce SF, Powell CA, D'Souza AR, Nicholls TJ, Minczuk M. Mitochondrial transcript maturation and its disorders. *J Inherit Metab Dis.* 2015 Jul;38(4):655-80. doi: 10.1007/s10545-015-9859-z. Epub 2015 May 28. PMID: 26016801; PMCID: PMC4493943.

5. Wittenhagen LM, Kelley SO. Impact of disease-related mitochondrial mutations on tRNA structure and function. *Trends Biochem Sci.* 2003 Nov;28(11):605-11. doi: 10.1016/j.tibs.2003.09.006. PMID: 14607091.

6. Hillen HS, Morozov YI, Sarfallah A, Temiakov D, Cramer P. Structural Basis of Mitochondrial Transcription Initiation. Cell. 2017 Nov 16;171(5):1072-1081.e10. doi: 10.1016/j.cell.2017.10.036. PMID: 29149603; PMCID: PMC6590061.

7. Tan BG, Gustafsson CM, Falkenberg M. Mechanisms and regulation of human mitochondrial transcription. Nat Rev Mol Cell Biol. 2024 Feb;25(2):119-132. doi: 10.1038/s41580-023-00661-4. Epub 2023 Oct 2. PMID: 37783784.

8. Hsieh AH, Mishanina TV. Nucleic Acid Sequence Determinants of Transcriptional Pausing by the Human Mitochondrial RNA Polymerase (POLRMT). Biochemistry. 2025 Oct 7;64(19):4081-4090. doi: 10.1021/acs.biochem.5c00236. Epub 2025 Sep 17. PMID: 40958658.

9. Kang JY, Mishanina TV, Landick R, Darst SA. Mechanisms of Transcriptional Pausing in Bacteria. J Mol Biol. 2019 Sep 20;431(20):4007-4029. doi: 10.1016/j.jmb.2019.07.017. Epub 2019 Jul 13. PMID: 31310765; PMCID: PMC6874753.

10. Stephen C, Mishanina TV. Alkaline pH has an unexpected effect on transcriptional pausing during synthesis of the Escherichia coli pH-responsive riboswitch. J Biol Chem. 2022 Sep;298(9):102302. doi: 10.1016/j.jbc.2022.102302. Epub 2022 Aug 4. PMID: 35934054; PMCID: PMC9472077.

11. Mayer A, Landry HM, Churchman LS. Pause & go: from the discovery of RNA polymerase pausing to its functional implications. Curr Opin Cell Biol. 2017 Jun;46:72-80. doi: 10.1016/j.ceb.2017.03.002. Epub 2017 Mar 28. PMID: 28363125; PMCID: PMC5505790.

12. Gressel S, Schwalb B, Cramer P. The pause-initiation limit restricts transcription activation in human cells. Nat Commun. 2019 Aug 9;10(1):3603. doi: 10.1038/s41467-019-11536-8. PMID: 31399571; PMCID: PMC6689055.

13. Dollinger R, Gilmour DS. Regulation of Promoter Proximal Pausing of RNA Polymerase II in Metazoans. J Mol Biol. 2021 Jul 9;433(14):166897. doi: 10.1016/j.jmb.2021.166897. Epub 2021 Feb 25. PMID: 33640324; PMCID: PMC8184617.

14. Snyder RJ, Shankar U, Delker D, Soerianto W, Burdick JT, Cheung VG, Watts JA. Guanine quadruplexes mediate mitochondrial RNA polymerase pausing. BMC Biol. 2025 May 13;23(1):129. doi: 10.1186/s12915-025-02229-4. PMID: 40361112; PMCID: PMC12076976.

15. Kang JY, Mishanina TV, Bellecourt MJ, Mooney RA, Darst SA, Landick R. RNA Polymerase Accommodates a Pause RNA Hairpin by Global Conformational Rearrangements that Prolong Pausing. Mol Cell. 2018 Mar 1;69(5):802-815.e5. doi: 10.1016/j.molcel.2018.01.018. PMID: 29499135; PMCID: PMC5903582.

16. Hwang S, Olinares PDB, Lee J, Kim J, Chait BT, King RA, Kang JY. Structural basis of transcriptional regulation by a nascent RNA element, HK022 putRNA. Nat Commun. 2022 Aug 15;13(1):4668. doi: 10.1038/s41467-022-32315-y. PMID: 35970830; PMCID: PMC9378689.

17. Widom JR, Nedialkov YA, Rai V, Hayes RL, Brooks CL 3rd, Artsimovitch I, Walter NG. Ligand Modulates Cross-Coupling between Riboswitch Folding and Transcriptional Pausing. Mol Cell. 2018 Nov 1;72(3):541-552.e6. doi: 10.1016/j.molcel.2018.08.046. PMID: 30388413; PMCID: PMC6565381.

18. Ling J, Roy H, Qin D, Rubio MA, Alfonzo JD, Fredrick K, Ibba M. Pathogenic mechanism of a human mitochondrial tRNAPhe mutation associated with myoclonic epilepsy with ragged red fibers syndrome. Proc Natl Acad Sci U S A. 2007 Sep 25;104(39):15299-304. doi: 10.1073/pnas.0704441104. Epub 2007 Sep 18. PMID: 17878308; PMCID: PMC2000536.

19. Xu C, Tong L, Rao J, Ye Q, Chen Y, Zhang Y, Xu J, Mao X, Meng F, Shen H, Lu Z, Cang X, Fu H, Wang S, Gu W, Lai EY, Guan MX, Jiang P, Mao J. Heteroplasmic and homoplasmic m.616T>C in mitochondria tRNAPhe promote isolated chronic kidney disease and hyperuricemia. JCI Insight. 2022 Jun 8;7(11):e157418. doi: 10.1172/jci.insight.157418. PMID: 35472031; PMCID: PMC9220945.

20. Viering D, Schlingmann KP, Hureaux M, Nijenhuis T, Mallett A, Chan MMY, van Beek A, van Eerde AM, Coulibaly JM, Vallet M, Decramer S, Pelletier S, Klaus G, Kömhoff M, Beetz R, Patel C, Shenoy M, Steenbergen EJ, Anderson G, Bongers EMHF, Bergmann C, Panneman D, Rodenburg RJ, Kleta R, Houillier P, Konrad M, Vargas-Poussou R, Knoers NVAM, Bockenhauer D, de Baaij JHF; Genomics England Research Consortium. Gitelman-Like Syndrome Caused by Pathogenic Variants in mtDNA. J Am Soc Nephrol. 2022 Feb;33(2):305-325. doi: 10.1681/ASN.2021050596. Epub 2021 Oct 4. PMID: 34607911; PMCID: PMC8819995.

Chapter 5 Summary and Conclusions

In this dissertation, I demonstrate how variations in mt-tRNA sequences influence both transcription of those sequences and the polycistronic transcript maturation. Although mt-tRNAs comprise only ~10% of the mitochondrial genome, they house over 50% of pathogenic mutations, highlighting their disproportionately large impact on mitochondrial function. While previous studies established the biological associations between mt-tRNA mutations and mitochondrial disease, the biochemical basis for many processing defects remained unclear – a gap filled in part by this dissertation work as summarized below. Understanding how mutations disrupt the mt-tRNA life cycle provides critical insight into the molecular origins of mitochondrial disease and identifies stages at which targeted therapeutic intervention may be most effective.

My work shows that an mt-tRNA mutation located within a “consensus elemental pause” sequence abolishes RNA polymerase pausing during transcription of the mt-tRNA gene. While the precise functional role of such pauses remains unclear, their disruption highlights an early stage in the tRNA life cycle that is sensitive to sequence variation. Additionally, my findings demonstrate that mt-tRNA variants located within the acceptor stem can directly compromise recognition and cleavage by the mitochondrial RNase P complex, impairing 5' leader excision – the first required step in mitochondrial RNA processing – thereby stalling mt-tRNA maturation. These defects can also propagate to downstream tRNAs within clusters, particularly when tRNAs are directly adjacent, as 3' processing of one tRNA is often coupled to 5' maturation of the next. Together, these findings demonstrate that disease-associated mutations disrupt multiple, mechanistically linked stages of the mt-tRNA life cycle.

In Chapter 2, I demonstrate that sequence variations within the acceptor stem, including a deletion that shortens the tRNA and disease-associated point mutations, impair downstream tRNA

processing by disrupting recognition by mitochondrial RNase P, resulting in defective 5' cleavage. Although pathogenic mt-tRNA variants have long been associated with defects in RNA maturation, the specific processing step affected remained unclear. I showed that mt-tRNA sequence variants not only altered interactions with the MRPP3 endonuclease, but also reduced binding affinity for the MRPP1/2 subcomplex, which is responsible for stabilizing and orienting the tRNA for processing and serves as a platform on which RNA processing factors exchange. This stabilizing and positioning role is particularly critical given that the majority of mt-tRNAs lack canonical structural features required for stable tertiary folding. I further showed that MRPP1/2 enforces directional processing by preventing ELAC2-mediated 3′ cleavage when the 5' leader remains attached, consistent with a 5'-to-3' maturation pathway. Although ELAC2 alone can cleave pre-tRNAs, its activity is less efficient and prone to miscleavage in the absence of MRPP1/2. In contrast, MRPP1/2-dependent processing ensures both efficiency and accuracy of cleavage, and my work revealed a previously unknown quality control role for MRPP1/2 in preventing miscleavage. Additionally, I demonstrate that defects in an upstream “leader” tRNA impair processing of downstream tRNAs within clusters, but only when these tRNAs are directly adjacent, indicating that physical continuity contributes to coordinated maturation. Although prior studies have observed these cluster effects from mt-tRNA level measurements in mitocybrid systems, they were unable to determine the mechanistic basis for these effects. My work demonstrated that defective 5' processing of an upstream tRNA can stall release of downstream tRNAs within a cluster, providing novel biochemical insights into coordination of processing events across adjacent transcripts. My work showed that impaired 5' cleavage is a major consequence of acceptor-stem variants and can serve as the initiating defect disrupting subsequent

maturation events, demonstrating a propagation of processing defects beyond the mutated tRNA itself.

In Chapter 3, I optimized a purification protocol for key components of the mitochondrial transcription machinery, including POLRMT, TFB2M, and TFAM. This work improved protein yield and purity relative to previous methods and resulted in a robust and reproducible protocol. The method has since been validated through its use by other research groups to investigate mitochondrial transcription mechanisms. Thus, this contribution provides a valuable technical foundation for advancing studies of mitochondrial gene expression.

In Chapter 4, I build upon previous work in mitochondrial transcription by investigating transcriptional pausing and its sensitivity to tRNA sequence variation. Initial promoter-based transcription assays presented technical limitations, including unintended incorporation of radiolabeled nucleotides into the DNA (instead of RNA) and challenges in resolving transcription intermediates. By systematically identifying and documenting these limitations, I establish a framework for future methodological improvements. Transitioning to a synthetic scaffold-based transcription system enabled characterization of POLRMT pausing behavior on mt-tRNA^{Phe}. Using this approach, I demonstrate for the first time that a disease-associated mutation (m.T616C) abolishes transcriptional pausing at a defined site. This finding provides direct evidence that sequence variation can disrupt transcriptional dynamics at an early stage of the tRNA life cycle. My results identify transcriptional pausing as a mutation-sensitive regulatory step in mitochondrial gene expression.

Collectively, this work integrates transcriptional and post-transcriptional mechanisms to provide a comprehensive view of how mt-tRNA variants disrupt mitochondrial gene expression. I demonstrate that mutations can impair tRNA maturation at multiple stages, including RNA

synthesis, RNA enzymatic processing, and coordinated RNA cluster maturation. Importantly, my work shows that defects arise earlier in the tRNA life cycle than previously understood and may propagate through multiple downstream processes.

While my doctoral work establishes a foundation for understanding the interplay between transcriptional pausing and tRNA processing, several questions remain. In particular, the functional role of transcriptional pausing in mitochondrial RNA biology and its direct impact on tRNA folding and modification require further investigation, such as studying protein-protein interactions between modifying enzymes and POLRMT during the transcription process. Additionally, integration of transcription and processing assays *in vitro* remains technically challenging due to the complexity of the system, the number of required components, and the complications/inefficiency of starting transcription *de novo* from promoter sequences. Continued methodological development will be necessary to fully reconstitute these processes and define their mechanistic relationships.

In conclusion, this dissertation identifies transcriptional pausing and tRNA processing as interconnected and pinpoints mutation-sensitive steps in the mt-tRNA life cycle. My work also adds to the existing body of evidence for a model in which pathogenic mt-tRNA variants disrupt processing by altering substrate architecture and enzyme recognition rather than solely through sequence changes at cleavage sites. This extends principles established in nuclear tRNA processing to the mitochondrial system and provides a framework for understanding the molecular basis and linking mtDNA sequence variation to mitochondrial dysfunction. These findings not only advance fundamental knowledge of mitochondrial gene expression but also highlight early stages of mt-tRNA maturation as potential targets for therapeutic intervention in human mitochondria.